Dissertation zur Erlangung des Doktorgrades
der Fakultät für Chemie und Pharmazie
der Ludwig-Maximilians-Universität München

Non-covalent dendrimer- and polymer-based modifications of adenovirus capsids for enhanced transduction of cancer cells

Alexandra Kerstin Maria Vetter

aus

Bühl, Deutschland

2013

Erklärung

Diese Dissertation wurde im Sinne von § 7 der Promotionsordnung vom 28. November 2011 von Herrn Prof. Dr. Ernst Wagner betreut.

Eidesstattliche Versicherung

Diese Dissertation wurde eigenständig und ohne unerlaubte Hilfe erarbeitet.

München, den

……
(Unterschrift der Autorin)

Dissertation eingereicht am:	04.06.2013
1. Gutachter:	Prof. Dr. Ernst Wagner
2. Gutachter:	PD Dr. Manfred Ogris
Mündliche Prüfung am:	11.07.2013

Phantasie ist wichtiger als Wissen,
denn Wissen ist begrenzt.

Albert Einstein

Meiner Mutter

TABLE OF CONTENTS

1 INTRODUCTION

1.1 Cancer gene therapy

Within the area of gene therapy, the treatment of malignant diseases is, with 64.3% of all gene therapy trials performed worldwide, the main area of application (Figure 1, The Journal of Gene Medicine, 2013). Cancer gene therapy employs DNA as a pharmaceutical agent to treat cancer. The method can either be used to introduce a functional gene to replace a mutated gene (gene replacement strategies) as performed with the tumor suppressor gene p53,[1] by delivering DNA that encodes for an enzyme e.g. the thymidine kinase gene of herpes simplex virus (HSV-TK) able to convert non-toxic prodrugs into active chemotherapeutic agents selectively within the tumor [2] (suicide gene therapy) or by priming the patient's immune system e.g. by transducing tumor cells so that they secrete granulocyte macrophage colony stimulating factor (GM-CSF) or interleukin-12 (gene based immunotherapy).[3] The two major methods by which the DNA is delivered include the use of naked DNA or DNA complexes as non-viral vectors and the utilization of recombinant viruses as viral gene transfer vehicles.

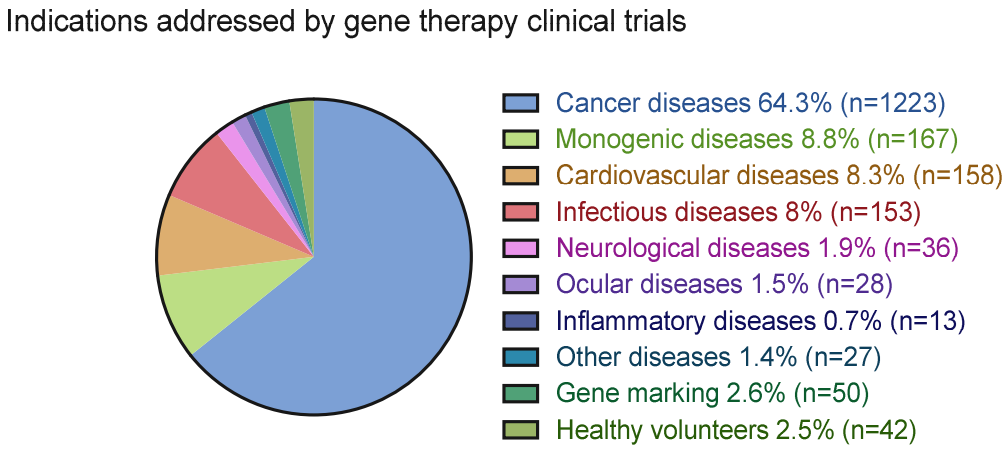

Figure 1. Percentage and absolute number of indications addressed by gene therapy clinical trials Adapted from www.wiley.co.uk/genmed/clinical (The Journal of Gene Medicine, 2013)

1.2 Adenovirus vectors in cancer gene therapy

To date adenovirus vectors are the most commonly studied and most widely used vectors in cancer gene therapy (Figure 2, The Journal of Gene Medicine, www.wiley.co.uk/genmed/clinical). Since its detection in adenoid tissue by Rowe in 1953,[4] there are currently 57 described serotypes [5] in humans belonging to the genus Mastadenovirus. Based on oncogenicity in rodents, hemagglutination properties of human,

monkey and rat erythrocytes, DNA sequence similarity and serologic profiles, the human adenoviruses can be further divided into species A -G.[6] Adenoviruses can be easily genetically manipulated to generate either replication incompetent or conditionally replicating viruses. Replication incompetent adenoviruses can be classified into three categories: vectors of the first generation contain deletions in the E1 regions required for viral replication and often have an additional E3 region deletion. Second generation vectors possess additional deletions in the E2 and E4 regions. Third generation vectors finally are devoid of all viral genes with the exception of inverted terminal repeats and DNA packing sequences. These gutless or helper-dependent vectors are characterized by a reduced immunogenicity and an extended transgene expression. In the case of replication incompetent adenoviruses, the anti-tumor activity is caused by the transgene delivered. In contrast conditionally replicating adenoviruses, also referred to as oncolytic adenoviruses, are able to selectively replicate in cancer cells, leading to the death of cancer cells through cell lysis, mediated during viral spread.[7] They hold great promise as potent, self amplifying cancer therapeutics, while showing no cross-resistance with chemo- and radiation therapies. [8] These oncolytic adenoviruses can be further armed with therapeutic transgenes like prodrug convertase transgenes (HSV-TK), pro apoptotic transgenes (p53, TRAIL) or immunoactivating transgenes (INF, GM-CSF).[8]

The most employed adenovirus vectors in clinical trials are serotype 5 (Ad) based vectors, belonging to species C, with a growing number of trials advancing to Phase III. The main focus lies on the delivery of the tumor suppressor gene p53 as gene replacement strategy, often combined with conventional chemotherapy.[9] One example is a US Phase III multicenter, open-label, randomized study, where the effectiveness and safety of bi-weekly intratumoral administration of Ad p53 (INGN 201) in combination with chemotherapy is compared with chemotherapy alone in 288 patients with recurrent squamous cell carcinoma of the head and neck. It is known that tumor cells expressing wild-type p53 are more sensitive to chemotherapeutic agents and radiation, than cells lacking functional p53.[9] Chemotherapy, in return, enhances expression of transduced genes from adenoviral vectors.[9] Also radiation enables a synergistic effect as it improves immediate adenoviral transduction efficiency and the duration of transgene expression.[10] Adenoviral gene therapy can therefore be used to support standard anti-tumor therapies like chemotherapy or radiation.

In China there are already two Ad-based products, which have been approved by the Chinese State Food and Drug Administration for the use in patients suffering from head and neck carcinoma: Gendicine™ [11] a replication-incompetent recombinant human Ad-p53

and Oncorine™ (H101) [12] a conditionally replicative adenovirus, carrying a deletion of the E1B-55 kDa/E3B genes (normally allowing the Ad to bind and inactivate the host p53 gene in order to promote its own replication),[13] developed to selectively replicate in tumor cells with dysfunctional p53 genes. The utilization of adenoviral vectors is especially beneficial, when temporary gene expression is desired, as in the case of cancer treatment.

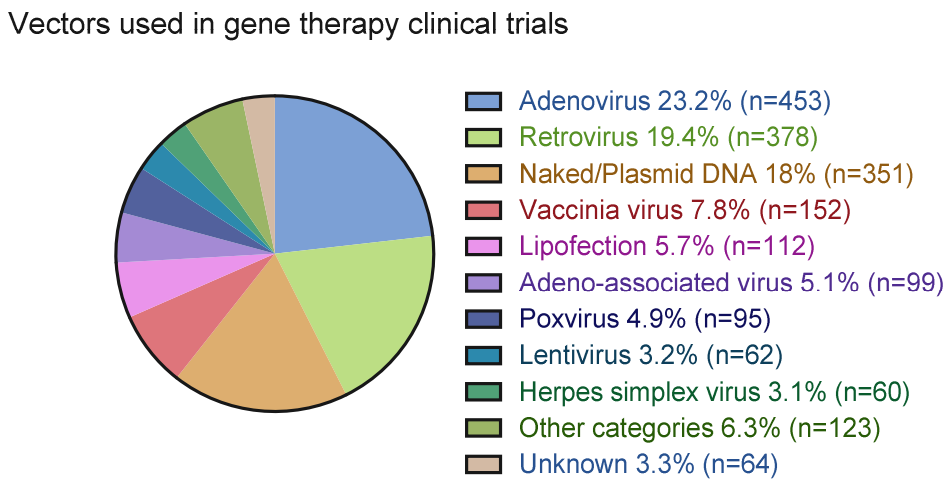

Figure 2. Percentage and absolute numbers of vectors used in gene therapy clinical trials
Adapted from www.wiley.co.uk/genmed/clinical (The Journal of Gene Medicine, 2013)

1.3 Adenovirus structure

The adenovirus is a non-enveloped double stranded DNA virus, with a genome size of about 36 kb,[14] showing an icosahedral symmetry and a size between 70 and 90 nm.[15] The viral particle is built out off 13 structural proteins (Figure 3).[16] Four proteins surround the genome forming a nucleoprotein core complex, composed of a core-penton bridging protein (V), histone-like protein (VII), Mu protein and terminal protein (TP) covalently bound to the 5' end of the genome.[17] Two more proteins are associated with the core, IVa2 [18] and the protease.[6] The capsid consists of seven proteins, namely the trimeric hexon (II), with its stabilizing minor capsid proteins (VI, VIII and IX), the pentameric penton base, the penton associated protein (IIIa), responsible to bridge hexon and penton and the trimeric fiber protein (IV), which protrudes at the 12 vertices of the icosahedral capsid.[19,20]

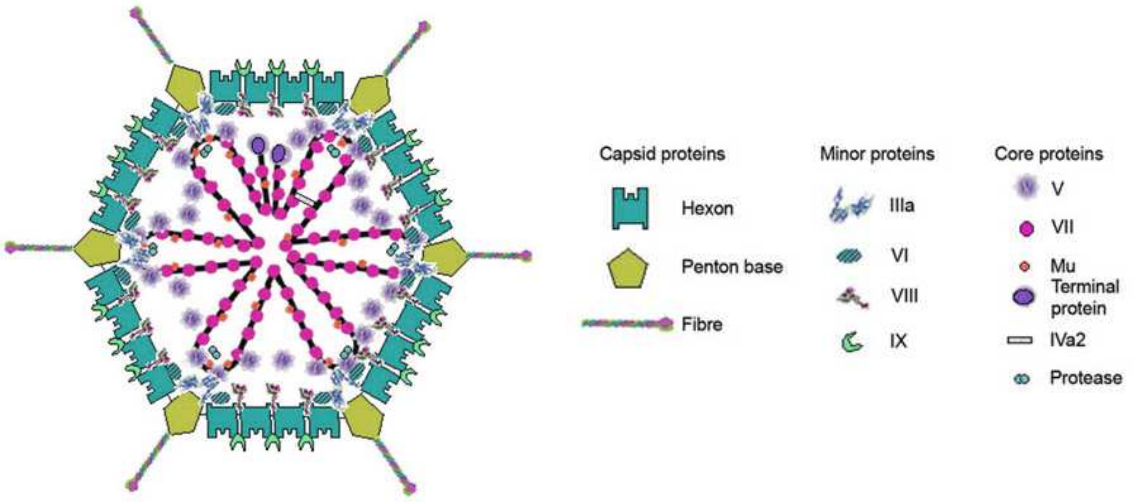

Figure 3. Adenovirus structure

Scheme of capsid and core proteins of an adenovirus (W.C. Russell, J. of General Virology, 2009)[6]

1.4 Entry pathway of adenovirus type 5 (Ad) in vitro

The adenovirus type 5 (Ad) infects its target cells through a two step entry pathway (Figure 4): the fiber knob protein of the Ad capsid binds to the coxsackie- and adenovirus receptor (CAR) for cell attachment,[21] as does the KKTK (Lys-Lys-Thr-Lys) motive of the fiber shaft to heparan sulfate proteoglycans (HSPG).[22] This is followed by an interaction of the RGD (Arg-Gly-Asp) motif in the penton base protein with the cell surface $\alpha_v\beta_3$ and $\alpha_v\beta_5$ integrins, leading to internalization.[23] Additional integrins including $\alpha_v\beta_1$, $\alpha_3\beta_1$, $\alpha_5\beta_1$ and $\alpha_M\beta_2$ have also been identified as receptors facilitating internalization, in vitro.[24-27] The internalization process is caused via clathrin-mediated endocytosis.[28] Partial capsid disassembly upon acidification of the endosome leads to exposure of protein VI, which then modulates endosomal escape by its lytic action.[29] Thereafter the nucleocapsid-hexon core is transported in a microtubule dependent manner to the nuclear pore complex, involving dynein for attachement.[30] After binding to the nuclear pore complex receptor CAN/Nup214 and recruitment of Hsc70, nuclear histone H1 and H1 import factors importin β and importin 7, complete capsid disassembly is facilitated and the viral genomic DNA delivered into the nucleus.[31]

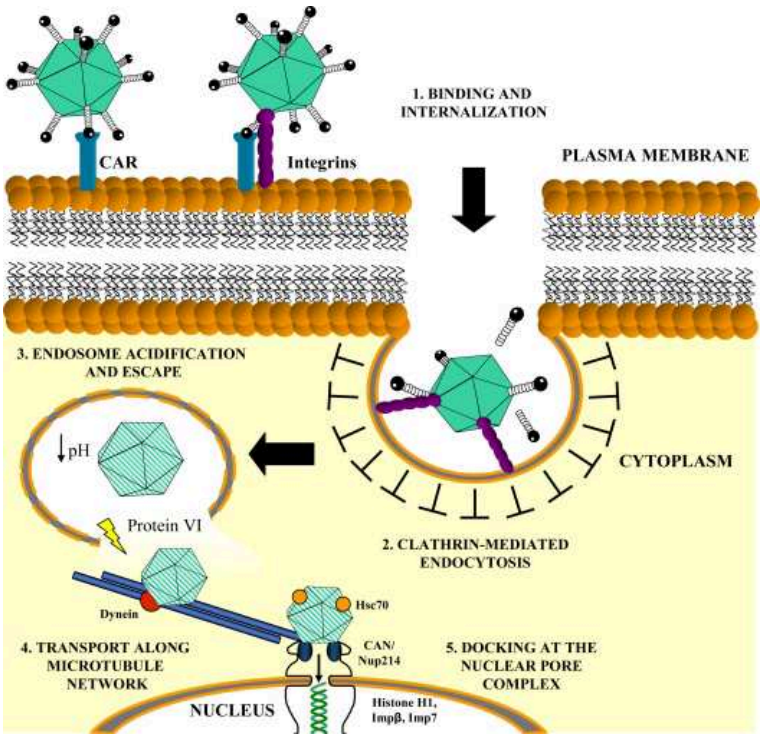

Figure 4. In vitro entry pathway of adenovirus type 5 (Ad) (L. Coughlan, Viruses, 2010)[16]

1. Ad attachment is mediated by binding of the fiber knob to CAR. **2.** Interaction between the RGD motif of the penton base and $\alpha_v\beta_{3/5}$ integrins triggers internalization by clathrin-mediated endocytosis. **3.** Partial disassembly of the capsid is induced upon acidification of the endosome. Endosomal escape is modulated through the lytic action of protein VI. **4.** The nucleocapsid-hexon core is translocated to the nuclear pore complex (NPC) along the microtubule network using the microtubule-associated motor, dynein. **5**. Final dissociation of the capsid at the NPC [32] allows the core DNA to extrude into the nucleus leading to subsequent transcription and in case of replication competent Ad, to induction of a replication cycle.

1.5 Advantages and disadvantages of Ad versus non-viral vectors

The adenovirus type 5 (Ad) is the most frequently used vector in gene therapy clinical trials as it has a number of features which favor effective gene transfer. Ad has the advantage of a high transduction efficiency in many cell types.[33] It can infect dividing as well as non-dividing and differentiated cells without integrating its DNA into the host genome, therefore exhibiting a limited rate of insertional mutagenesis.[14] Additionally Ad can accommodate large segments of foreign DNA, with a volume of up to 7.5 kb for first-generation vectors and up to 36 kb in the case of gutless vectors.[34] The transgenic protein can be expressed at high levels of up to 35% of the total cellular protein. Titers up to 10^{13} VP/ml can be produced [35] and virus biology is well characterized. Moreover the vectors are stable, when administered into the bloodstream. Still the in vivo application of Ad faces significant hurdles (Figure 5):

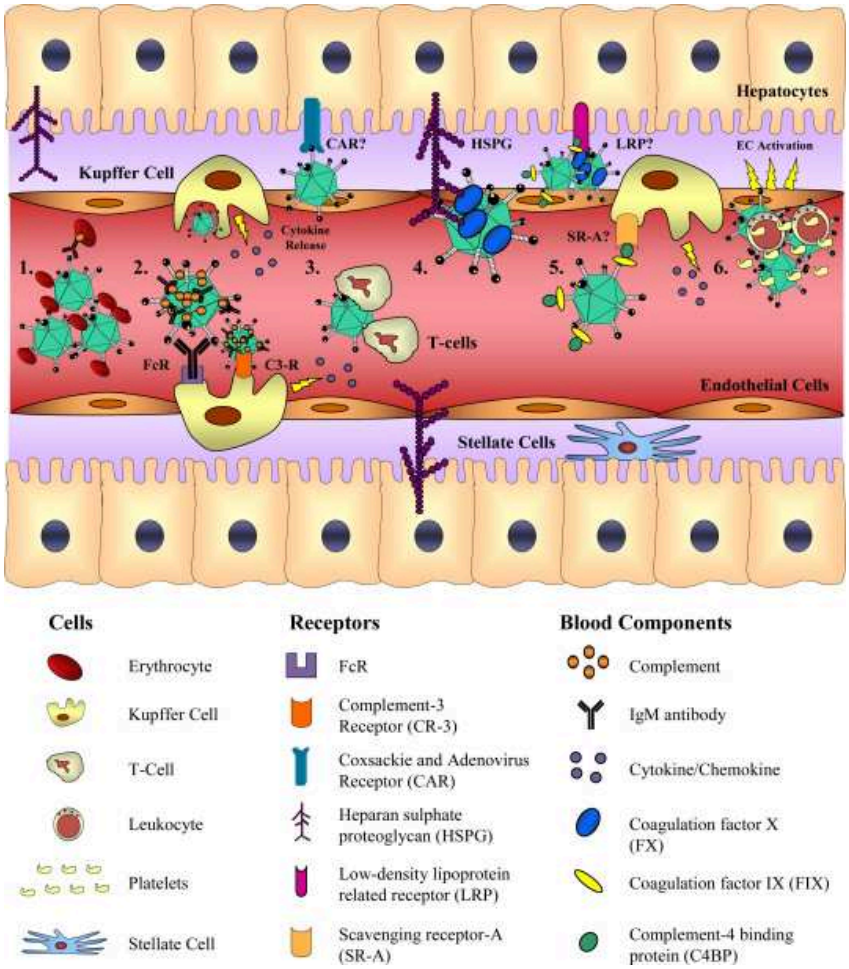

Figure 5. Interactions of Ad with blood components in vivo (L. Coughlan, Viruses, 2010)[16]

1. Binding of Ad to CAR-expressing erythrocytes can cause trapping of virus in the circulation. In the presence of antibody and complement, Ad can bind human erythrocytes via CR-1. **2.** Opsonization of Ad with natural IgM and/or complement promotes Kupffer cell (KC) uptake via complement receptor-3 (CR-3) or Fc Receptor. **3.** Ad interactions with CD4+ T-cells. **4.** FX binding to the Ad hexon promotes hepatocyte entry through HSPGs (heparan sulphate proteoglycans). **5.** FIX/C4BP binding to the fiber knob has been proposed to mediate hepatocyte entry via HSPGs or LRP (Low density lipoprotein receptor), and has been suggested to direct KC uptake [36]. **6.** Ad binding to platelets has been shown to enhance uptake by KCs.[37] Von Willebrand factor (vWF) and P-selectin have been associated with the formation of activated platelet-leukocyte aggregates which are cleared by scavenging macrophages.[38]

After intravenous application of Ad the majority of the particles are scavenged by resident liver macrophages, called Kupffer cells (KCs) and spleen macrophages. Following opsonization of Ad by immunoglobulin M antibodies and complement system, uptake in KCs is directed via complement receptor-3 (CR3) or Fc receptor interations.[39,40] Also scavenging receptor-A (SR-A) has been proposed to be involved in Ad uptake by KCs, presumably recognizing the negative charge of the virus capsid.[41] Besides being rapidly

removed from the blood circulation, scavenging by KCs is accompanied by the release of inflammatory cytokines contributing to the acute liver toxicity. After saturation of the reticuloendothelial system the Ad is predominantly taken up by hepatocytes.[42] A recently identified high affinity interaction between coagulation factor X and the hexon protein, leads to this hepatocyte infection after intravenous application in vivo.[43-45] Additionally most humans possess antibodies against Ad, due to Ad contact early in life. This leads to neutralization of Ad by preexisting antibodies, causing a strong reduction of target cell infection.[46-48] Yet another problem to solve is that the transduction efficiency is limited by the level of viral receptors on target cells, which are often downregulated on cancer cells, correlating with the aggressiveness of the tumor.[49] On the other hand, non-target cells may express high levels of receptors precluding target selectivity. An important difference between mouse and man, which has to be taken into consideration, when establishing a mouse model, where the vector is applied intravenously, is the fact that in humans Ad binds to erythrocytes leaving only 1% unbound. This on the one hand increases circulation times, but on the other hand precludes vector extravasation into target tissue.[50] In principal adenoviral vectors are well tolerated, proven through several phase I clinical trials, showing minimal side effects like shivering, light fever, chills, local pain and diarrhea after intratumoral administration of $1x10^{12}$ viral particles.[9] Despite this, a general skepticism still pervades since the death of 18 year old Jesse Gelsinger in 1999, who participated in a Phase I clinical trial for ornithine transcarbamylase deficiency. 98 h following intravascular administration of $3.8x10^{13}$ virus particles he died due to systemic inflammatory response syndrome, disseminated intravascular coagulation, accumulation of ammonia in the blood due to the underlying metabolic deficiency and ultimately multiorgan failure.[35] This tragic incident led to several considerations. By minimizing the transcribed viral genes through the further development of second and third generation vectors, measuring vector concentration in plaque forming units (PFU) and additionally in viral particles (VP) and taking into account liver function and underlying diseases before systemic administration of Ad, safety could have been improved.[51]

As an alternative to viral vectors, synthetic gene delivery systems have evolved, like cationic lipids or polymers,[52] which are able to condense DNA forming a positively charged complex that can enter the cell and escape the endosome via a proton sponge effect.[53] In contrast to viral vectors, which are restricted mainly to DNA and RNA delivery, non-viral vectors are able to deliver proteins, synthetic oligonucleotides and small compounds beside DNA and RNA.[52] Such vectors have the advantage that no preformed antibodies exist, which could prevent a successful infection. In addition non-viral vectors

have the ability to carry large therapeutic genes (52 kb) [54] and cheap large scale manufacture is possible.[55] Furthermore, modification with hydrophilic polymers, like polyethyleneglycol (PEG), enables prolonged circulation of drugs and gene vectors in the bloodstream, avoiding entrapment by reticuloendothelial cells in the liver, spleen and lung therefore allowing accumulation in tumor tissue.[56] Synthetic delivery systems can also be designed in a modular way, which allows the incorporation of cell targeting and internalizing ligands considerably improving their efficiency and specificity.[57] Still, there are major hurdles for non-viral gene delivery vectors to overcome like poor nuclear import and the absence of a transcriptional enhancer, making them far less effective compared to their viral counterparts.[58]

The limited clinical applicability of adenoviral vectors, caused by several vector–host interactions, could be widened by using polycationic coating to cover the sides responsible for interaction. A combination of both systems would be therefore beneficial to achieve a high transgene expression level even in cells not accessible by Ad itself and at the same time enable e.g. protection from inactivation by neutralizing antibodies.

1.6 Transductional targeting

1.6.1 Genetic modification strategies

Transductional targeting, which is based on directed binding of Ad to and uptake in target cells, away from its natural tropism, is primarly achieved by genetic targeting strategies. The genetic incorporation of targeting ligands is tolerated at specific sites of the Ad capsid including the C-terminus [59] and the H1 loop [60] of the fiber, the penton base,[61] certain hypervariable regions of the hexon [62] and the pIX protein.[59] Therefore it is important that the inserted ligand doesn't disrupt adequate capsid assembly. Besides a limitation in size of the inserted ligand, functionality of the targeting peptide must be retained without the necessity for major post-translational modifications.[16] Ligands successfully inserted into the H1 loop and C-terminus of the fiber include RGD [63] and polylysine motifs binding to $\alpha_v\beta_{3/5}$ integrins and heparan sulphate proteoglycans respectively. Furthermore genetic pseudotyping is used, where e.g. the adenovirus type 5 fiber is substituted by fibers derived from species B adenoviruses, leading to CAR-independent target cell infection via receptors including CD46 [64], CD80 and CD86.[65] A drawback of this approach is, that genetic pseudotyping has been shown to alter intracellular trafficking of Ads, leading to inefficient endosomal escape [66] or a slow-down in nuclear translocation.

1.6.2 Chemical modification: non-covalent versus covalent

Additionally, transductional targeting can be gained chemically either via non-covalent or covalent surface modification of the viral capsid. Due to its net negative surface charge, Ad capsids can be easily coated with (poly)cationic molecules by non-covalent charge interaction. This allows for a fast screening of suitable polycationic coating agents. Fasbender et al. were the first to demonstrate the prominent increase in binding and subsequent transgene expression of Ad non-covalently coated with cationic lipids on differentiated airway epithelia, in vitro, as well as nasal epithelium of mice, in vivo.[46] Other researchers confirmed these findings by using cationic lipids, (proteo)- liposomes or cationic polymers such as poly L-lysine or polyethylenimine.[46,67-72] Non-covalent coating offers the possibility that adenoviral infectivity is potentially retained and transduction efficiency elevated through increased cellular binding and uptake, while intracellular trafficking is not negatively influenced. As certain polycations, like linear polyethylenimine (LPEI), a gold standard of non-viral gene delivery systems, suffer from undeniable toxicity due to crosslinking of erythrocytes in the lung,[73] there is a search for well tolerated and efficient Ad coating reagents. PAMAM dendrimers, used in this study, are well-known drug carriers exhibiting a considerably lower toxicity compared to LPEI when applied systemically,[74] and having the additional advantage over LPEI to have a defined structure, a defined size and a defined molecular weight due to the synthesis procedure. The word dendrimer is derived from the Greek words dendri- (tree branch-like) and meros (part of). The expression was coined by Tomalia et al. in 1985 in the first full paper on PAMAM dendrimers.[75] Dendrimers are composed of three architectural components: a core (I), an interior of shells with repeating branching units (II) and terminal functional groups (III) (Figure 6).

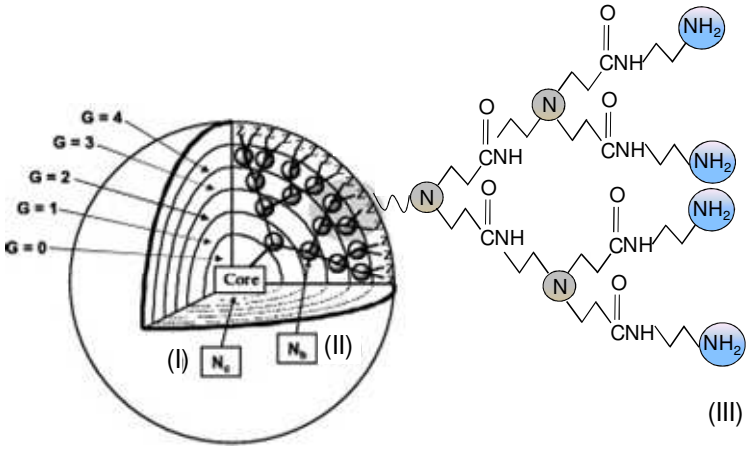

Generation	Surface Groups	Molecular Formula	MW	Diameter (nm)
2	16	$C_{144}H_{292}N_{58}O_{28}$	3284	2.6
3	32	$C_{304}H_{612}N_{122}O_{60}$	6937	3.6
5	128	$C_{1264}H_{2528}N_{506}O_{252}$	28854	5.7

Figure 6. Structure, molecular weights and sizes of PAMAM dendrimers (modified from D.A. Tomalia, Progress in Polymer Science, 2005)[76]

PAMAM dendrimers used in this study are composed of a diaminobutane core and iterative branches built out of methyl acrylate and ethylendiamine by iterative alkylation-amidation, with each generation doubling in surface groups (primary amines).

Besides non-covalent coating approaches, covalent coating using hydrophilic polymers was investigated in order to mask surface epitopes and prevent inactivation by neutralizing antibodies and unwanted interactions with blood components and non-target tissue. First attempts were made using amine reactive polyethylene glycol (PEG), known to solubilise drugs and enable prolonged circulation of liposomes.[77] Small PEG moieties proved to shield vector particles from neutralizing antibodies,[78] but detargeting of Ad away from hepatocytes was only feasible, when large PEG moieties above 20 kDa were used including extensive modification of at least 10,000 amine groups of the Ad capsid.[79] A more effective strategy in covering the sites relevant for hepatocyte transduction was investigated by coupling of PEG moieties to a cysteine genetically incorporated into the hyper variable region 5 (HVR 5) of the hexon protein. Depending on the size of the PEG moiety used, Ad was either detargeted from hepatocytes but taken up from KCs (2 kDa), evading KCs but targeted to hepatocytes (5 kDa) or detargeted from both cell types but also reduced in its overall infectivity (20 kDa). With this strategy higher particle uniformity can be gained and less polymer is needed compared to conventional amine PEGylation (maximum of 720 PEG moieties per viral capsid).[80]

Besides PEG, hydrophilic polymers based on N-(2-hydroxypropyl)methacrylamide (HPMA), bearing multiple side chains carrying amino-reactive groups at their ends are used for coating. Unlike PEG, HPMA is not fusogenic preventing enhanced infection through non-specific membrane activity.[81] These polymers form a dense, multivalent coverage, with each polymer having several points of attachment to the virus.[82] While the physical size of the virus is effectively unchanged, HPMA coated adenovirus is unable to bind to its natural receptors on target cells and shows no transduction efficiency in vitro. Binding of anti-adenovirus antibodies to the virus particles is reduced by about 80% by this coating method [82] and can be even more reduced by the use of HPMA polymers bearing additionally quaternary ammonium groups, which can electrostatically interact with the acid region of the hexon protein.[83] HPMA coated virus also shows extended plasma circulation kinetics with a half life of over 60 min, whereas uncoated adenovirus was cleared from the circulation within 2 min. Along with the absence of hepatocyte infection and the reduction of binding to human erythrocytes,[50] these coated viruses provide the opportunity to reach disseminated tumor sites by passive accumulation through the enhanced permeability and retention (EPR) effect.[84] With the main advantage of stability of covalent versus non-covalent coated vector particles, methods have to be developed to increase infectivity of target cells by the addition of suitable targeting ligands.[85]

While chemical modifications of oncolytic adenoviruses would only mediate targeting of the inoculated virus, progeny virions produced in the tumor would default to their genetically encoded tropism.[8] Additionally, as multiple Good Manufacturing Practice (GMP)-grade reagents, for use in patients, have to be combined, the approach using chemical modification is more difficult for clinical translation, than having one genetically modified vector.[8] On the other hand, one can argue that with the chemical modification approach, progeny viruses once extravasated from the tumor site would be recognized by the immune system, abolishing uncontrolled viral spread and infection of non-target cells.

1.6.2 Targeting ligands

Polymer coating strategies enabling ablation of viral tropism and non specific uptake into tumor cells, in vivo, can be raised in their efficiency and safety profile, when adding targeting ligands for cancer restrictive receptors. First targeting experiments with coated adenoviral vectors were performed using the high affinity ligand fibroblast growth factor 2 (FGF2),[82] binding the 4 FGF receptors upregulated in a number of diseases characterized by hyper proliferation, including malignancies [86,87] and dermal wound healing.[88]

To date a range of internalizing receptors have been used for retargeting purposes, e.g. the epidermal growth factor receptor, known to be overexpressed on several cancer types and associated with disease progression.[89] Successful EGFR retargeting ligands include murine EGF (mEGF)[90] and Cetuximab.[85] As both FGF and mEGF are potential mitogens, the EGFR-antibody Cetuximab, which stimulates internalization of EGFR similarly to EGF, but inhibits EGFR phosphorylation,[85] while at the same time directing antibody dependent cellular toxicity,[91] is a more suitable ligand for clinical use. Alternatively the peptide ligand GE11 (YHWYGYTPQNVI) discovered by screening a phage display library can be used to target the EGFR, showing much lower mitogenic activity than the natural ligand EGF.[92] Besides EGFR targeting ligands, a laminin derived peptide (YESIKVAVS) was incorporated on polymer coated adenovirus to permit tumor-specific targeting via $\alpha_6\beta_1$ integrins, whose expression is upregulated during progression of prostate cancer,[93] leading to increased migratory and invasive phenotypes.[94] For all of the retargeting strategies it is essential, that ligands retain their biological efficacy after chemical coupling, are efficiently presented and accessible for target receptor binding, allow subsequent vector internalization and permit successful dissociation and delivery to the nucleus.[16]

1.7 The ideal adenovirus vector

An ideal vector would combine several characteristics, including increased circulation half life, prevention from scavenging by Kupffer cells and spleenic macrophages, detargeting from hepatocytes (either through genetically FX binding ablation or chemical capsid modification), protection from neutralizing antibodies, infection via disease restrictive receptors, additional safety through target tissue specific expression using e.g. tissue specific promoters or microRNA binding sites, a transgene with bystander effect like the sodium iodide symporter (NIS) [95] to overcome hampered spreading of oncolytic Ad within a solid tumor mass, while maintaining the transduction efficiency of a wild type Ad.

1.8 Aims of the thesis

Adenovirus type 5 vectors (Ads) are the most commonly used vectors in cancer gene therapy. Despite showing high transduction efficiency in many cell types, transduction efficiency of cancer cells is often low due to downregulation and heterogeneous distribution of viral receptors. Therefore methods have to be established to increase the transduction efficiency of these Ad refractory cancer types.

Non-covalent coating has been proven to enhance transduction of hardly transducable cancer cell lines, while highly effective, low toxicity coating agents are still being sought. To avoid infection of off target organs like liver and spleen, strategies have to be established to, not only prevent host-vector interactions and uptake of the adenovirus via its natural ubiquitously expressed receptors, but to target the Ad to cancer specific receptors. Additionally, due to high seroprevalence of neutralizing antibodies to human Ad5, strategies have to be developed to protect the Ad from being inactivated.

The overall aim of the thesis was therefore the in vitro evaluation and optimization of non-covalent coating strategies of adenovirus vectors for their use as gene transfer vehicles to solid tumors, in vivo.

Specific aims:

1) To enable high transduction efficiency in otherwise adenovirus refractory cancer cells, by the use of PAMAM dendrimers for non-covalent charge based coating.
2) To characterize the shielding potency of non-covalent PAMAM dendrimer coating with respect to preexisting immunity.
3) To increase specificity for cancer cells by the use of the peptide ligand GE11, targeting the epidermal growth factor receptor (EGFR).
4) To evaluate the biodistribution of non-covalently coated adenovirus vectors after intravenous injection.
5) To establish a SKOV-3 LucEGFP intraperitoneal mouse model, enabling an alternative application route to intravenous injection, and the ability of a two colored evaluation, using Ad-mCherry.

Overall, this work should demonstrate the feasibility and potential advantages of non-covalent adenovirus capsid modifications for in vivo tumor delivery.

2 MATERIALS AND METHODS

2.1 Chemicals, reagents, polymers and dendrimers

DMSO (Dimethylsulfoxide purissimum), EtOH (absolute ethanol), DTT (DL-Dithiothreitol) and TNBS (2,4,6-Trinitrobenzenesulfonic acid solution) were obtained from Sigma-Aldrich GmbH (Munich, Germany). Water was used as purified, de-ionized water. NHS-PEG-OPSS (ω-2-Pyridyldithio polyethylene glycol α- succinimidylester, 2 kDa) was synthesized by Rapp Polymere GmbH (Tübingen, Germany), peptide GE11 (CYHWYGYTPQNVI-OH, TFA salt, >95% purity) by Biosyntan GmbH (Berlin, Germany), and LPEI (22 kDa) as recently described.[96] Recombinant murine EGF (mEGF) was purchased from Peprotech (Hamburg, Germany). Amine terminated PAMAM dendrimers (generations G2, G3 and G5, DAB core, molecular weight 3,284 Da, 6,937 Da and 28,854 Da, respectively) were purchased from Dendritic Nanotechnologies (Mount Pleasant, MI, 48858, USA), branched PEI (BPEI, 25 kDa) was purchased from Sigma Aldrich and used after gelfiltration (Sephadex G25 superfine, HR 10/30) as a 1 mg/mL stock solution in HBS. HEPES (4-(2-hydroxyethyl)-1-piperazineethanesulfonic acid) was obtained from Biomol GmbH (Hamburg, Germany), H-L-Cysteine from IRIS Biotech GmbH (Marktredwitz, Germany) and MacroPrep High S from BioRad GmbH (Munich, Germany). Dialysis was performed with Spectra/Por membranes (molecular mass cut-off 1, 3.5 or 10 kDa) from Spectrum Laboratories Inc. (Breda, Netherlands). Cell culture 5x lysis buffer and D-luciferin sodium salt were purchased from Promega (Mannheim, Germany). Cell culture media, antibiotics, L-alanine-L-glutamine and non essential amino acids (NEAA) were obtained from Biochrom (Berlin, Germany). Fetal calf serum was purchased from Gibco (Life Technologies, Carlsbad, USA). 1% Phosphotungstic acid solution was obtained from Science Services (Munich, Germany). Carbon coated 200 mesh copper grids were bought from Plano GmbH (Wetzlar, Germany). Human factor X was purchased from Cell Cystems (Troisdorf, Germany). QIAamp DNA mini kit was bought from Qiagen (Hilden, Germany). Brilliant II SYBR Green qPCR Master Mix was purchased from Agilent Technologies (Santa Clara, USA).

2.1.1 Conjugate syntheses

Conjugate syntheses and cyanine 5 labeling were performed by Wolfgang Rödl.

Synthesis of PAMAM-PEG-OPSS

Synthesis of PAMAM G2-PEG-OPSS was carried out in principle as described recently for LPEI-PEG-OPSS [97] with some modifications. In brief, 1.4 µmol of PAMAM G2 (MW = 3284 Da) in EtOH was reacted with 4.2 µmol NHS-PEG-OPSS (2 kDa) dissolved in DMSO for 3 h, under agitation, at 37 °C. Thereafter, 2 M HEPES pH 7.4, 3 M NaCl and water were added to give a final concentration of 20 mM HEPES and 0.6 M NaCl and the pH adjusted to 7.4 using hydrochloric acid. The reaction mixture was loaded on a cation-exchange column (Macro-prep High S; 10/10; BioRad, Munich, Germany) and fractionated with a salt gradient from 0.6 to 3 M NaCl in 20 mM HEPES, pH 7.4. The product eluted between 2 and 2.6 M NaCl and was dialyzed overnight (o.n.), at 4 °C, against HBS (20 mM HEPES pH 7.4, 150 mM NaCl). Dialysis was performed with Spectra/Por membrane (molecular mass cut-off 1, 3.5 or 10 kDa for PAMAM G2, G3 or G5 respectively). The PAMAM G2 content of the conjugate was determined by TNBS assay, which is used for detection of primary amines.[98] Briefly 10 µL TNBS (2,4,6-Trinitrobenzenesulfonic acid) were mixed with 320 µL Borax 0.1 M. Afterwards 1, 2, 4, 6, 8 or 10 µL sample were pipetted into a 96-well plate in duplicate and mixed with 100 µL Borax and 2.5 µL of the prepared TNBS/Borax mixture. After 15 min incubation the absorption of the yellow product was measured at 405 nm using a microplate reader (Tecan, Grödig, Austria) and the amount of PAMAM G2/µL was estimated using a PAMAM G2 standard curve. To ascertain the quantity of linker coupled to the PAMAM G2, the amount of dithiopyridine (PDP) after reduction of an aliquot with dithiothreitol (DTT) was evaluated by spectrophotometric measurement of released pyridine-2-thione (ε_{343} = 8080 M^{-1} x mol^{-1}).[99] This resulted in a molar ratio of PAMAM G2/PDP of 1/0.6. PAMAM G3-PEG-OPSS and PAMAM G5-PEG-OPSS were synthesized with a molar ratio of 1/0.63 for PAMAM G3/PDP and 1/1.1 for PAMAM G5/PDP respectively. For the covalent coupling of PAMAM-PEG-OPSS to the Ad-Cys, new charges for all three generations were synthesized, with the help of Wolfgang Rödl, exhibiting a PEG-OPSS/PAMAM ratio of 1/1.1 for PAMAM G2, 1/0.94 for PAMAM G3 and 1/0.89 for PAMAM G5.

Synthesis of PAMAM-PEG-GE11

For PAMAM G2-PEG-GE11 synthesis, 1.98 µmol GE11 in 75 µL 30% acetonitrile, 70% H_2O and 0.1% TFA (trifluoroacetic acid) and 0.79 µmol PAMAM G2-PEG-OPSS in 3.6 mL HBS were mixed and incubated at ambient temperature. The reaction was considered to be finished once all pyridine-2-thione was released. The release was controlled during the reaction at 343 nm and recalculated relative to the used PDP. Purification and analysis was carried out, as described above, with the difference of using a salt gradient from 0.6 to 3 M NaCl in 20 mM HEPES including 10% acetonitrile, pH 7.4. The amount of GE11 was calculated via the extinction coefficient at 280 nm (ε=9970 M^{-1} x mol^{-1}). PAMAM G3-PEG-GE11 and PAMAM G5-PEG-GE11 were synthesized accordingly. The molar ratio of PAMAM G2, PAMAM G3 and PAMAM G5 to GE11 was 1/0.75, 1/0.5 and 1/0.47 respectively.

Synthesis of PAMAM-PEG-Cys

PAMAM G2-PEG-Cys was synthesized by mixing one part of PAMAM G2-PEG-OPSS with four parts of cysteine at ambient temperature. Purification was carried out on a gel-filtration column (Sephadex G-25; HR10/30 column; 20 mM HEPES, pH 7.4) to remove pyridine-2-thione and unreacted cysteine. PAMAM G3-PEG-Cys and PAMAM G5-PEG-Cys were synthesized respectively.

Cyanine 5 labeling

Cyanine 5 (Cy5) labeling of PAMAM G5 was performed with amine-reactive FluroLink Cy5 monofunctional dye (GE Health Care, Life Sciences, Freiburg, Germany) in principle as described.[100] In brief, 2 mg PAMAM G5 in 1 mL HBS was mixed with 69 nmol Cy5 dissolved in 40 µL water free DMSO. After 2 h at ambient temperature the sample was purified by gel filtration to remove unreacted dye. The molar ratio of PAMAM G5/Cy5 was 1/0.3.

2.2 Antibodies

Goat anti-human IgG-peroxidase antibody was bought from Sigma-Aldrich (St. Louis, USA). Mouse anti-human CAR antibody (clone RmcB) was obtained from Millipore (Schwalbach, Germany). Mouse anti-human transferrin receptor, mouse anti-human epidermal growth factor receptor (clone H11) and mouse IgG control antibody were purchased from Dako (Copenhagen, Denmark). Mouse anti-human CD51/61 ($\alpha_v\beta_3$ integrin)

was purchased from Biolegend (San Diego, USA). Goat anti-human Alexa 488 and goat anti-human Alexa 647 antibody were obtained from Invitrogen (Eugene, USA). Privigen®, human anti-Ad IgG was bought from CSL Behring (Marburg, Germany).

2.3 Adenovirus vectors

Ad-Luc [$1x10^{10}$ viral particles per microliter (VP/µL)], $5x10^{8}$ plaque-forming units per microliter (PFU/µL) was purchased from Vector Biolabs (Philadelphia, PA 19104, USA) and amplified in HEK 293 cells in the lab of Per Holm. The virus was purified by two consecutive, continuous cesium chloride (CsCl) gradient centrifugations and desalted by size-exclusion chromatography (Disposable PD-10 desalting columns, GE Healthcare, Munich, Germany). Viral titer was determined by AdEasy™ Viral Titer Kit (Stratagene, Waldbronn, Germany) and viral particle number by absorption measurement at 260 nm. Ad-Alexa Fluor488 (Ad-Alexa488, $1x10^{8}$ VP/µL, $5x10^{6}$ PFU/µL), enhanced green fluorescent protein encoding Ad (Ad-EGFP, $5x10^{8}$ VP/µL, $1x10^{8}$ PFU/µL), enhanced green fluorescent and luciferase fusion protein encoding Ad (Ad-EGFPLuc, $1x10^{9}$ VP/µL, $6x10^{7}$ PFU/µL) and mCherry encoding Ad (Ad-mCherry, $1x10^{9}$ VP/µL, $5x10^{8}$ PFU/µL) are Ad5-based E1-deleted first-generation vectors. All were amplified in the E1-transcomplementing N52E6 cell line in the lab of Florian Kreppel.[101] The Ad-EGFP and Ad-EGFPLuc carry a hCMV-promoter controlled EGFP or EGFPLuc expression cassette respectively, whereas the Ad-mCherry carries an EF1α-promotor controlled mCherry expression cassette. Vectors were purified by one CsCl density step gradient followed by one subsequent continuous CsCl density gradient and were desalted by PD-10 size exclusion columns (GE Healthcare). The titers for infectious and physical particles were determined by a DNA-based slot blot assay [102] and the physical particle titer was confirmed by measuring the optical density at 260 nm. Ad-CMV-hNIS [103] (Ad-NIS) ($1.1x10^{9}$ VP/µL, $5x10^{7}$ PFU/µL) was prepared by Richard D. Anderson from ViraQuest Inc. (North Liberty, USA).

Alexa 488 labeling

For random labeling, $5x10^{11}$ AdEmpty (no transgene) vector particles were incubated with a 20-fold excess of amine reactive Alexa Fluor488-5TFP (Invitrogen, Darmstadt, Germany) over the 18,000 amino groups present at the capsid surface. After incubating over night, at ambient temperature, the reaction mixture was made up to a final volume of 2.5 mL with PBS. The labeled vector particles were then purified from excess dye by PD10 column purification (GE Healthcare).

2.4 Coating of Ad with PAMAM dendrimers or LPEI and BPEI polymers

The complexes of Ad and PAMAM generation 2, 3, 5, LPEI or BPEI were formed (unless otherwise stated) by separately diluting the indicated amounts of Ad in Opti-MEM® (Invitrogen, Darmstadt, Germany) and polycation in HEPES buffered Glucose (HBG; 20mM HEPES, 5% glucose, pH 7.4). Viral particles were added to the polycation solution, immediately gently mixed with a pipette and allowed to incubate for 30 min at ambient temperature (20 -25 °C) before further use.

2.5 Biophysical Characterization

2.5.1 Transmission electron microscopy (TEM)

Sample preparation was performed similar to the method shown by Chen et al. [104] with some modifications. A 20 µL drop containing either $1x10^{10}$ VP of Ad-Luc in water or Ad complexed with 455 ng PAMAM G5 in PBS, which equals 950 molecules per adenovirus, was put on a sheet of parafilm. A plasma cleaned carbon coated 200 mesh copper grid (Plano GmbH, Wetzlar, Germany) was placed on top of the drop (filmed side down) for 5 min and excess liquid was blotted off using filter paper. Subsequently the grid was incubated with 20 µL of a 1% phosphotungstic acid solution (PTA) (Science Services, Munich, Germany) for 3 min and drained as before. All solvents were filtered with a 0.02 µm spin column filter (Whatman, Dassel, Germany) before use. Air dried grids were analyzed within 48 h by Kulpreet Virdi using a JEOL 2011 TEM (JEOL Ltd. Tokyo, Japan) fitted with a lanthanum hexaboride thermal emitter and operating at an accelerating voltage of 200 kV and at low dose.

2.5.2 Zeta potential and particle size measurement

Ad-Luc ($5x10^{10}$ VP/mL in PBS/HBG, pH 7.4) and Ad/PAMAM G5 complexes (formed as described in 2.4, but with Ad diluted in PBS instead of Opti-MEM® to reduce background signal) were analyzed on a Zetasizer Nano ZS (Malvern Instruments, Malvern Hills, UK) at 25 °C in triplicates for measurement of the zeta potential. Size measurement of Ad-EGFP, Ad-NIS and Ad-Luc only or coated with PAMAM G5 was performed by photon correlation spectroscopy (PCS). Measurements were conducted on a Coulter N4 Plus (Beckman Coulter, Brea, USA) with 90° angle PSC analysis using $2x10^{11}$ VP or $1x10^{11}$ VP respectively in a total volume of 2 mL PBS/HBG mixture.

2.5.3 Gel electrophoresis and silver staining

To analyze the purity of different Ad preparations gel electrophoresis followed by silver staining was performed. $5x10^9$ VP of Ad-EGFP, Ad-NIS and Ad-Luc were mixed with 2x loading buffer (0.2% bromophenol blue, 200 mM DTT, 20% glycerine, 4% SDS, 100 mM Tris HCl, pH 6.8) and denatured for 2 min at 96 °C. Gel electrophoresis was performed at 120 V for 1.5 h using a 3.5% stacking and a 10% resolving gel. The gel was fixed with a fixative solution (50% methanol, 12% acetic acid, 0.5mL/L 37% formaldehyde solution) o.n. at 4 °C. After pretreatment with sodium thiosulfate solution (127 mg/L) for 1 min, the gel was incubated with a silver nitrate solution (silver nitrate 2 g/L, 0.5 mL/L 37% formaldehyde solution) for 20 min. Formaldehyde containing developer solution (0.5 mL/L 37% formaldehyde, 60 g/L sodium carbonate, 2.5 mg/L sodium thiosulfate) was used to reduce silver ions to metallic silver and the reaction was stopped by addition of 12% acetic acid in 50% methanol for 5 min.

2.6 Biological characterization

2.6.1 Cell culture

Human cancer cell lines were maintained as follows. HuH7 hepatoma cells (JCRB0403; Japanese Cancer Research Resources Bank, Tokyo, Japan) were cultivated in Ham's F12/DMEM (1:1), SKOV-3 ovarian carcinoma cells (HTB-77; American Type Culture Collection [ATCC], Manassas, VA), SKOV-3 LucEGFP stably transfected cells (kindly provided by Izumi Ohno, laboratory of Nori Kasahara) HepG2 hepatoma cells (HB-8065, ATCC) and DU145 prostate carcinoma cells (ACC 261; German Collection of Microorganisms and Cell Culture [DSMZ], Braunschweig, Germany) in RPMI 1640, A549 lung carcinoma cells (CCL-185, ATCC) and U87MG glioblastoma cells (HTB-14, ATCC) in DMEM. All cell culture media were supplemented with 10% fetal bovine serum, 100 units/mL penicillin, 100 µg/mL streptomycin and 1% L-Alanine-L-Glutamine (200 mM). Medium for U87MG cells was additionally supplemented with 1% NEAA (non-essential amino acids) and cell culture flasks where coated with 0.1 mg/mL Collagen A before use. All cells were passaged twice a week and cultured at 37 °C in 5% CO_2.

2.6.2 Receptor level estimation

Cells, $6x10^5$ in 100 µL FACS buffer (10% FCS in PBS), were incubated with either mouse anti-CAR, mouse anti-EGFR, mouse anti-TfR, mouse anti-CD51/61 (1:200 dilution) or mouse IgG control antibody (1:100 dilution) for 1.5 h on ice and then washed twice with FACS buffer. Thereafter cell were stained with Alexa-488-labeled goat anti-mouse

(1:400 dilution) or Alexa-647-labeled goat anti-mouse (1:200 dilution) secondary antibody for 1 h on ice, washed, counterstained with DAPI (1 µg/mL) and analyzed on a Cyan ADP flow cytometer (Dako, Glostrup, Denmark). DAPI fluorescence was excited at 405 nm and detected with a 450/50 bandpass filter, Alexa-488 fluorescence was excited at 488 nm and detected with a 530/40 nm bandpass and Alexa-647 fluorescence was excited at 635 nm and emission was detected with a 665/20 nm bandpass filter. $4x10^4$ events (living cells) were collected per sample, using forward scatter (FS) versus sideward scatter (SS) to exclude cell debris and apoptotic cells, FS versus pulse width to exclude duplets and FS versus violet one channel to exclude necrotic cells. The percentage of CAR and EGFR positive cells was determined compared to control IgG stained cells. The mean fluorescence intensity (MFI) corresponds to the arithmetic mean of the living cell population.

2.6.3 Cellular uptake and co-localization studies

For flow cytometry analyses, $5x10^4$ cells were seeded in 24-well plates 24 h prior to transduction. On the day of transduction cells were 70-80% confluent. Medium was removed and 250 µL of Opti-MEM® containing Ad-Alexa488 only (10,000 VP/cell, MOI 500) or complexed with various amounts of PAMAM G5-Cy5 dendrimer were incubated with cells for 2 h, at 37 °C, and in 5% CO_2. Thereafter the cells were washed twice with PBS, harvested with Trypsin/EDTA, fixed with 2% paraformaldehyde (PFA) for 30 min at ambient temperature and analyzed by flow cytometry as described above using a FACS Canto II flow cytometer (Becton, Dickinson, Germany) (Alexa 488: excitation at 488 nm, emission at 530/30 bandpass, Cy5: excitation at 633 nm, emission at 660/20 bandpass). For laser scanning microscopy (LSM) studies, $2x10^4$ cells were seeded in Collagen A (0.1 mg/mL) coated Labtek™ chamber slides, 24 h prior to transduction. PAMAM or LPEI coated Ad was incubated with cells for 2 h at 37 °C, thereafter cells were washed three times with PBS and fixed with 4% PFA for 30 min. Nuclei were stained using DAPI (1 µg/mL). Samples were analyzed with a confocal laser scanning microscope (LSM 510 META; Carl Zeiss, Jena, Germany) equipped with an argon laser emitting ultraviolet light at 364 nm, a second argon laser emitting light at 488 nm and two helium/neon lasers delivering light at 543 nm and 633 nm. A 63x oil immersion objective (Carl Zeiss) was used and data acquisition done in multitrack mode (DAPI: excitation at 364 nm, emission at 385-470 nm bandpass, Alexa 488: excitation at 488 nm, emission at 505-530 nm bandpass, Cy5: excitation at 633 nm, emission at 650 nm longpass). The data was analyzed with AxioVision 4.6 software (Carl Zeiss).

2.6.4 Transduction studies

Cells were seeded at a density of $1x10^4$ cells/well in 96-well plates 24 h prior to transduction and were 70-80% confluent on the day of transduction. The medium was removed and 60 µL of serum free Opti-MEM® (or up to 100% FCS in DMEM for stability studies) containing Ad-Luc or Ad-EGFPLuc (MOI 100) alone or complexed with various amounts of dendrimer or polymer were incubated with cells for 2 h (or 45 min for EGFR-targeting experiments) at 37 °C. To show the specificity of PAMAM G2-PEG-GE11, cells were pre-incubated with 10 µg/well mEGF for 45 min at 37 °C. DNA/PAMAM polyplexes were also formed within 30 min at RT and incubated with cells for 2 h at 37 °C accordingly. The infection solution was replaced by fresh serum-containing medium and after 48 h cells were lysed using 5x cell lysis buffer in a 1:10 dilution. Luciferase activity of a 35 µl aliquot was quantified on a Centro LB 960 luminometer (Berthold Technologies, Bad Wildbad, Germany).[74] Two nanograms of recombinant luciferase correspond to $1x10^7$ relative light units (RLU).

2.6.5 Cell viability assay (MTT)

The influence on cell metabolism of the Ad/PAMAM, Ad/LPEI and Ad/BPEI complexes was evaluated using a MTT colorimetric assay. 10 µL of MTT [3-(4,5-dimethylthiazol-2-yl)-2,5-diphenyltetrazolium bromide, 5mg/mL] were added to the cells, 48 h after transduction and incubated for 2 h at 37 °C. Thereafter the supernatant was removed and the plate kept at -80°C for 30 min. The purple formazan crystals were dissolved in 100 µL/well dimethyl sulfoxide (DMSO). Absorbance was measured at 590 nm with background correction at 630 nm using a microplate reader (Tecan, Grödig, Austria). The relative cell viability (in %) was calculated by [A] sample /[A] control x 100.

2.6.6 Neutralization assay

A549 cells were seeded at a density of $5x10^4$ cells/well in 24-well plates 24 h prior to transduction. On the day of transduction cells were 70-80% confluent. Complexes of Ad-EGFP and dendrimer were pre-formed at ambient temperature for 30 min. Thereafter, 50 µL Ad or Ad/PAMAM G5 containing $2.5x10^7$ VP were mixed with 10 µL diluted human IgG containing anti-Ad antibodies (Privigen®, CSL Behring, Marburg, Germany) and incubated for a further 30 min; the final IgG concentration was in the range of 0.08-3.3 mg/mL. Cells were transduced with a MOI of 100, under serum free conditions, in a total volume of 250 µL in Opti-MEM®. After incubating for 2 h, 1 mL fresh serum-containing

medium was added and the medium replaced after 24 h. After 48 h, the cells were analyzed for EGFP expression by flow cytometry collecting $2x10^4$ gated events per sample.

2.6.7 ELISA

For the indirect ELISA, $6x10^{10}$ viral particles (VP) were heat-inactivated for 10 min at 60 °C. A volume of 50 µL/well containing $6x10^8$ of these VP in coating buffer (0.2M Na_2CO_3/$NaHCO_3$ pH 9.5) were added to a 96-well maxisorb flat bottom plate (Nunc, Thermo Scientific Fisher, Schwerte, Germany) and incubated o.n. at 4 °C with gently agitation. The coated wells were then blocked with 3% BSA in PBS for 1 h at RT. Human IgG (Privigen®, 100 mg/mL) was diluted gradually 1:2 starting from a 1:250 dilution. In order to prove that there was no interaction between PAMAM and anti-Ad IgG, the Privigen® dilutions were pre-incubated with 100 ng PAMAM dendrimer or HBG, as control, for 30 min, before application to the immobilized Ad, for 2 h at RT. A 1:2000 dilution of a peroxidise anti-human IgG antibody was added for 1 h at RT before the addition of o-phenylendiamine dihydrochloride containing substrate solution, pH 5, for 5 min. The colour reaction was stopped by adding 1M H_2SO_4 and the absorbance measured at 485 nm with background correction at 630 nm, using a microplate reader.

2.6.8 Factor X binding assay

SKOV-3 cells were seeded at a density of $2x10^4$ cells/well in 96-well plates 24 h prior to transduction. On the day of transduction cells had reached 70-80% of confluency. Cells were washed once with PBS and additive-free medium or medium containing factor X at a physiological concentration (8 µg/mL) was applied. Naked Ad versus Ad/PAMAM was added at a particle MOI (pMOI) of 1000 and incubated with cells for 3 h at 37 °C. After transduction, cells were washed once with PBS before adding fresh growth medium supplemented with 10% FCS, 1% stable glutamine and 1% penicillin/streptomycin. After 72 h the cells were analyzed for EGFP expression using FACS with $2x10^4$ gated events per sample.

2.6.9 Targeting studies

For targeting studies $5x10^4$ cells were seeded in 24-well plates 24 h prior to transduction and were transduced with Ad-EGFP alone or coated with PAMAM G2-PEG-GE11 or PAMAM G2-PEG-Cys at a MOI of 100 under serum-free conditions in a total volume of 250 µL. After 45 min incubation at 37 °C the solution was replaced by 1 mL fresh serum-containing medium. After 48 h, cells where harvested and $2x10^4$ gated cells were analyzed for EGFP expression using flow cytometry.

For LSM imaging $2x10^4$ cells, seeded in Collagen A-coated chamber slides, were treated accordingly and after 48 h fixed with 4% PFA for 30 min before evaluation by laser scanning microscopy, as described earlier.

2.7 In vivo experiments on biodistribution

For studies on biodistribution of Ad versus Ad/PAMAM G5 female BALB/cAnNCrl (BALB/c) mice were used. Mice were obtained from Charles River (Sulzfeld, Germany) and maintained in pathogen-free, individually ventilated cages (Tecniplast, Hohenpeissenberg, Germany) in the animal facility of PD Dr. Florian Kreppel and Prof. Dr. Stefan Kochanek at the University of Ulm. Mice were fed with sterilized diet for laboratory rodents (Ssniff, Soest, Germany) and experiments started, when mice were 6-8 weeks old. Animal experiments were approved by the Animal Care Commission of the Government of Baden-Württemberg and were in accordance with institutional guidelines.

$3x10^{10}$ VP of an EGFP encoding Ad, with or without PAMAM coating (250 ng or 1500 ng), were injected intravenously by Matthias Kron into the tail vein of mice in a total volume of 200 µL PBS/HBG 1:1 mixture. For comparative studies, two different mouse strains, female BALB/cAnCrl and CD1 nu/nu mice were selected, obtained from Charles River (Sulzfeld, Germany) and maintained under specific pathogen-free conditions in individually ventilated cages at the animal facility of the Klinikum rechts der Isar (Munich, Germany). Mice had access to sterilized diet for laboratory rodents and water, ad libitum. Experiments started, when mice were 5-7 weeks old. Then $2.2x10^{10}$ VP of an EGFP encoding Ad, with or without PAMAM coating (300 ng), was injected intravenously, by Geoffrey Grünwald, into the tail vein of mice, in a total volume of 200 µL Opti-MEM/HBG 1:1 mixture. The experimental protocol was in accordance with institutional guidelines and approved by the regional governmental commission for animals (Regierung von Oberbayern, Munich, Germany). 72 h after injection, mice were sacrificed by an overdose of isoflurane (Abott, Ludwigshafen, Germany) inhalation and the liver (after

perfusion with PBS), lung, kidney and spleen were taken out. One piece of each organ was fixed for 24 h in 2% PFA followed by 24 h in 30% sucrose and embedding in Tissue-Tek® for histological sections; one piece was snap-frozen in liquid nitrogen and stored at -80°C for DNA isolation and in the case of the liver a second piece was snap-frozen and used for homogenization.

2.7.1 Fluorometry of liver homogenates

After PBS perfusion and snap freezing in liquid nitrogen, 0.5 g of each mouse liver was homogenized in a conical tissue grinder (Wheaton, Millville, NJ) using 1 ml RIPA buffer [50 mM Tris, 1% NP-40, 0.25% sodium desoxycholate, 150 mM NaCl, 1 mM EDTA, 1 mM phenylmethylsulfonyl fluoride (PMSF), ad 1 L with demineralized water, pH 7.4] and incubated for 10 min at RT. After centrifugation at 20,000 *g* for 10 min at 4 °C, 500 µL of the clear supernatant fraction were transferred into a new 1.5 mL reaction tube. Centrifugation was repeated, as described above, and 200 µL of the clear supernatant fraction was removed and diluted 1:500 in RIPA buffer before measurement of the EGFP fluorescence at 488 nm excitation and 512 nm emission wavelength with a LS50B spectrometer (Perkin Elmer, Waltham, USA) and the Spex dM300 software version 3.32e (SPEX instruments SA. Inc, NJ, USA).

2.7.2 Cryosections

A piece of liver, lung, spleen and kidney was fixed o.n. in 2% PFA, followed by an o.n. incubation in 30% sucrose before embedding in Tissue-Tek® (Sakura, Zoeterwoude, Netherlands) and storing at -80 °C. 6 µm sections were cut using a Leica CM3050S-cryostat (Leica Biosystems, Wetzlar, Germany). Sections were put on microscope slides, covered with fluorescent mounting medium (Dako, Copenhagen, Denmark) and analyzed with a confocal laser scanning microscope (LSM 510 META; Carl Zeiss, Jena, Germany).

2.7.3 Quantitative real time PCR (qPCR)

DNA isolation from mice tissue was undertaken using the QIAamp DNA mini kit (Qiagen) according to the manufacturer's protocol. Additionally an ethanol precipitation was performed to increase purity of the samples. QPCR was carried out by amplification of the Ad E4 gene with a Stratagene 3005P qPCR machine and the MxPro MX3005P v4.01 software using 2x Brilliant II SYBR® Green qPCR Master Mix and the following primers: E4 sense (5`-TAGACGATCCCTACTGTACG-3′), E4 anti-sense (5`-

GGAAATATGACTACGTCCGG-3′), as well as murine β-actin-sense (5′-CAAGGAGTGCAAGAACACAG-3′) and murine β-actin-antisense (5′-GCCTTGGAGTGTGTATTGAG-3′) for later normalization for cellular DNA content. Forty cycles with the following thermal protocol were performed: melting (95 °C, 30 sec) annealing (60 °C, 30 sec) and elongation (72 °C, 20 sec). Samples were run in duplicate and the averaged C_T values for the E4 adenoviral gene were normalized against the β-actin C_T values of the same sample. On every plate β-actin standard ranging from $1x10^0$ to $1x10^5$ copies and an E4 standard ranging from $1x10^{-1}$ to $1x10^4$ copies was run in parallel. Copy numbers of Ad/cell were calculated using the E4 standard equation.

2.8 Establishment of a SKOV-3 intraperitoneal cancer mouse model

2.8.1 In vitro characterization of SKOV-3 LucEGFP cells

2.8.1.1 Quantification of the luciferase and EGFP expression level

To quantify the luciferase expression level of SKOV-3 LucEGFP cells, 2,000, 5,000 and 10,000 cells/well (n=6) were seeded in a 96-well plate. After 24 h the cells were lysed and a luciferase assay was performed, as described earlier. The EGFP expression level was analyzed by FACS for mean fluorescence intensity (MFI) in the FITC channel as well as percentage of EGFP positive cells performing diagonal gating of FITC versus PE-Texas Red. A549 cells were used as control for laser adjustment.

2.8.1.2 Receptor level estimation

Receptor level estimation was performed as described in 2.6.2, using an Alexa 647 labeled secondary antibody (1:200 dilution).

2.8.2 Establishment of a dual color system

2.8.2.1 Cloning of Ad-mCherry

For cloning of the mCherry construct, 1 µg of pCpG-hCMV EF1α-TNF and pCpG-hCMV SCEP-mCherry, cloned by Rudolf Haase, were digested for 2 h at 37 °C using 0.3 µL HindIII and SpeI-HF enzyme [New England Biolabs GmbH (NEB), Frankfurt am Main, Germany] in a final volume of 20 µL. Digestion products were separated on a 2% agarose gel at 80-100 mV and gel extraction performed according to the QIAquick gel extraction kit (Qiagen, Hilden, Germany). Ligation of the EF1α-promotor with the mCherry containing backbone was performed in a molar ratio of 1:3 (vector: insert) with 0.5 µL T4

DNA ligase (NEB) in a volume of 10 µL for 1 h at 30 °C. Transformation via heat shock at 42 °C for 1 min and 45 sec, with pre and post incubation on ice for 2 min, was performed with DB 3.1 chemo competent cells prepared by Ursula Biebl. Afterwards 1 mL of LB medium was added and the bacteria were incubated at 37 °C for 1.5 h under continuous agitation (350 rpm). Afterwards the bacteria were centrifuged for 6 min at 6000 rpm. Bacterial pellet was resuspended in 100 µL LB, spread on Zeocin (25 µg/mL) (Roche, Mannheim, Germany) or Ampicillin (100 µg/mL) plates (1.5% agar in LB medium) and incubated at 37 °C o.n. for clonal selection. Plasmid preparation was carried out using a QIAprep Spin Miniprep Kit (Qiagen) according to the manufacturer's instructions. To verify the insertion of the EF1α promoter, the plasmid was cut with the restriction enzymes SmlI and NheI. The pCpG-hCMV EF1α-mCherry construct was additionally verified by sequencing, employing GATC Biotech (Constance, Germany). In the final step, performed by Sandra Behmüller, the pCpG-hCMV EF1α-mCherry was digested with PacI (NEB) o.n as was the pGs66 [101] backbone. Separation was performed using a 1% agarose gel at 100-120 mV. Bands were cut out using a dark reader and equivalent goggles. After phenol extraction and precipitation with isopropanol and ethanol, ligation was performed o.n. at RT. Therefore vector and insert were separately heated up to 42 °C for 20 min, before pipetting the ligation mix on ice. Transformation was performed by electroporation using XL2-blue ultracompetent cells (Stratagene, La Jolla, USA).

2.8.2.2 Transduction of SKOV-3 LucEGFP using Ad-mCherry

For LSM and FACS analysis $2.5x10^4$ SKOV-3 LucEGFP were seeded in 24-well plates and transduced with Ad (MOI 125) only or coated with PAMAM generation 2, 3, 5 or the respective targeting and control constructs PAMAM-PEG-GE11 and PAMAM-PEG-Cys of each generation for 2 h at 37 °C. FACS analysis was carried out with an excitation at 488 nm for EGFP and mCherry, while use of different filters (530/40 nm for EGFP; 680/30 nm for mCherry) allowed for separate detection of the two fluorophores. $2x10^4$ gated cells were analyzed. LSM was performed using a 488 nm argon laser for excitation of EGFP and a 543 nm helium-neon laser for excitation of mCherry, while using a 505-530 nm band pass and 560 nm long pass filter respectively for detection.

2.8.3 In vivo characterization of SKOV-3 LucEGFP cells

2.8.3.1 Luciferase imaging

Luciferase imaging of Rj:NMRI-nu (nu/nu) mice (Janvier, Le Genest-St-Isle, France) carrying intraperitoneally (i.p.) implanted SKOV-3 LucEGFP tumors was performed twice a week using an IVIS Lumina imaging system and the Living Image software 3.2 (Caliper Life Sciences, Hopkinton, USA). Mice were anesthetized with 3% isoflurane in oxygen, 100 µL luciferin solution (c=60 mg/mL, in PBS) (Promega, Fitchburg, USA) was injected i.p. and light efflux recorded after 10 min, with an acquisition time of 2 sec. For quantification of the bioluminescent signal, a region of interest (ROI) was adjusted to the abdominal cavity and the signal measured as emitted photons/sec.

2.8.3.2 Hematoxylin and eosin staining

Organs were fixed with 4% PFA, embedded in paraffin, cut in 5 µm sections and mounted on microscopic slides. Hematoxylin and eosin staining of liver, spleen, stomach and small intestine was performed by Alke Schropp according to a standard protocol. Briefly, slides were immersed in xylene for 15 min, twice, followed by absolute EtOH, 96% EtOH and 70% EtOH for 5 min each. After a brief rinse in distilled water, slides were stained with hematoxylin (Merck, Darmstadt, Germany) for 5-30 sec, rinsed with tap water for 10 min and stained with eosin (Chroma, Münster, Germany) for 10 min. Thereafter slides were rinsed with tap water for 3 min and immersed in 70% EtOH and 96% EtOH for 3 min and absolute EtOH for 5 min. Before embedding in Eukitt® (O. Kindler GmbH & Co, Freiburg, Germany), slides were immersed in xylene for 10 min, twice. Images of H/E staining were taken with an Olympus BX41 microscope using an Olympus DP25 U-TV1X-2 camera and the Olympus cellSensEntry 1.5 software (Olympus, Hamburg, Germany) in the group of Prof. Dr. Angelika Vollmar.

2.9 Statistical analysis

Results are presented as mean ± standard deviation. Statistical significance was evaluated by an unpaired two tailed t-test using Graph Pad Prism 6.0. P-values < 0.05 were considered significant.

3 RESULTS

3.1 Biophysical characterization of Ad and Ad/PAMAM complexes

For the in vitro evaluation and optimization of non-covalent coating strategies of Ad vectors using PAMAM dendrimers, complexes were first characterized biophysically, starting with transmission electron microscopy (TEM) studies.

3.1.1 Coating efficiency shown by transmission electron microscopy

The structure of uncoated Ad (Ad-Luc) and Ad/PAMAM G5 complexes was analyzed by transmission electron microscopy (TEM) using phosphotungstic acid (PTA) stained samples (Figure 7). Uncoated Ad capsids displayed the characteristic hexon structure as well as the icosahedral shape of the adenoviral particle. In contrast, when coated with 455 ng PAMAM G5 (equals 950 molecules/Ad) capsids revealed a rough surface structure, indicating complete coating of the Ad particles. In general, single coated particles were observed, but also smaller numbers of dimers or moderate numbers of aggregates, similar to uncoated Ad, occurred.

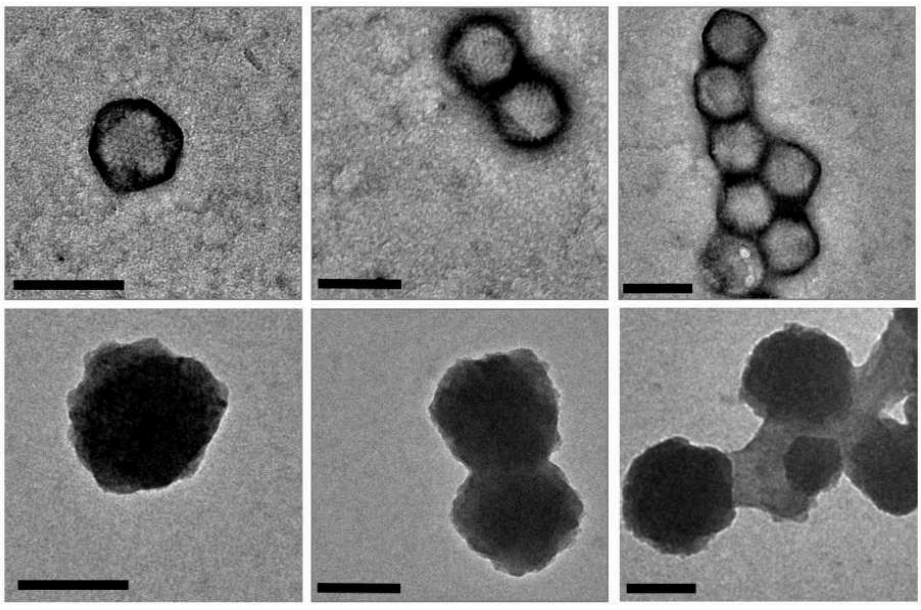

Figure 7. TEM images of uncoated versus PAMAM G5 coated Ad
(A) Transmission electron micrographs of PTA stained Ad (top row) and Ad/PAMAM G5 complexes (bottom row); magnification: A and D 40,000x, B and E 30,000x, C and F 25,000x; scale bars: 100 nm. Representative images are shown.

To identify the amount of PAMAM, that is needed to show complete coating in TEM images, also 100 ng (equals 208 molecules/Ad) and 10 ng (equals 21 molecules/Ad) were tested (Figure 8). While coating with 100 ng PAMAM G5 still led to fully coated Ad/PAMAM particles, coating with 10 ng produced around 50% of uncoated complexes.

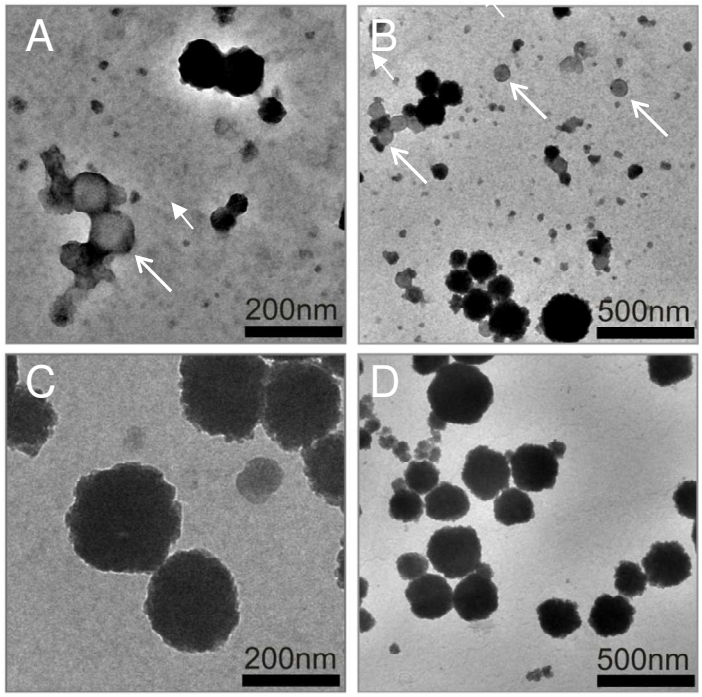

Figure 8. TEM images of 10 ng versus 100 ng PAMAM G5 coated Ad
(A) Transmission electron micrographs of PTA stained Ad/PAMAM G5 10 ng (top row) and Ad/PAMAM G5 100 ng (bottom row); magnification: A and C 15,000x, B and D 6,000x. White arrows depict examples of uncoated Ad. Representative images are shown.

3.1.2 Zeta potential measurement

For measuring the surface charge, $5x10^{10}$ viral particles (VP) in PBS were coated with indicated amounts of PAMAM G5 diluted in HBG. Uncoated Ad exhibited a negative surface charge with a zeta potential corresponding to -17.4 ± 1.6 mV. In sharp contrast, a zeta potential corresponding to +3.4 ± 0.7 mV was measured, when Ad was coated by 20 µg PAMAM G5 (Figure 9).

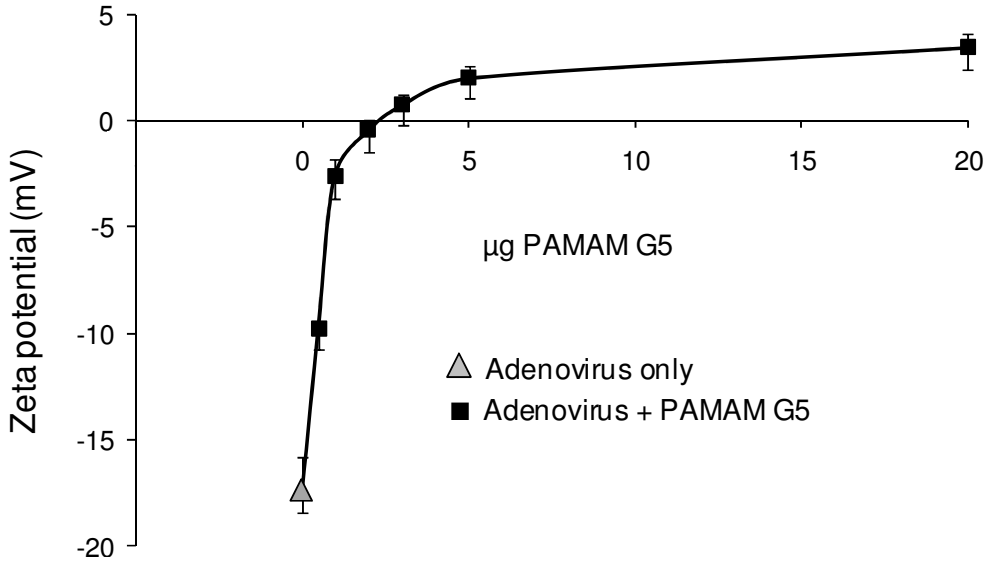

Figure 9. Zeta potential measurement of uncoated versus PAMAM G5 coated Ad

Zeta potential of Ad versus Ad/PAMAM G5 complexes was measured by laser doppler micro-electrophoresis using a Zetasizer Nano ZS and $5x10^{10}$ VP in 1 mL solvent plus the indicated amounts of PAMAM G5 dendrimer. Triple measurements of one sample ± variation of the median are shown.

3.1.3 Size measurement

For measurement of the size of the uncoated Ad compared to the Ad/PAMAM G5 complexes two experiments were taken into account. Representative images gained by TEM were analyzed with the Gatan Digital Micrograph software (Figure 10). Capsid diameters of 70-83 nm were measured for uncoated Ad (A, B) and 143-160 nm for PAMAM G5 coated Ad (C, D) revealing a doubling in size after coating with 455 ng PAMAM G5 (equals 950 molecules/Ad).

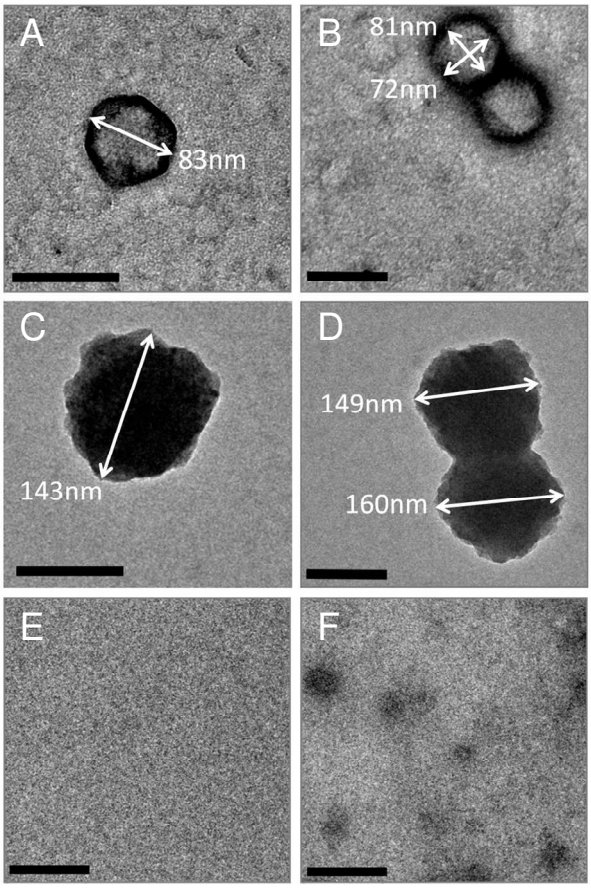

Figure 10. Size of Ad and PAMAM G5 coated Ad measured by TEM

(A-F) Electron micrographs of PTA stained Ad (A, B) and Ad/PAMAM G5 complexes (C, D) were analyzed with Gatan Digital Micrograph software (Gatan Inc., Pleasanton, California). Background staining is displayed for water alone (E) and PAMAM G5 dendrimer in PBS (F). magnification: A and C 40,000x, B, D, E and F 30,000x; scale bars: 100 nm. Representative images are shown.

Additionally, size measurement by dynamic light scattering (DLS), using a Beckman–Coulter N4Plus, was performed (Figure 11B). DSL measures the Brownian motion relative to the hydrodynamic diameter of the particles. The smaller the particles the higher the Brownian motion, measured by a higher fluctuation rate of the intensity of the scattered light. $2x10^{11}$ VP Ad-EGFP, Ad-NIS or Ad-Luc were prepared in 2 mL PBS. After the sizes of the VP were measured, samples were separated into two parts and mixed with PAMAM G5 (958 ng and 4791 ng) diluted in HBG, referring to 200 and 1000 molecules PAMAM G5/Ad respectively. For the Ad-EGFP from the lab of Florian Kreppel a high sample uniformity with a poly dispersity index (PDI) of only 0.04 and a size of 118 ± 28 nm could be found. For the Ad-NIS a PDI of 0.07 and a size of 115 ± 37 nm were measured and for the Ad-Luc a PDI of 0.44 and a size of 145 ± 63 nm was found. Whereas the Ad-EGFP revealed a homogeneous size distribution after coating, in all 3 rounds of measurement,

Ad-NIS as well as Ad-Luc showed several peaks after coating with 200 PAMAM G5 molecules/Ad and a broader size distribution, when coated with 1000 PAMAM G5 molecules/Ad as illustrated in the intensity profiles depicted in figure 11A.

A

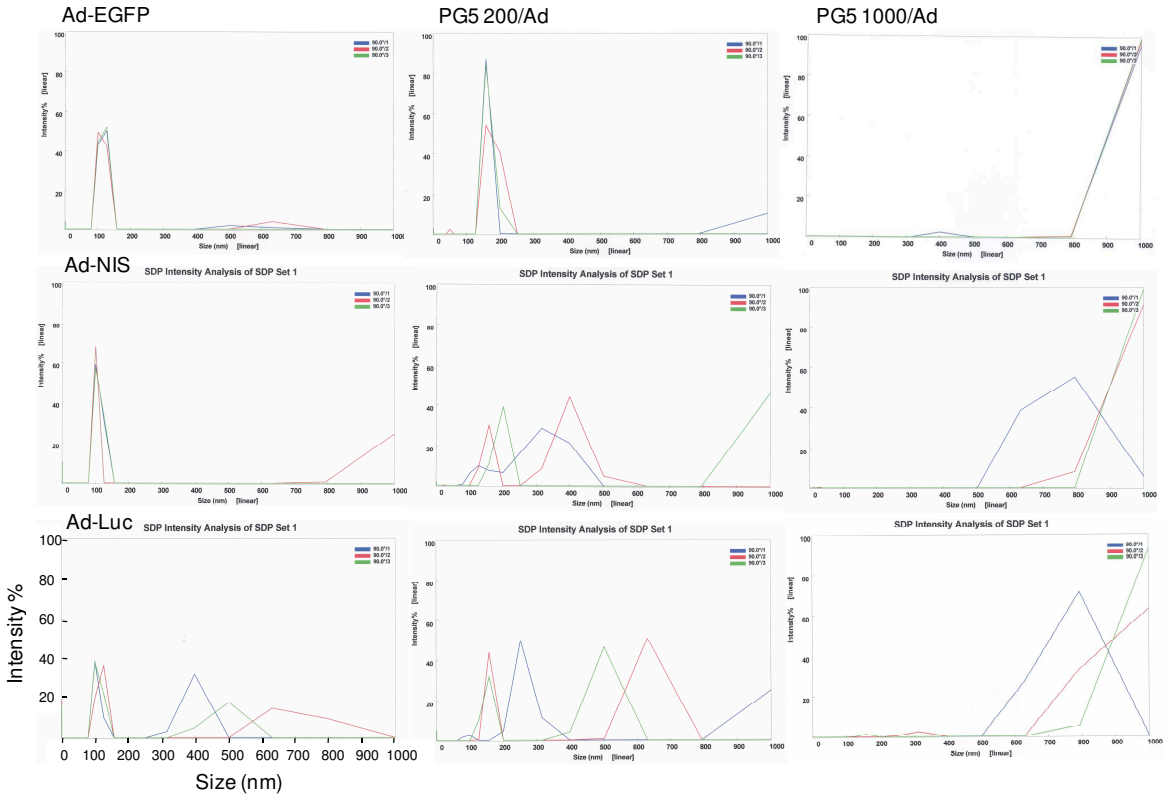

B

Ad sample	PG5/Ad	Solvent	PDI	Size [nm]
Ad-EGFP	0	PBS	0.04	118 ± 28
Ad-EGFP	200	PBS/HBG	0.14	168 ± 61
Ad-EGFP	1000	PBS/HBG	0.41	1128 ± 490
Ad-NIS	0	PBS	0.07	115 ± 37
Ad-NIS	200	PBS/HBG	0.35	231 ± 99
Ad-NIS	1000	PBS/HBG	0.41	1010 ± 374
Ad-Luc	0	PBS	0.44	145 ± 63
Ad-Luc	200	PBS/HBG	0.59	264 ± 120
Ad-Luc	1000	PBS/HBG	0.22	862 ± 298

Figure 11. Size of Ad and PAMAM G5 (PG5) coated Ad measured by dynamic light scattering Size measurement of $2x10^{11}$ VP of Ad-EGFP, Ad-NIS or Ad-Luc only in 2 mL solvent or $1x10^{11}$ VP plus the indicated amount of molecules PAMAM G5/Ad. (A) Intensity profiles, showing the size distribution as well as the occurrence of each size in % intensity. (B) Results on size measurement as well as poly dispersity index (PDI) for each Ad preparation gained as unimodal results from the PCS Control Software Version 2.02 (Beckman Coulter). Triplicate measurements of one sample ± variation of the median are shown.

3.2 Comparing purity of different adenovirus preparations

When considering a non-covalent coating approach based on charge interaction, it is of importance to have a pure virus preparation uncontaminated by cellular proteins, which might interfere with the coating process. Therefore three different adenovirus preparations from three different laboratories were compared using a silver staining technique (Figure 12). When $5x10^9$ VP of Ad-EGFP or Ad-NIS were used, a characteristic band pattern was seen, where the 108 kDa hexon band was the highest molecular weight band and with 720 copies was the most prominent band. Only when higher concentrations were used ($1x10^{10}$ VP), impurities above the hexon band did occur for Ad-NIS. Contrary to this, Ad-Luc showed impurities around 60 kDa and above 100 kDa with $5x10^9$ VP. This later led to the exchange of the Ad-Luc, which was purified by two continuous density gradients against Ad-EGFPLuc, which was purified by one density step gradient followed by one continuous density gradient and showed the higher purity.

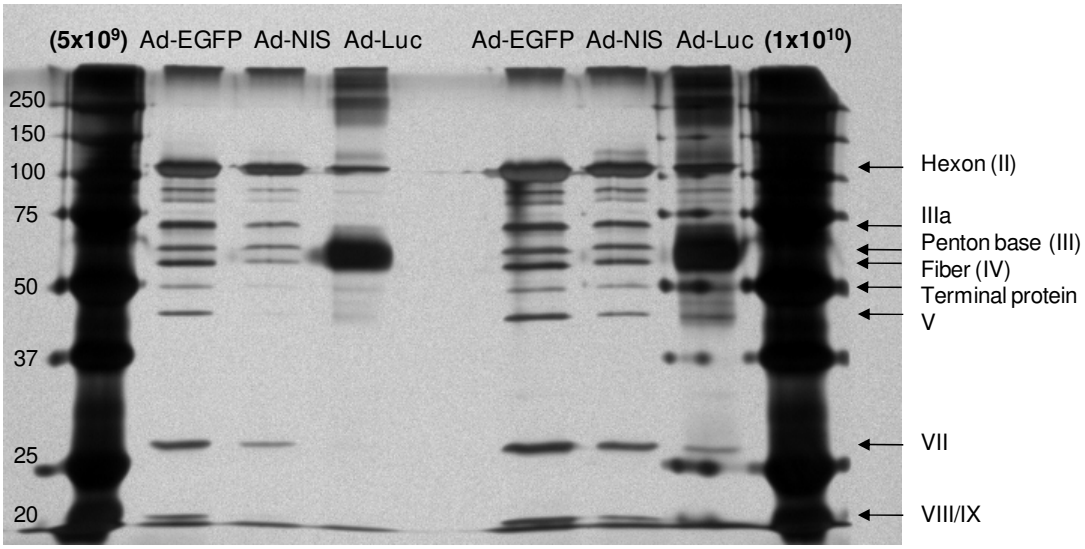

Figure 12. Silver staining of different Ad preparations after electrophoretic separation on a polyacrylamide gel

$5x10^9$ VP of Ad-EGFP, Ad-NIS and Ad-Luc were separated by gel electrophoresis at 120 V for 1.5 h. Silver staining was performed to investigate for potential impurities. From left to right: Protein ladder, Ad-EGFP (from Florian Kreppel), Ad-NIS (from Richard Anderson, ViraQuest Inc.) and Ad-Luc (from Per Holm).

3.1 Stability of the Ad/PAMAM complexes

3.1.1 Co-localization of Ad-Alexa488 and PAMAM G5-Cy5

As stability is a major issue for non-covalent Ad coating, U87MG and HuH7 cells were incubated with Ad-Alexa488/PAMAM G5-Cy5 complexes for 2 h at 37 °C to find out if Ad and PAMAM G5 remained co-localized in the transduction medium and during the cell binding process (Figure 13 and 14). Almost all Ad positive spots exhibited a correlating red signal from the Cy5-labeled PAMAM, which is seen as yellow fluorescence in Figure 13C and F. In addition, numerous PAMAM signals were found especially on HuH7 cells (Figure 13E and F), which did not correlate with Ad fluorescence.

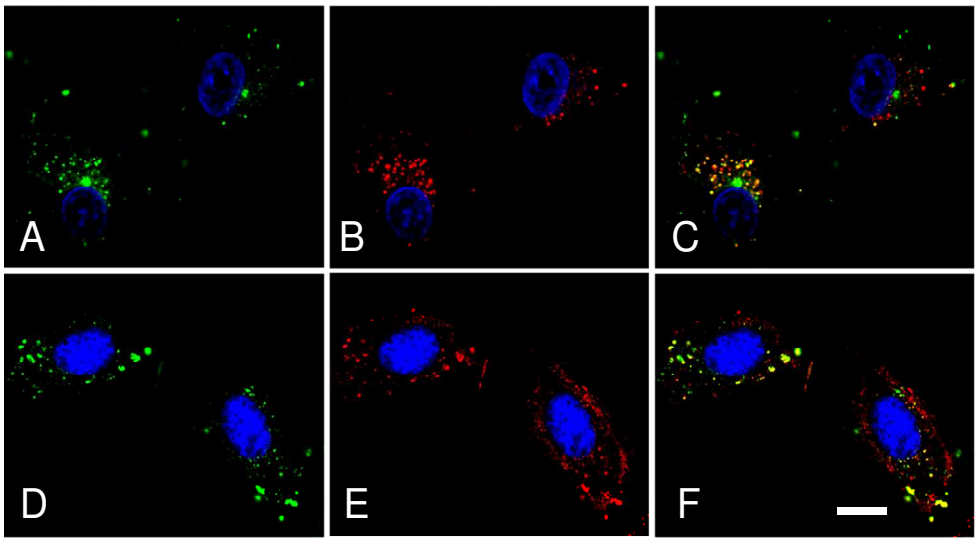

Figure 13. Co-localization of Alexa488-labeled Ad and Cy5-labeled PAMAM G5 dendrimer
U87MG and HuH7 cells seeded in chamber slides were transduced with Ad-Alexa488 coated with PAMAM G5-Cy5 (MOI 500, 10,000 virus particles/cell). After a 2 h incubation period at 37 °C cells were analyzed by LSM. Central sections of U87MG (A-C) or HuH7 (D-F) incubated with Ad-Alexa488 coated with 100 ng of PAMAM G5-Cy5 are shown. (A, D) Alexa488 signal (green) (B, E) PAMAM G5-Cy5 signal (red). (C, F) Overlay; DAPI signal in blue, co-localization Alexa488 signal and Cy5 signal in yellow.

This was also confirmed using the histo and profile tool within the Zeiss 510 META software, where all Alexa488 signals were accompanied by a corresponding more or less prominent PAMAM G5-Cy5 signal, but there were also PAMAM G5-Cy5 peaks without Alexa488 signal (Figure 14A). This demonstrated that PAMAM was present in excess, when using 100 ng of PAMAM G5, where the free dendrimer in solution was subsequently internalized by the cells. Co-localization was also observed near the nucleus, indicating that the complexes co-translocated together to the nuclear membrane.

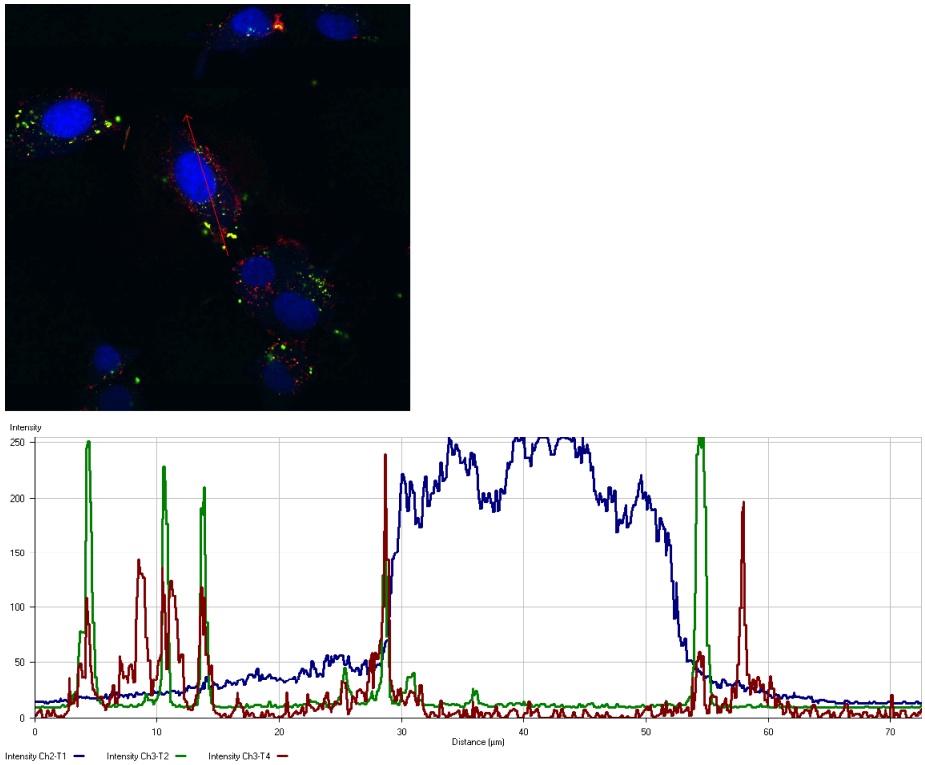

Figure 14A. Qualitative co-localization analysis of Ad-Alexa488 and PAMAM G5-Cy5

HuH7 cells seeded in chamber slides were transduced with Ad-Alexa488 coated with PAMAM G5-Cy5 (MOI 500, 10,000 virus particles/cell). After a 2 h incubation period at 37 °C, cells were fixed with 4% paraformaldehyde, stained with DAPI and analyzed by LSM. The top panel shows a central section of cells. The red arrow denotes the line along which the intensity profile in the lower panel was analyzed. Lower panel: Intensity profile of Ad-Alexa488 signal (green line), PAMAM G5-Cy5 (red line) and DAPI (blue line).

In addition, the co-localization coefficients for the signals were calculated (Figure 14B): in both cell lines the overlap coefficient after Manders [105] ranged between 0.7 and 0.8, indicating a high degree of correlation.

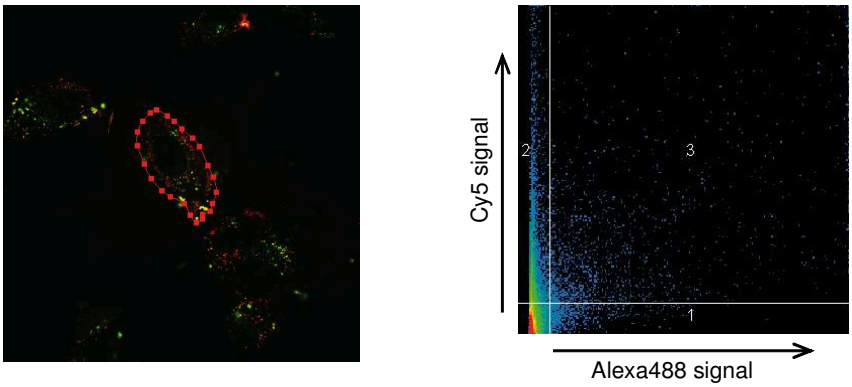

Scatter region	Number pixels	Area (µm2)	Relative area (%)	Mean intensity Alexa488-Channel (Ad)	Mean intensity Cy5-Channel (PAMAM)	Overlap coefficient (Manders)
1	929	36	1.2	39	13	
2	6732	262	9.0	12	53	
3	1654	64	2.2	72	69	0.8

Figure 14B. Quantitative co-localization analysis of Ad-Alexa488 and PAMAM G5-Cy5
The top left panel shows a central section of the cells (green signal: Ad-Alexa488, red signal: PAMAM G5-Cy5) with a red line following the outer cell margins encircling the analyzed area. The top right scatter plot shows the co-localization analysis from the encircled area indicating 3 scatter regions (region 1: Alexa488 signal only; region 2: Cy5 signal only; region 3: co-localization of Alexa488 and Cy5 signal); the weighted pixel signal is color-coded with the intensity increasing from blue to red. The table summarized the results from the co-localization analysis and indicates the overlap coefficient according to Manders.[105]

3.1.2 Transduction in the presence of FCS

Furthermore it was investigated how the presence of fetal calf serum (FCS) influences the transduction efficiency of Ad/PAMAM complexes in terms of interfering with the PAMAM coating. In the first experiment the effect of 2% and 10% FCS on transduction was investigated (Figure 15A). When using 10% FCS, the absolute level of luciferase expression was reduced both for naked Ad-Luc (2.9-fold) and coated Ad (between 1.8- and 2.8-fold), but the beneficial effect of PAMAM coating, when looking at the fold increase of Ad/PAMAM versus Ad in the respective transduction media, remained stable even in the presence of 10% FCS (Figure 15A). To mimic in vivo conditions transductions with higher FCS concentrations up to 100% were also performed. When comparing the absolute transgene expression levels in Opti-MEM versus their 100% FCS counterparts, a reduction of 1.5-fold for Ad-EGFPLuc, 4.2-fold for Ad/PAMAM G5 10 ng and 2.6-fold for Ad/PAMAM G5 100 ng respectively could be seen (Figure 15B). The relative fold increase in transduction efficiency remained stable up to 25% FCS. In the presence of

100% FCS 36% of the relative fold increase could still be maintained for Ad coated with 10 ng and 58% when Ad was coated with 100 ng PAMAM G5 (Figure 15C).

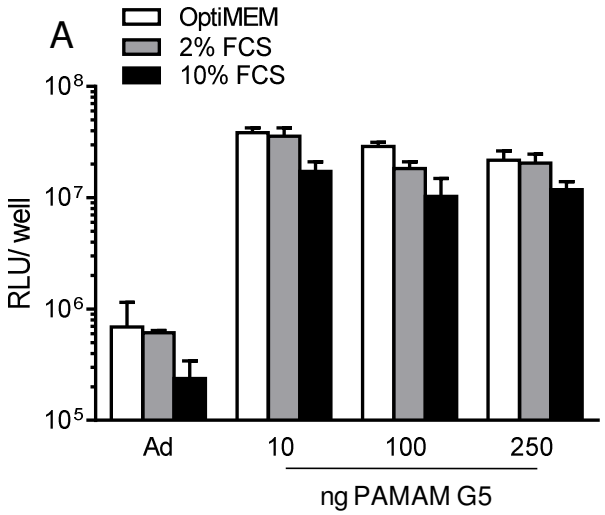

Figure 15A. Influence of FCS on transduction efficiency

U87MG cells were transduced with Ad-Luc only or coated with 10 ng, 100 ng or 250 ng of PAMAM G5 in Opti-MEM (white bars) or DMEM supplemented with 2% (gray bars) or 10% FCS (black bars), and the luciferase level was quantified after 48 h. Mean values (n=5) plus std.dev. are shown.

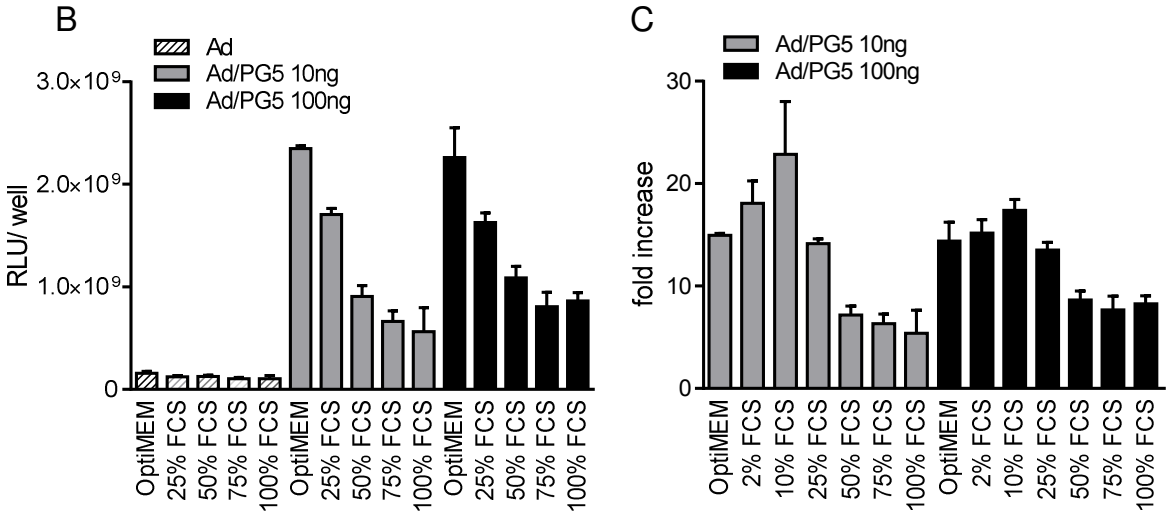

Figure 15B-C. Influence of FCS in concentrations up to 100% on transduction efficiency

U87MG cells were transduced with Ad-EGFPLuc only (striped bars) or coated with 10 ng (grey bars) or 100 ng (black bars) of PAMAM G5 in Opti-MEM or DMEM supplemented with 2%-75% FCS or pure FCS and the luciferase level was quantified after 48 h (Figure 15B). Additionally, the fold increase in transduction efficiency of Ad/PAMAM versus Ad in the respective transduction media was calculated (Figure 15C). Mean values (n=3) plus std.dev. are shown.

3.3.3 Storage under different temperature conditions

Coated Ad particles were usually prepared immediately prior to use. For certain applications however it would be advantageous to prepare larger amounts of stock, which would then require storage. The effect on transduction efficiency after storing coated Ad, for 24 h under different conditions, was therefore tested. After coating, particles were stored at 4 °C, room temperature or 37 °C for 24 h, and thereafter U87MG or HuH7 cells transduced and the transduction efficiency was compared with freshly coated Ad (Figure 16). Transduction efficiency of coated Ad was only slightly lower or unaffected (depending on the amount of PAMAM G5 used for coating), when stored at 4 °C, than of freshly coated Ad samples. However, when stored at RT and especially at 37 °C, most of the beneficial effect on transduction due to coating was lost.

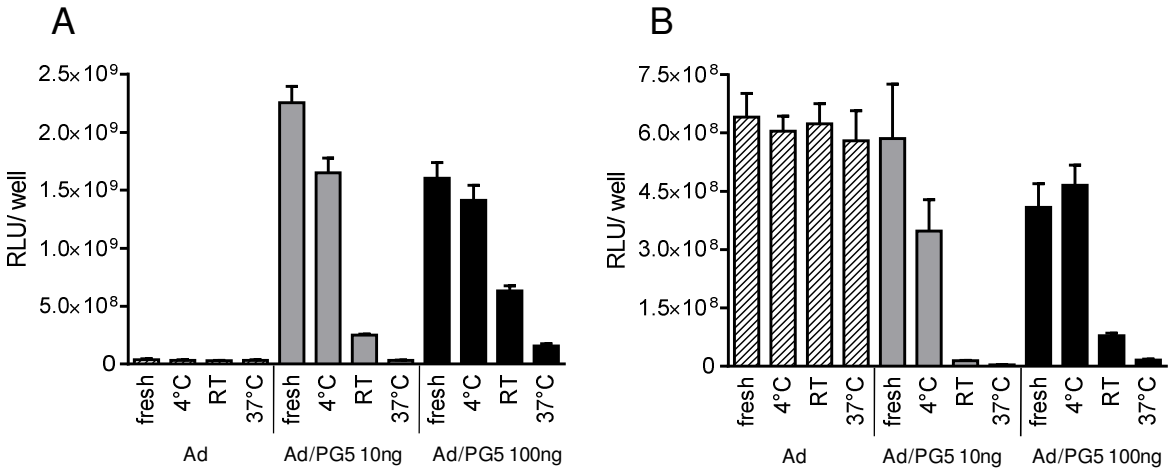

Figure 16. Stability of Ad/PAMAM complexes stored at various temperature conditions
$1x10^4$ U87MG (A) and HuH7 (B) cells were transduced in 96-well plates with a MOI of 100 of Ad-EGFPLuc alone (striped bars) or complexed with 10 ng (grey bars) or 100 ng PAMAM G5 (black bars) either freshly prepared or stored for 24 h at 4 °C, RT (20-25 °C) or 37 °C. Luciferase expression level was evaluated 48 h after transduction, expressed as relative light units per well (RLU/well). Mean values (n=5) plus std.dev. are shown.

3.3.4 Importance of complex formation before application to cells

Preformed complexes of Ad/PAMAM G5 were compared with a consecutive addition of Ad followed by PAMAM G5 into the transduction medium, or alternatively by pre-incubating the cells with PAMAM G5 for 30 min followed by application of Ad (Figure 17 A). The latter was performed to rule out a stimulation of macropinocytosis by free PAMAM. The best transduction result gained on U87MG by Ad coated with 10 ng PAMAM G5 could not be reached by consecutive application or preinbubation with 10 ng

PAMAM G5. Whereas consecutive application of Ad and 100 ng PAMAM G5 led to results comparable to the preformed complexes, when using an incubation time of 2 h. In the next step shorter incubation times of 15, 30 and 60 min were undertaken and the preformed complexes were compared with the consecutive addition. While consecutive application of Ad and 10 ng PAMAM G5 caused transgene expression levels comparable to naked Ad, the values for consecutive addition of Ad and 100 ng PAMAM G5 increased with incubation time reaching 68% of the transgene expression levels of preformed complexes after an incubation time of 1h.

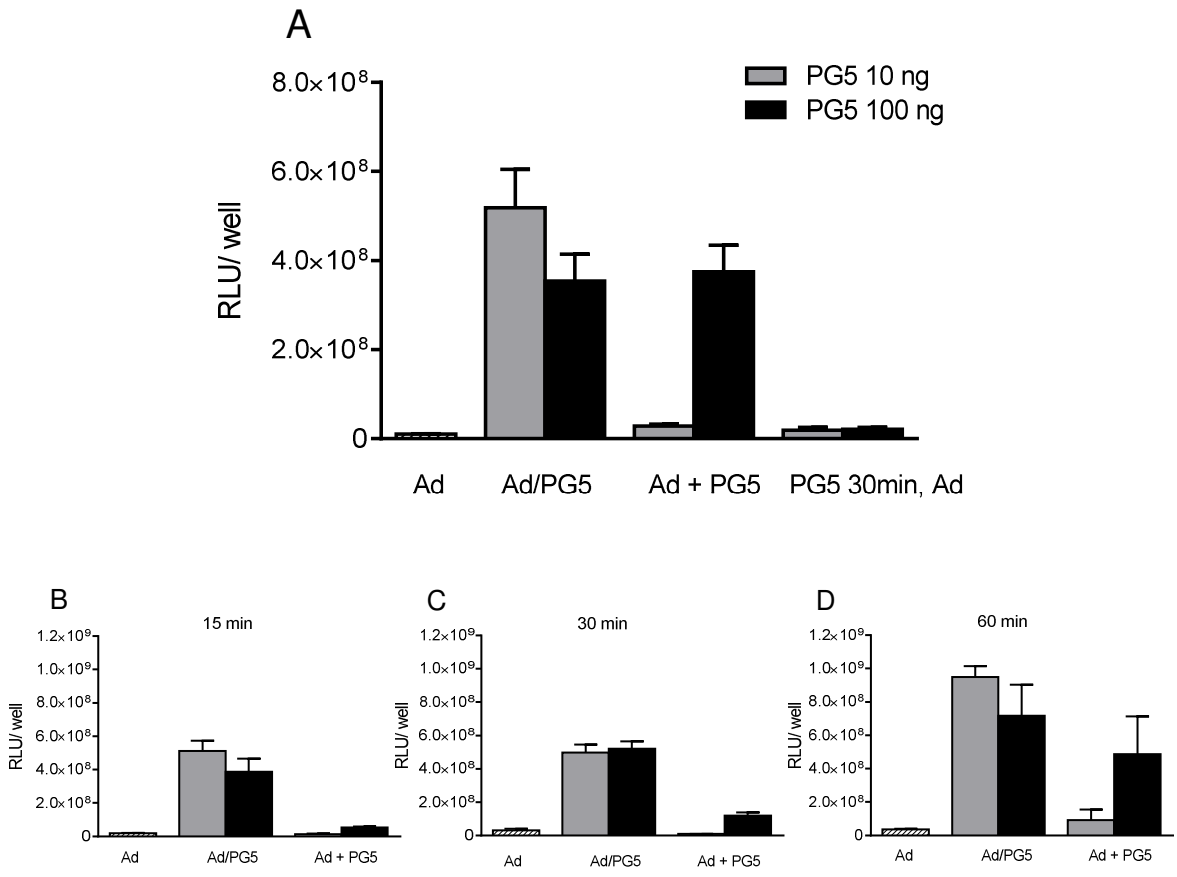

Figure 17. The importance of complex formation before application to cells

(A) 1x10^4 U87MG cells were transduced in a 96-well plate for 2 h with a MOI of 100 of uncoated Ad-EGPFLuc or preformed Ad/PAMAM G5 complexes versus Ad and PAMAM G5 consecutively added or PAMAM G5 applied for 30 min before addition of Ad. (B) Ad or Ad/PAMAM G5 complexes versus Ad and PAMAM G5 consecutively added were incubated with cells for 15, 30 or 60 min. 48 h after transduction, luciferase expression level was analyzed and expressed as relative light units per well (RLU/well). Mean values (n=5 for A and n=3 for B,C) plus std.dev. are shown.

3.4 Receptor status of different cancer cell lines

Six different cancer cell lines were tested for their coxsackie- and adenovirus receptor (CAR) and integrin $\alpha_v\beta_3$ levels to predict which cell lines would be easily infected by Ad alone and which might benefit from polycation coating. Additionally, cells were stained for the epidermal growth factor receptor (EGFR) and the transferrin receptor (TfR) as possible receptors for targeting (Figure 18). Receptor levels of additional cell lines can be found in the appendix (Figure S1, supplementary information).

U87MG and HuH7 were used in further studies as representative cell lines with low and high CAR levels respectively. In terms of targeting, HepG2 was used as a low EGFR expressing cell line and A549 as an EGFR overexpressing cell line.

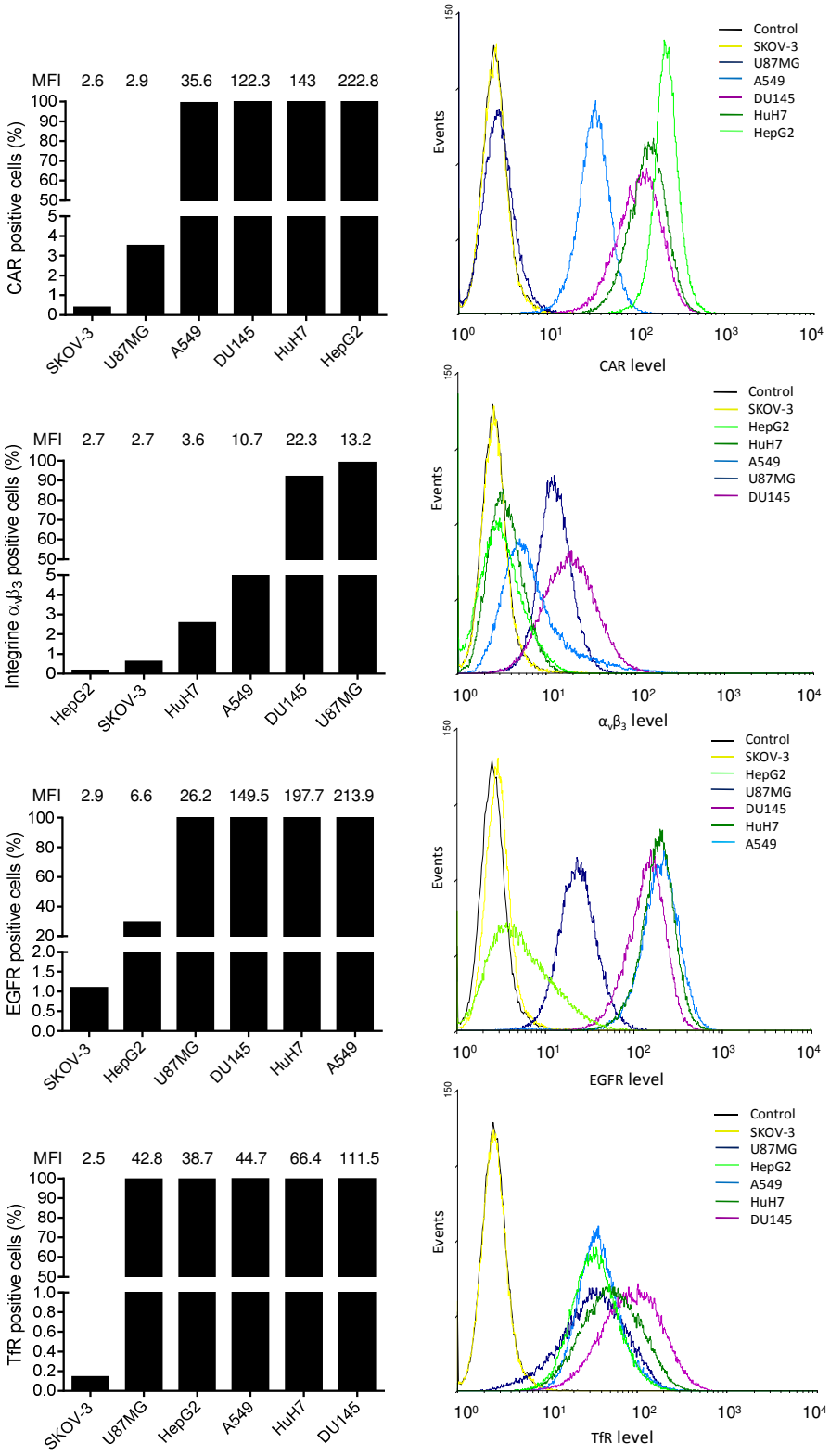

Figure 18. Receptor level estimation of CAR, integrin $\alpha_v\beta_3$, EGFR and TfR

Indicated cell lines were stained for CAR, integrin $\alpha_v\beta_3$, EGFR and TfR and analyzed by flow cytometry. Control staining was performed with mouse IgG control antibody. The diagrams on the left display the percentage of receptor positive cells for each cell line as well as the mean fluorescence intensity (MFI) in the FITC channel above each column. The histograms on the right illustrate the shift of Alexa 488 positive cells for every cell line.

3.5 Cellular uptake of fluorescently labeled Ad and Ad/polycation complexes

3.5.1 Cellular uptake of Ad versus Ad/PAMAM G5 complexes

To study the uptake behavior of uncoated versus coated Ad, Ad-Alexa488 was coated with Cy5-labeled PAMAM G5. Two cell lines with different CAR expression levels were compared: the human glioblastoma cell line U87MG expressing low CAR levels (3.5% CAR positive, MFI 3), and the human hepatocellular carcinoma cell line HuH7, where all cells are positive for CAR (100%, MFI 143). U87MG and HuH7 were infected with 10,000 particles per cell of Ad-Alexa488 alone or complexed with 2.5, 10 or 100 ng of PAMAM G5. Cells were incubated with Ad for 2 h at 37 °C, thereafter fixed and cellular association and internalization analyzed by flow cytometry and LSM (Figure 19).

Total cellular association of uncoated Ad as seen by FACS analysis was higher on HuH7, when compared to U87MG cells. After virus coating with 10 ng of PAMAM G5, a 6-fold increase in MFI was seen on U87MG (Figure 19A). A further increase in PAMAM G5 concentration to 100 ng did not lead to an additional increase in signal, whereas coating with 2.5 ng led to a slightly lower signal shift. On HuH7 cells, the already high cellular association of Ad was increased approximately 3-fold using 10–100 ng of PAMAM G5 (Figure 19B).

LSM studies were conducted to study intracellular uptake and distribution of Ad and Ad/PAMAM G5 within the cell (Figure 19C–H): In the low CAR expressing U87MG cells low uptake of uncoated Ad (Figure 19C) was observed, whereas with PAMAM G5 coated Ad highly effective internalization occurred, especially when 10 ng of PAMAM G5 were used and the Ad/PAMAM G5 particles were small and evenly distributed (Figure 19D). Ad/PAMAM G5 complexes were found in close proximity to the nucleus after incubation for 2 h, at 37 °C, indicating that the intracellular trafficking was not grossly, negatively influenced. HuH7 cells on the other hand exhibited a significant uptake of uncoated Ad due to their high level of CAR (Figure 19F), while Ad complexed with PAMAM G5 tended to form aggregates at the cell membrane. The aggregation process has already been observed with low amounts of PAMAM G5, i.e., 10 ng (Figure 19G), which was even more pronounced when 100 ng of PAMAM G5 were used (Figure 19H).

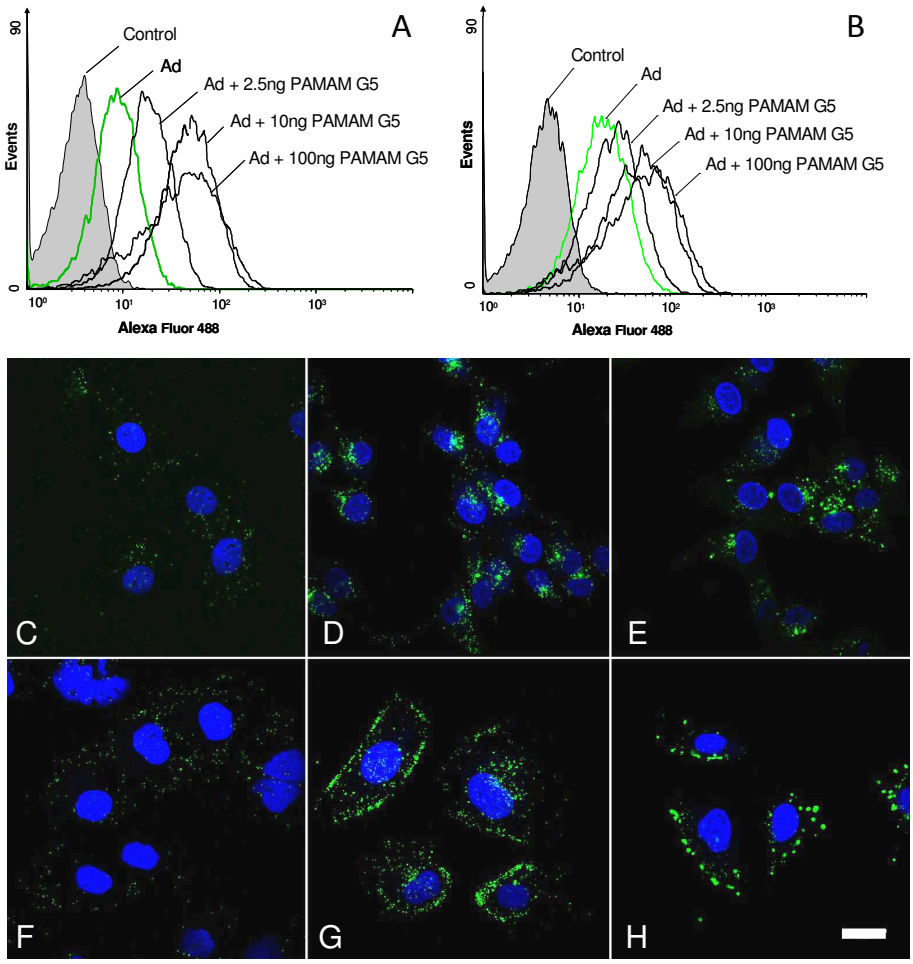

Figure 19. Influence of PAMAM G5 coating on cellular uptake

U87MG (low CAR) and HuH7 (high CAR) were transduced with Ad fluorescently labeled with amine reactive Alexa Fluor488-5TFP, either alone or coated with PAMAM G5 (MOI 500, 10,000 VP/cell). After a 2 h incubation period at 37 °C cells were analyzed by either flow cytometry (A, B) or LSM (C-H). (A, B) U87MG (A) or HuH7 cells (B) were incubated with Ad-Alexa488 alone or coated with 2.5, 10 or 100 ng of PAMAM G5. Cells without virus served as control; $2x10^4$ gated events per sample are shown. (C-H) U87MG (C-E) and HuH7 cells (F-H) seeded in chamber slides were incubated with Ad-Alexa488 alone (C, F), coated with 10 (D, G) or 100 ng (E, H) of PAMAM G5 and fixed with 4% PFA, and the nuclei were counterstained with DAPI and analyzed by LSM; for most cells central sections of cells are shown; in panel G some cytoplasmic virus signal (green) appears above the nucleus; Alexa488 signal in green, DAPI signal in blue, scale bar represents 20 µm.

3.5.2 Cellular uptake of Ad/PAMAM G5 compared to Ad/LPEI complexes

In order to see if differences between the aggregation and uptake behavior between Ad/PAMAM G5 and Ad/LPEI occured, Ad-Alexa 488 was coated with 10 ng of either polycation and incubated with cells for 2 h at 37 °C (Figure 20). Coating with LPEI (22 kDa) led to excessive particle aggregation and reduced uptake resulting in only a few Ad

particles reaching the nuclear membrane in U87MG (A) and HuH7 cells (B) after 2 h compared to PAMAM G5 coated Ad shown in D and in E for U87MG and HuH7 cells respectively.

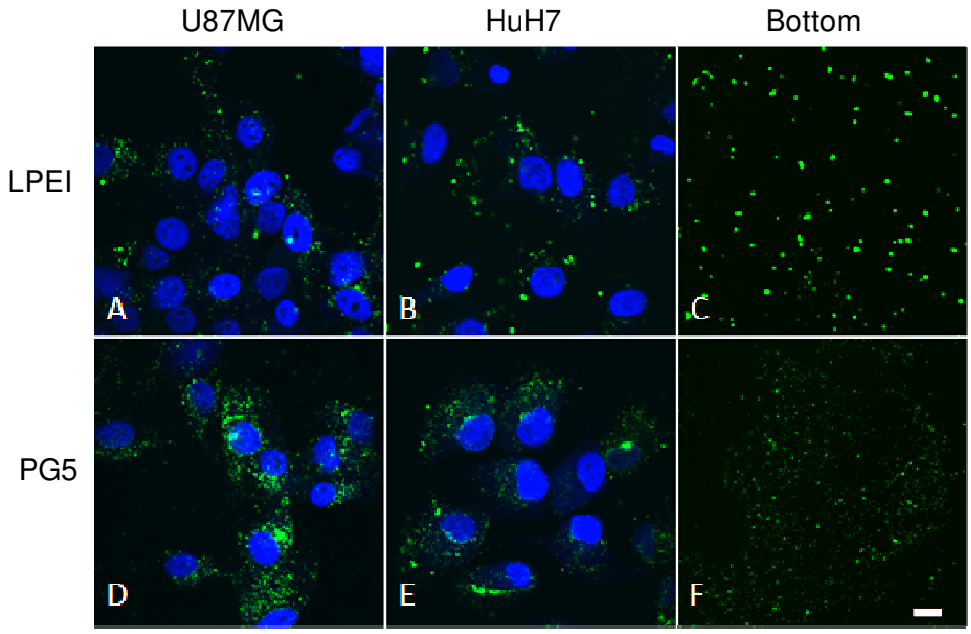

Figure 20. Cellular uptake and aggregation behavior of Ad/LPEI and Ad/PAMAM G5

U87MG and HuH7 were transduced with LPEI and PAMAM G5 (PG5) coated Ad-Alexa488 (MOI 500, 10,000 VP/cell). After 2 h at 37 °C cells were fixed and analyzed by LSM. Central sections of U87MG (A: Ad/LPEI, D: Ad/PG5) and HuH7 (B: Ad/LPEI 5, E: Ad/PG5) transduced with Ad-Alexa488 coated with 10 ng LPEI or PAMAM G5 respectively are shown. C (Ad/LPEI) and F (Ad/PG5) show the size of the complexes sticking to the bottom of the chamber slide. Alexa488 signal is illustrated in green, DAPI signal in blue.

3.5.3 Solvent optimization

While optimizing the coating process, PAMAM G5 and Ad were diluted separately in different buffers, including the low ionic buffer HEPES buffered glucose (HBG, pH 7.4), PBS and Opti-MEM. The most efficient transduction was obtained with Ad diluted in Opti-MEM and PAMAM G5 in HBG, as shown for HuH7 (Figure 21). Hence, all further studies were conducted in this buffer system with the exception of zeta potential measurements, where PBS was used instead of Opti-MEM for Ad dilution, and TEM, where water was used for Ad dilution and PBS for the Ad/PAMAM G5 complex to reduce background signal and background staining.

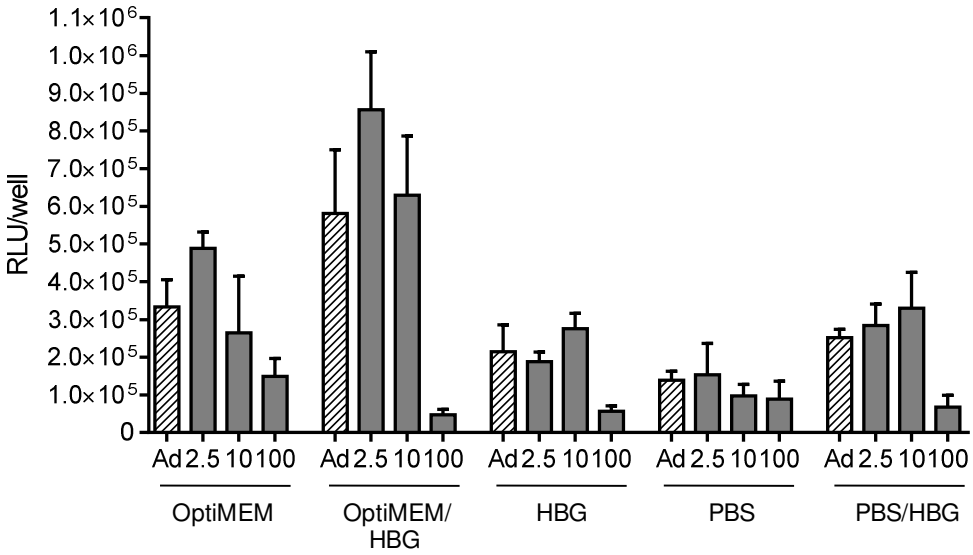

Figure 21. The effect of different solvents on transduction efficiency

$1x10^4$ HuH7 hepatoma cells were transduced in 96-well plates with Ad-EGFPLuc (MOI 100) alone or complexed with 2.5, 10 and 100 ng PAMAM G5 in the indicated solvents and solvent mixtures. The luciferase expression level was evaluated 48 h after transduction and expressed as relative light units per well (RLU/well). Mean values (n=3) plus std.dev. are shown.

3.6 Evaluation of the transduction benefit through coating

3.6.1 Influence of PAMAM G5 and LPEI coating on Ad-Luc mediated transduction and metabolic activity of low CAR or high CAR cell lines

To further investigate the differences between U87MG as low CAR level cell line and HuH7 as high CAR level cell line, and to distinguish differences in uptake of Ad/PAMAM G5 versus Ad/LPEI, transduction studies based on evaluation of the luciferase transgene expression were performed. U87MG and HuH7 cells were transduced with a MOI of 100 ($2x10^7$ VP/well) of uncoated Ad (Ad-Luc) or Ad coated with PAMAM G5 or LPEI ranging from 2.5 ng to 1,000 ng per well (Figure 22). In U87MG, uncoated Ad induced only very low luciferase expression levels, whereas PAMAM G5 coating induced an increase in luciferase expression of up to 36-fold using the optimum amount of 10 ng PAMAM G5 (Figure 22A). Although HuH7 were highly transducted with uncoated Ad, lower doses of PAMAM G5 (2.5 ng) further increased luciferase expression by approximately 30%, whereas with higher PAMAM G5 doses the luciferase activity decreased below the level achieved with uncoated Ad (Figure 22B). In addition, LPEI (22 kDa), a linear polycation and a gold standard in polymer mediated non-viral gene therapy, was evaluated. On U87MG cells, LPEI elevated Ad mediated luciferase expression by a maximum of only 6.5-fold; In HuH7 cells, all LPEI concentrations tested had a negative effect on Ad

activity. A MTT assay revealed that cells treated with PAMAM G5 maintained high cell viability even when 1,000 ng/well of PAMAM G5 were applied (Figure 22 C,D). In contrast, LPEI induced toxicity from 50 ng/well and above and resulted in a cell viability of only 3% when incubated with 1,000 ng/well.

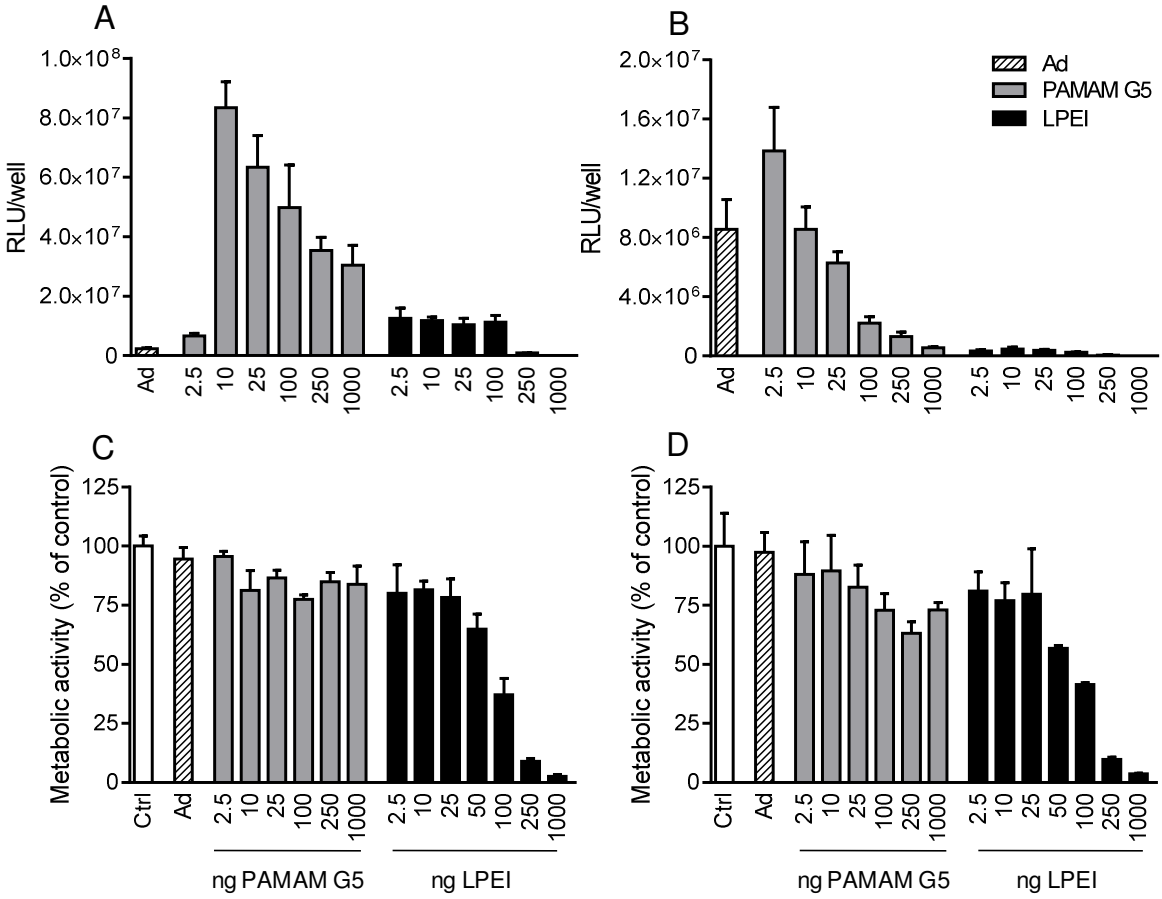

Figure 22. The influence of PAMAM G5 and LPEI coating on transduction efficiency and metabolic activity

$1x10^4$ U87MG glioblastoma (A,C) and HuH7 hepatoma (B,D) cells were transduced in 96-well plates with $2x10^7$ Ad-Luc particles/well (MOI 100) either alone (striped bars) or complexed with the indicated amounts of PAMAM G5 (grey bars) or LPEI (black bars). Luciferase expression level was evaluated 48 h after transduction for U87MG (A) and HuH7 (B) and expressed as relative light units per well (RLU/well). MTT assays were also performed for U87MG (C) and HuH7 (D) after 48h. Untreated cells served as control (white bars) with 100% viability. Mean values (n=3) plus std.dev. are shown.

As a further control, 25 kDa branched PEI (BPEI) was used for Ad coating (Figure 23), which is similar to 22 kDa LPEI in that it consists of ethylenimine subunits, but in addition it is randomly branched and therefore exhibits primary, secondary and tertiary amines similar to PAMAM dendrimers. As seen in the previous experiment, PAMAM G5 was

greatly superior to LPEI on both cell lines tested. When comparing LPEI to BPEI, LPEI worked two times better on U87MG and almost five times better on HuH7 than BPEI. The reduction in metabolic activity (Figure 23 C,D) was comparable to that seen for LPEI, showing toxicity from 100 ng per well and upwards retaining only 4% cell viability when 1,000 ng of BPEI per well was applied.

For further studies, the transduction efficiency using LPEI was compared with the different PAMAM dendrimers.

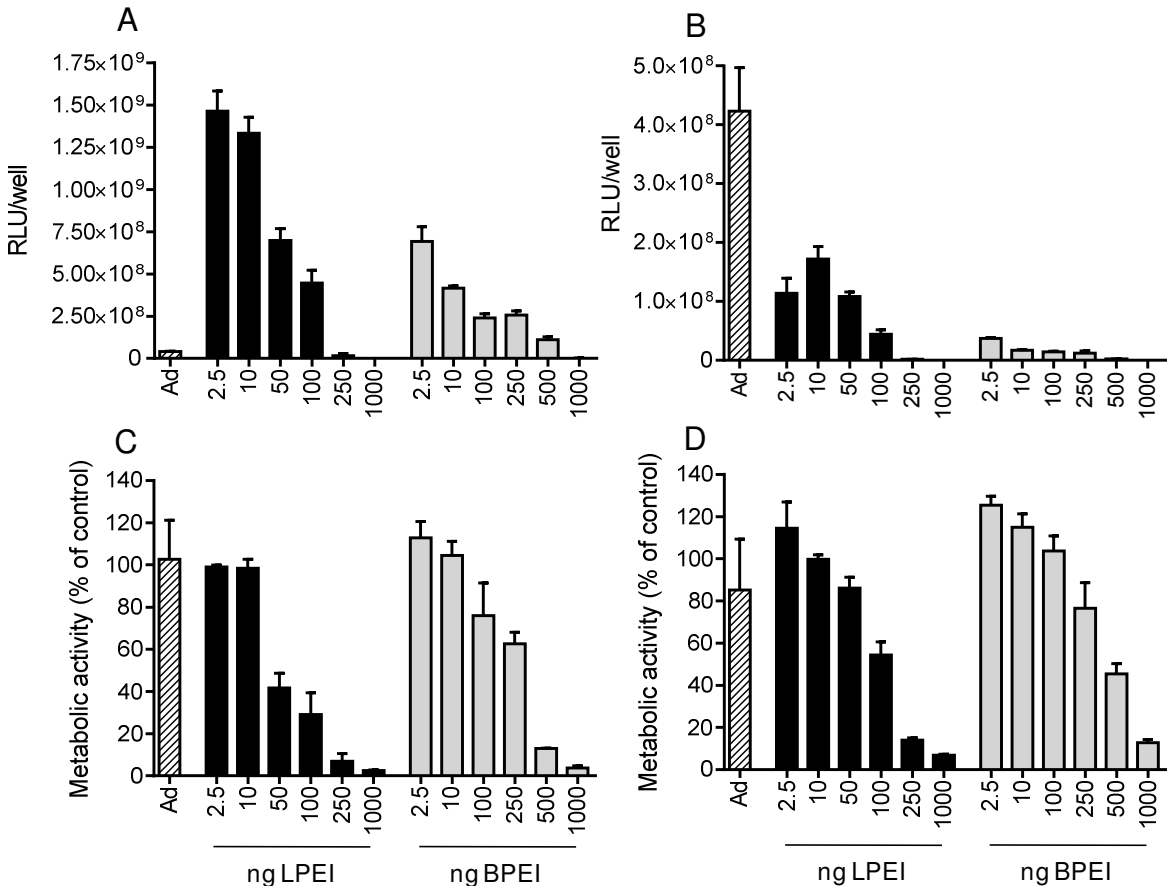

Figure 23. The influence of LPEI and BPEI coating on transduction efficiency and metabolic activity

$1x10^4$ U87MG glioblastoma (A,C) and HuH7 hepatoma cells (B,D) were transduced in 96-well plates with $2x10^7$ Ad-Luc particles/well (MOI 100) either alone (striped bars) or complexed with the indicated amounts of LPEI (black bars) or BPEI (light grey bars). Luciferase expression level was evaluated 48 h after transduction for U87MG (A) and HuH7 (B) and expressed as relative light units per well (RLU/well). MTT assays were also performed for U87MG (C) and HuH7 (D) after 48h. Untreated cells served as control (white bars) with 100% cell viability. Mean values (n=3) plus std.dev. are shown.

3.6.2 Comparison of PAMAM G2, G3, G5 and LPEI on 5 human cancer cell lines

The transduction experiments comparing uncoated versus coated Ad were then extended to five human cancer cell lines with a range of CAR expression levels (low CAR level in SKOV-3 ovarian carcinoma (MFI 2.6, 0.4% positive) and U87MG glioblastoma (MFI 3, 3.5% positive), medium CAR level in A549 lung carcinoma (MFI 35.6, 99.2% positive), high CAR level in DU145 prostate carcinoma (MFI 122.3, 99.9%) and HuH7 hepatocellular carcinoma (MFI 143, 100%). The benefit of PAMAM G5 coating in relation to the lower generation PAMAMs, namely PAMAM G2 and G3, as well as LPEI was examined (Figure 24A-E). For U87MG cells, which express low levels of CAR, the highest transduction efficiency was observed with PAMAM G5 followed by G3, G2 and LPEI with the best transduction achieved using 10 ng PAMAM G5, 50 ng PAMAM G3 and 250 ng PAMAM G2, following the trend: the lower the PAMAM generation the more coating material is required. In HuH7 an inverse effect was seen, where the best transduction efficiency occurred using PAMAM G2 followed by G3, G5 and LPEI.

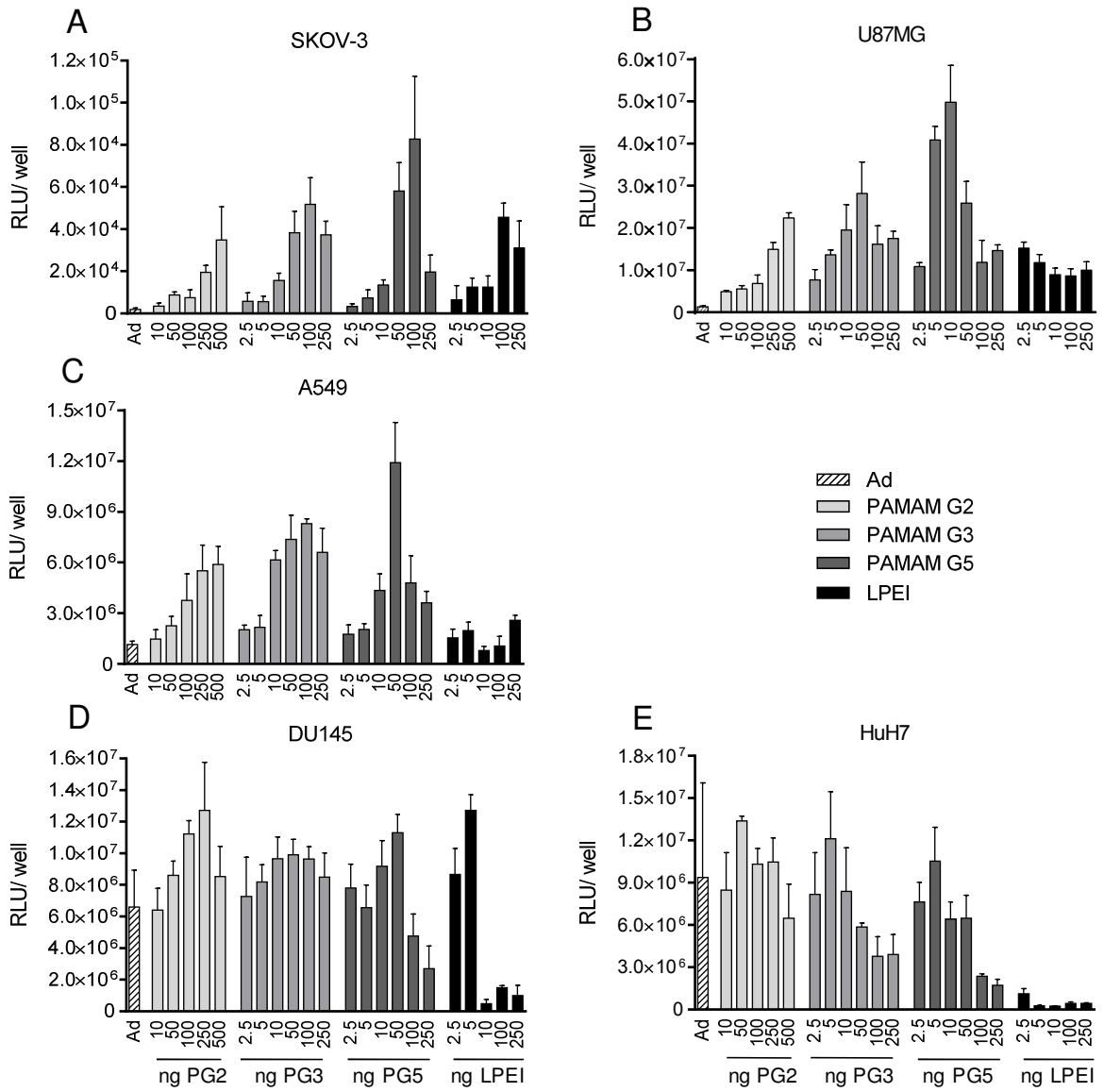

Figure 24 A-E. The coating benefit of PAMAM G2, G3, G5 and LPEI

$1x10^4$ SKOV-3 ovarian carcinoma, U87MG glioblastoma, A549 lung carcinoma, DU145 prostate carcinoma and HuH7 hepatoma cells were transduced in 96-well plates with $2x10^7$ Ad-Luc particles/well (MOI 100) either alone (striped bars) or complexed with the indicated amounts of PAMAM G2 (white bars), PAMAM G3 (light grey bars), PAMAM G5 (dark grey bars) or LPEI (black bars). Luciferase expression level was evaluated 48 h after transduction, expressed as relative light units per well (RLU/well). Mean values (n=3) plus std.dev. are shown.

MTT assays for all the polycations tested pointed to the absence of toxicity for PAMAM G2, G3 and G5 using concentrations up to 1000 ng/well, while LPEI displayed toxicity from 50 ng/well and above (Figure 24F-G).

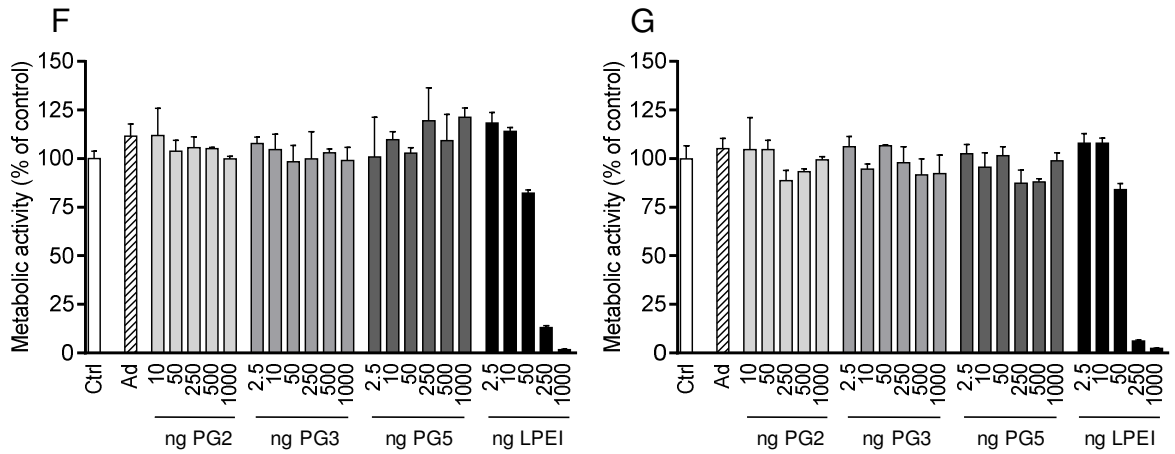

Figure 24 F-G. Metabolic activity of U87MG and HuH7 cells after transduction with uncoated Ad and PAMAM G2, G3, G5 and LPEI coated Ad

After 48 h MTT assays were performed for U87MG (F) and HuH7 cells (G). Untreated cells served as control (white bars) with 100% cell viability. Mean values (n=3) plus std.dev. are shown.

3.6.3 Correlation of CAR level and transduction improvement by PAMAM G5 coating

When taking the highest transduction efficiencies gained with PAMAM G5 (PG5) coating in the five cell lines tested, a clear inverse correlation between the CAR expression level (Figure 25A) and the benefit gained through transduction with Ad/PAMAM G5 complexes compared to uncoated Ad can be observed (Figure 25B). In contrast, no correlation was observed between $\alpha_v\beta_3$ integrin expression levels and improved transduction efficiency due to PAMAM coating. SKOV-3 cells, which are virtually CAR negative, showed the greatest increase in transduction efficiency (46-fold) using 100 ng of PAMAM G5 for coating, followed by U87MG cells which showed a 38-fold increase with 10 ng PAMAM G5. For A549 cells a 10-fold increase was found, with an optimum of 50 ng of PAMAM G5, whereas DU145 and HuH7 cells, which exhibit high levels of CAR, revealed only a 1.7 and 1.3-fold increase with a maximum at 50 ng and 5 ng of PAMAM G5 respectively.

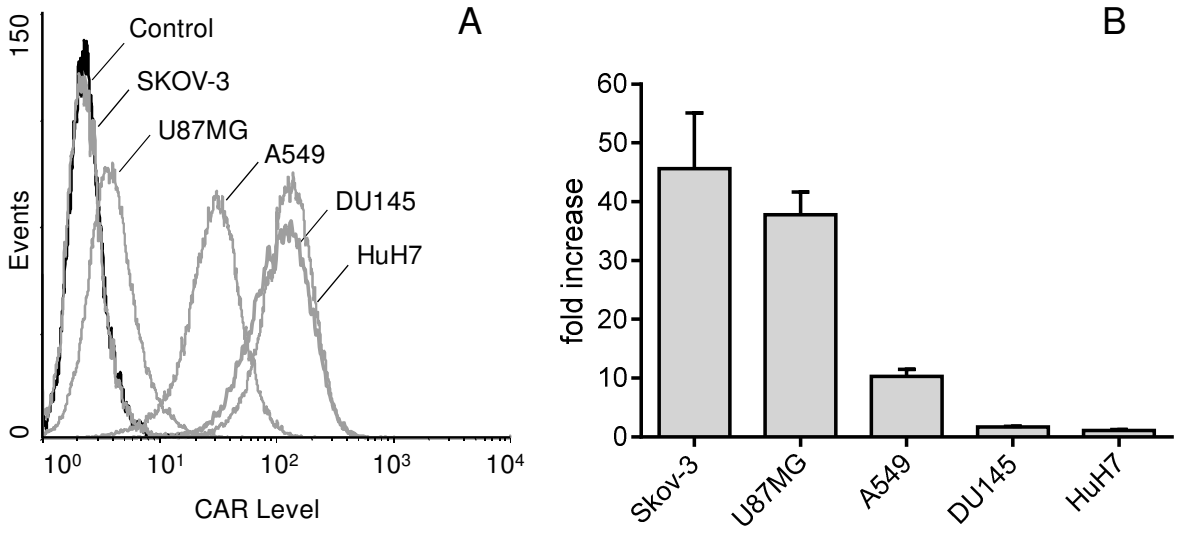

Figure 25. Correlation between CAR level and increase in transduction efficiency obtained with PAMAM G5

(A) Indicated cell lines were stained for CAR and analyzed by flow cytometry. Control staining was performed with mouse IgG control antibody. (B) Cell lines were transduced in 96-well plates at MOI 100 with Ad-Luc alone or coated with an optimized amount of PAMAM G5 (SKOV-3, 100 ng/well; U87MG, 10 ng; A549, 50 ng; DU145, 50 ng; HuH7, 5 ng), and the luciferase activity was quantified after 48 h. Relative transduction efficiency was expressed as ratio between luciferase activity obtained with PAMAM G5 coated Ad-Luc and uncoated Ad-Luc. Mean values (n=3) plus std.dev. are shown.

3.6.4 PAMAM mediated gene delivery: a direct comparison of Ad and plasmid

As PAMAM dendrimers can be used for both, plasmid [74] and Ad delivery, a side-by-side comparison of both systems was conducted using the same polycations and in each case a CMV promoter driven EGFPLuc transgene expression cassette. U87MG and HuH7 cells were transduced with either an optimal amount of Ad (MOI 100, corresponding to 1×10^6 infectious and 1.5×10^7 total VP) or plasmid at an optimal amount of 400 ng/well (corresponding to approximately 5.7×10^{10} plasmid molecules) (Figure 26). In the low CAR cell line U87MG, optimal amounts of plasmid condensed with optimal amounts of the most effective PAMAM (400 ng of plasmid condensed with 800 ng of PAMAM G5) still only reached luciferase levels about 5-fold below Ad transduced cells; compared to coated Ad the level was 102-fold lower. In the CAR positive HuH7 cells, plasmid/PAMAM complexes were 55-fold less efficient compared to the naked Ad and 83-fold less efficient than the coated Ad. When taking into account that a 57,000-fold excess of DNA molecules over infectious Ad particles was used, Ad coated with PAMAM G5 dendrimer led to

5.8×10^6 and 4.7×10^6-fold increases in transgene expression level versus DNA/PAMAM polyplexes in U87MG and HuH7 cells respectively.

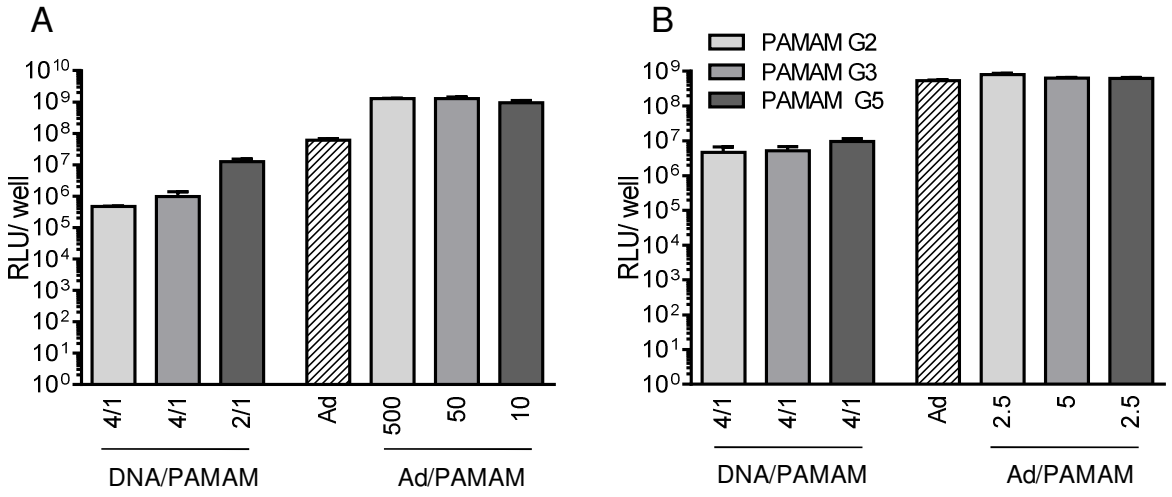

Figure 26. Comparision of DNA/PAMAM polyplexes with PAMAM coated Ad
$1x10^4$ U87MG (A) or HuH7 cells (B) were transfected in 96-well plates with either DNA/PAMAM polyplexes (400 ng DNA, optimum w/w of 4/1 or 2/1 PAMAM G2/G3/G5 to DNA) or Ad-EGFPLuc coated with the indicated amounts of PAMAM G2 (light grey bars), PAMAM G3 (medium grey bars) or PAMAM G5 (dark grey bars). Luciferase expression level was evaluated 48 h after transduction, expressed as relative light units per well (RLU/well). Mean values (n=3) plus std.dev. are shown.

3.7 Protection ability of PAMAM dendrimer coating from inhibition by neutralizing antibodies

In order to study the ability of the PAMAM G5 dendrimer to protect the Ad from neutralizing antibodies, uncoated Ad-EGFP or preformed Ad/PAMAM G5 complexes with 25 or 100 ng PAMAM G5 were incubated for 30 min with increasing concentrations of human IgG (Privigen®, obtained from pooled plasma taken from 60,000 donors, stock 100 mg/mL) before transducing A549 cells. FACS analysis for EGFP 48 h after transduction revealed that uncoated Ad was rapidly inactivated by IgG exposure reaching a baseline level of 0.5% positive cells, when incubated with 0.8 mg/mL of IgG (1:120 dilution), while PAMAM coated Ad was still able to transduce 65% of the cells, on average, with the same IgG concentration. At IgG concentrations reaching 3.3 mg/mL (1:30 dilution), 100 ng of PAMAM G5 still helped to protect the Ad from inhibition by neutralizing antibodies, therefore enabling infection of 47% of the cells on average (Figure 27 and S3, supplementary information).

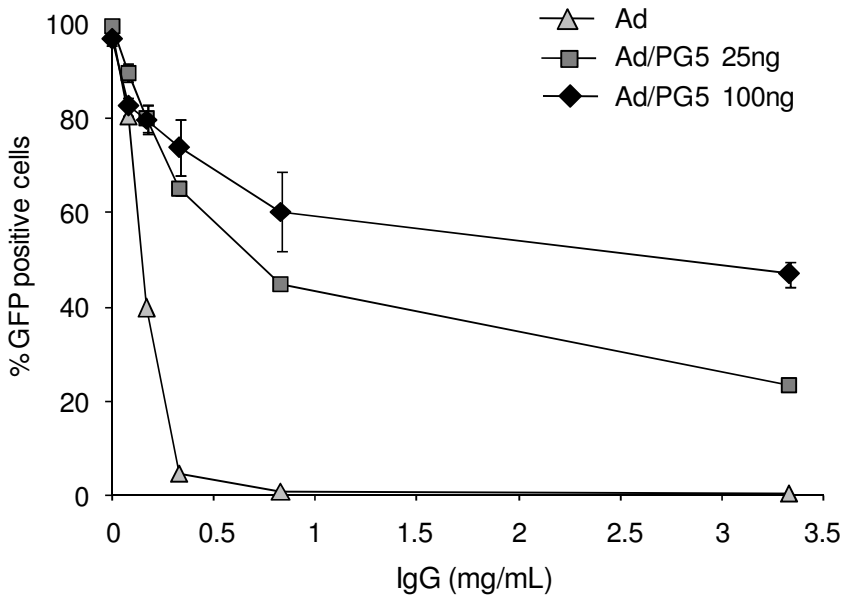

Figure 27. The protective effect of PAMAM G5 coating on transduction in the presence of anti-adenovirus neutralizing antibodies

$5x10^4$ A549 cells seeded in 24-well plates were transduced with Ad-EGFP alone (triangles) or coated with 25 ng (squares) or 100 ng (diamonds) of PAMAM G5 at a MOI of 100. A range of IgG concentrations (Privigen®) were incubated with uncoated Ad or Ad/PAMAM G5 complexes for 30 min before application to A549 cells. After 48 h, EGFP expression was analyzed by flow cytometry. Representative data from 3 independent experiments are shown. Mean values (n=2) ± std.dev. are illustrated.

To rule out the possibility, that free PAMAM G5 inactivates the anti-Ad IgG contained in Privigen® an indirect ELISA was performed to check for PAMAM G5-Privigen® interaction. Therefore immobilized Ad was incubated with anti-Ad IgG dilutions (1:250 to 1:512,000), which were either preincubated for 30 min at RT with 100 ng PAMAM G5 in HBG or HBG buffer only. Both conditions tested enabled approximately the same amount of HRP-labeled goat anti-human-IgG antibody to bind to the immobilized Ad, leading to almost identical absorbance curves of the o-phenylenediamine dihydrochloride (OPD) containing substrate solution.

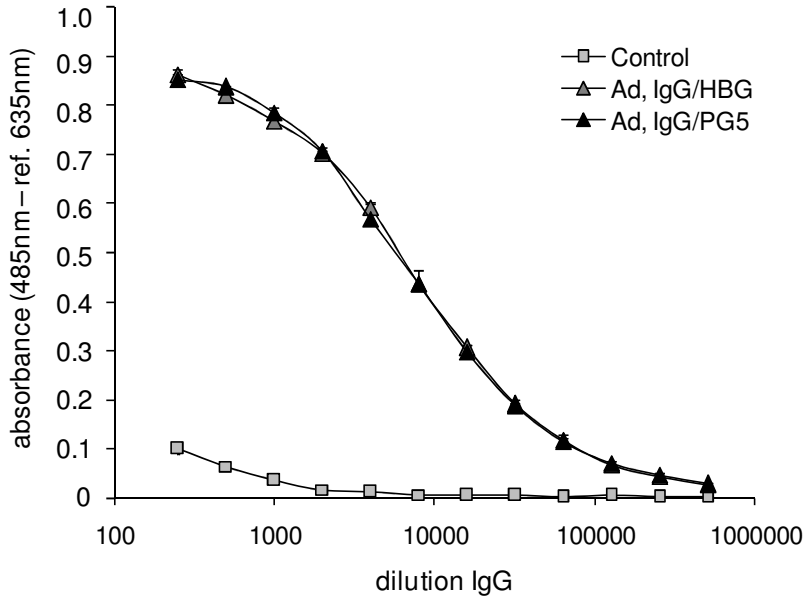

Figure 28. Testing the interaction of anti-Ad IgG with PAMAM G5 using an indirect ELISA
$6x10^8$ VP/well were added to a Nunc Maxisorb 96-well plate and allowed to adhere o.n. at 4°C, while two rows were coated with coating buffer only for control samples (squares). Privigen® dilutions were either incubated with 100 ng PAMAM G5 for 30 min at RT (black triangles) or incubated with HBG buffer (grey triangles) only, before addition to the immobilized Ad. A HRP-labeled secondary antibody was used, followed by an OPD (o-phenylenediamine dihydrochloride) substrate solution. Absorbance was measured at 485 nm with background correction at 635 nm. Mean values (n=3 for samples, n=2 for control) ± std.dev. are shown.

Beside PAMAM G5, PAMAM G3 and PAMAM G2 were also tested for their ability to protect the Ad from neutralizing antibodies. PAMAM G5 gave superior protection compared to PAMAM G3 followed by PAMAM G2 especially when high IgG concentrations were used.

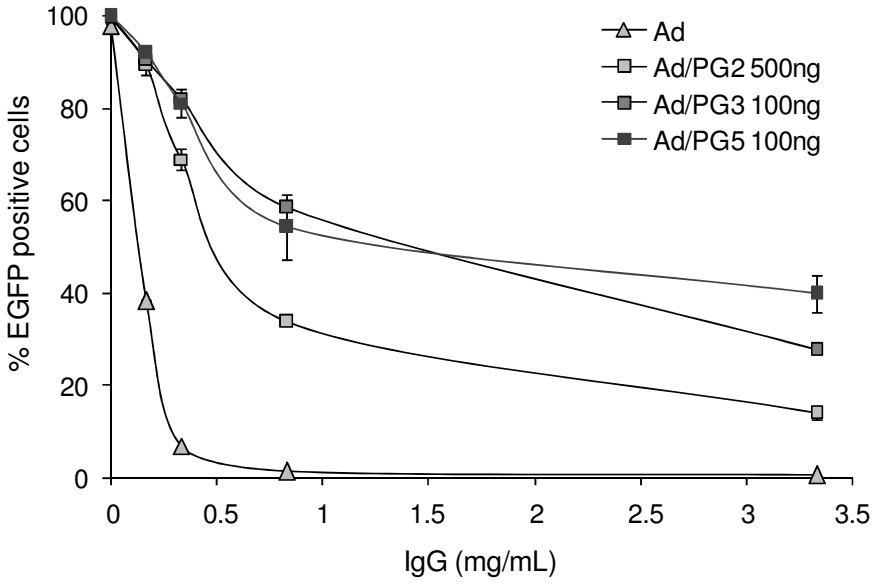

Figure 29. Comparison of the protective ability of PAMAM G2, G3 and G5 coating against neutralizing antibodies

$5x10^4$ A549 cells seeded in 24-well plates were transduced with Ad-EGFP alone (triangles) or coated with 500 ng PAMAM G2 (light grey squares), 100 ng PAMAM G3 (dark grey squares) or 100 ng PAMAM G5 (black sqares) at a MOI of 100. A range of IgG concentrations (Privigen®) were incubated with uncoated Ad or Ad/PAMAM complexes for 30 min before application to A549 cells. After 48 h, EGFP expression was analyzed by flow cytometry. Mean values (n=2) ± std.dev. are shown.

3.8 Factor X binding assay

Besides inactivation by neutralizing antibodies, which becomes important when thinking about a clinical application, two main cellular interactions are responsible for loss of vector as well as appearance of toxicity after intravenous injection. The majority of adenovirus vectors injected intravenously are scavenged by Kupffer cells, macrophages which are located in the liver.[39] Additionally the adenovirus type 5 is known to bind coagulation factor X (FX) with its hexon protein, leading to hepatocyte transduction.[43-45] To examine the potential of PAMAM G5 to abolish FX-hexon interaction and therefore hepatocyte transduction a factor X binding assay was performed (Figure 30). Ad-EGFP coated with increasing amounts of PAMAM G5 was incubated with SKOV-3 cells with or without addition of physiological concentrations of factor X (8 µg/mL) into the transduction media. Two controls were investigated in parallel, one where FX binding was genetically ablated through exchange of the hyper variable region 5 (HVR5) by the peptide CKS 17 binding TGF beta, and a second one where FX binding was chemically ablated due to covalent coupling of a 750 Da MeO-PEG-Mal to HVR5 of an Ad containing a genetically

incorporated cysteine. Like the Ad-EGFP, both were coated with increasing amounts of PAMAM G5 and 72 h after transduction, cells were analyzed for EGFP expression. Independently of the PAMAM G5 concentration used, both control vectors failed to show an increase in transduction efficiency in the presence of FX, proving the FX binding ablation. In contrast Ad-EGFP, when coated with amounts as small as 10 ng of PAMAM G5 caused even higher EGFP levels in the presence of FX than uncoated Ad. This led to the hypothesis that both, PAMAM G5 and FX, contributed to uptake via heparan sulfate proteoglycans (HSPGs). Only when the amounts of PAMAM particles exceeded the amounts of FX molecules, could a reduction in transgene expression in the presence of FX be seen.

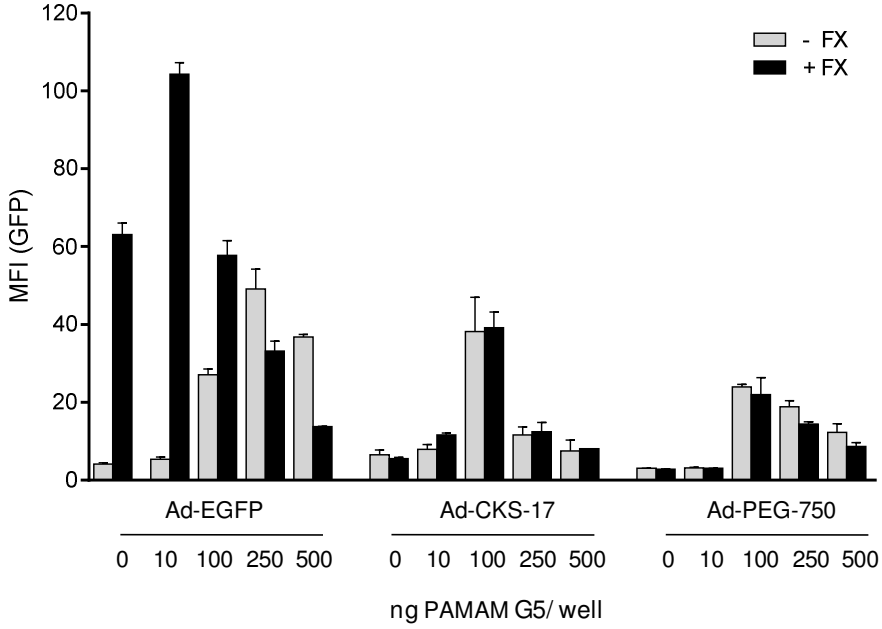

Figure 30. Factor X binding assay

$2x10^4$ SKOV-3 cells seeded into 96-well plates were transduced with 1000 VP/cell Ad-EGFP or the genetically FX-binding ablated Ad-CKS-17 and the chemically FX-binding ablated Ad-PEG-750 Da as controls in the presence (black bars) or absence (light grey bars) of FX at a concentration of 8 µg/mL. After 72 h, EGFP expression was analyzed by flow cytometry. Mean values (n=2) ± std.dev. are shown.

3.9 Targeting of Ad to the epidermal growth factor receptor (EGFR)

Having a system at hand that increases uptake in CAR positive, and to a much stronger extent in CAR negative cell lines, the aim was to increase the specificity of uptake and therefore transgene expression for tumor cells expressing distinct receptors on their surface. EGFR, upregulated in several cancer types like head and neck, ovarian and breast cancer and a common target of antitumor therapies,[85,90] was chosen as the target receptor.

As EGF, the natural ligand for the EGFR, has a mitogenic potential, we used GE11, a peptide ligand known to bind the EGFR without receptor activation.[92] The peptide was coupled to a PAMAM G2 dendrimer via a 2 kDa PEG spacer and a PAMAM G2-PEG-Cys conjugate with a distal cysteine was used as control for Ad coating (Figure 31). In HepG2 cells, which express only low levels of EGFR (MFI 6.6, 29.3% EGFR positive), no significant difference in transgene expression was observed between PAMAM-PEG-Cys and PAMAM-PEG-GE11 coated Ad-EGFP, either by flow cytometry (Figure 31A) or by laser scanning microscopy (Figure 31 C,D). In contrast, the GE11 conjugate was able to induce a significantly higher increase (up to 2.3-fold) in EGFP expression in the highly EGFR positive lung carcinoma cell line A549 (MFI 213.9, 100% EGFR positive) when compared to PAMAM-PEG-Cys coating (Figure 31 B: flow cytometry, E and F: laser scanning microscopy), especially with lower amounts of conjugate.

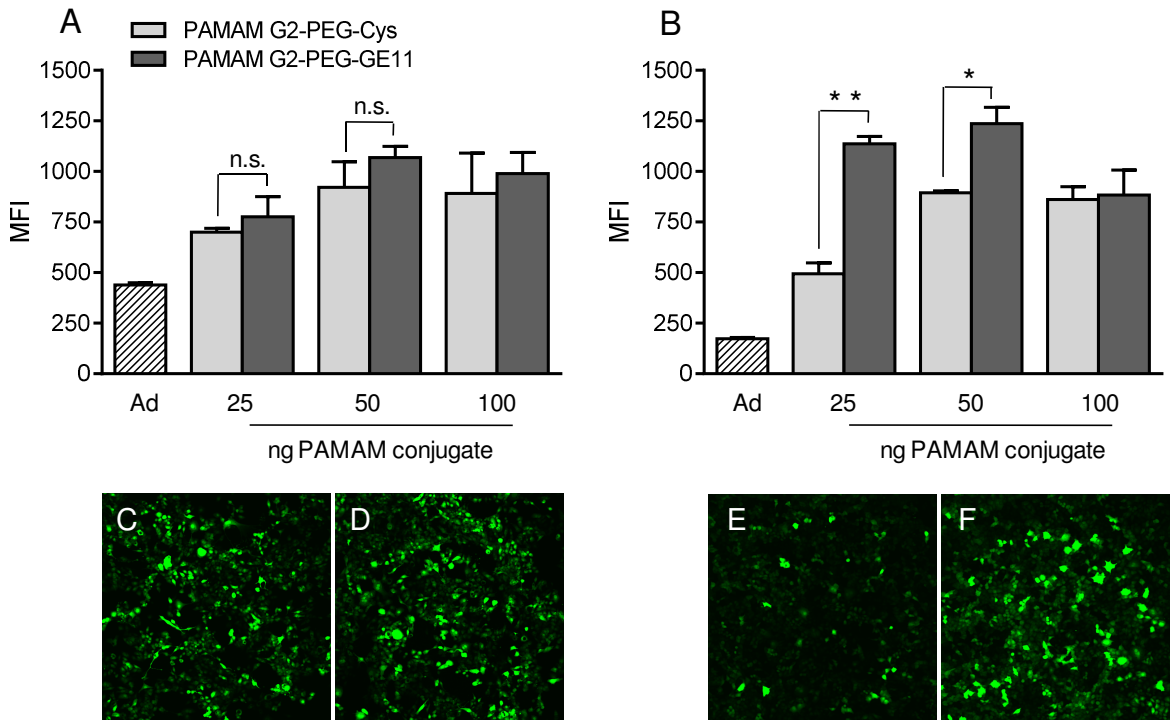

Figure 31. Targeting of Ad to the EGFR using PAMAM G2-PEG-GE11 for coating

HepG2 (A, C, D) or A549 cells (B, E, F) seeded in 24-well plates (A, B) or chamber slides (C-F) were transduced at a MOI of 100 with Ad-EGFP alone or coated with the indicated amounts of PAMAM G2-PEG-GE11 or PAMAM G2-PEG-Cys. EGFP expression was analyzed 48 h after transduction. (A, B) MFI of transduced cells (striped bars: Ad-EGFP, light gray bars: PAMAM G2-PEG-Cys coated Ad, dark gray bars: PAMAM G2-PEG-GE11 coated Ad. (C-F) Laser scanning microscopy of cells transduced with Ad-EGFP coated with 25 ng of PAMAM G2-PEG-Cys (C, E) or PAMAM G2-PEG-GE11 (D, F). * $p<0.05$, ** $p<0.01$, PAMAM G2-PEG-Cys versus PAMAM G2-PEG-GE11, t test unpaired.

To further specify the GE11 targeting effect, the EGFR was downregulated before application of the PAMAM-PEG-GE11 versus its control construct. To find the most effective condition for EGFR downregulation, cells were pre-incubated for 45 min at 37 °C with Cetuximab, an antibody known to cause internalization of the EGFR after binding,[85] or with murine EGF (mEGF), as a substitute for the natural ligand (Figure 32). Thereafter FACS analysis to determine the EGFR level was undertaken, where untreated cells stained for EGFR served as control. From the concentrations tested, 0.1 µg/well worked best for Cetuximab leading to a 1.4-fold reduction in the mean fluorescence intensity (MFI) of the Alexa 488 signal, whereas mEGF in a concentration of 10 µg/well induced a 4.2-fold reduction. Therefore the use of 10 µg/well mEGF was continued for receptor downregulation before transduction.

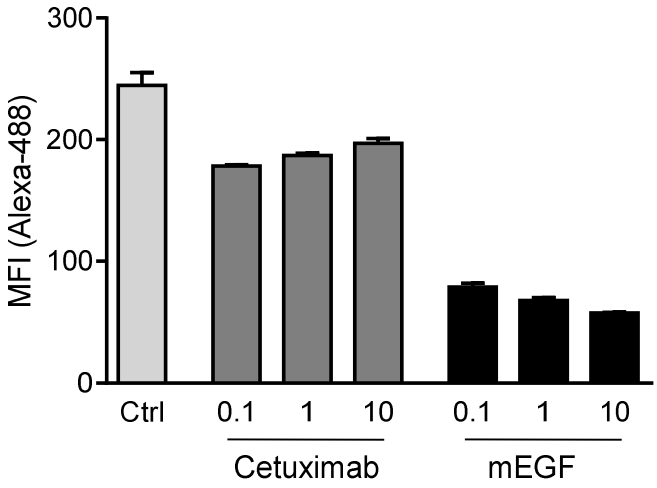

Figure 32. Downregulation of the EGFR using Cetuximab and mEGF

$1x10^4$ A549 cells were seeded in a 96-well plate and incubated with increasing amounts of Cetuximab or mEGF (0.1, 1 and 10 µg/well) for 45 min at 37 °C. Thereafter cells were stained with mouse anti-EGFR followed by Alexa 488 labeled secondary antibody and analyzed by flow cytometry. Untreated cells stained for EGFR served as control. Mean values of Alexa488 signal (MFI) plus std.dev. are shown (n=2).

According to the transduction with Ad-EGFP, transduction using Ad-EGFPLuc and PAMAM G2-PEG-GE11 versus its control construct PAMAM G2-PEG-Cys was performed (Figure 33A). Pre-incubation with mEGF reduced transgene expression of the PAMAM G2-PEG-GE11 coated Ad-EGFPLuc significantly, whereas PAMAM G2-PEG-Cys coated Ad-EGFPLuc was unaffected, further proving the specificity of the system (Figure 33B).

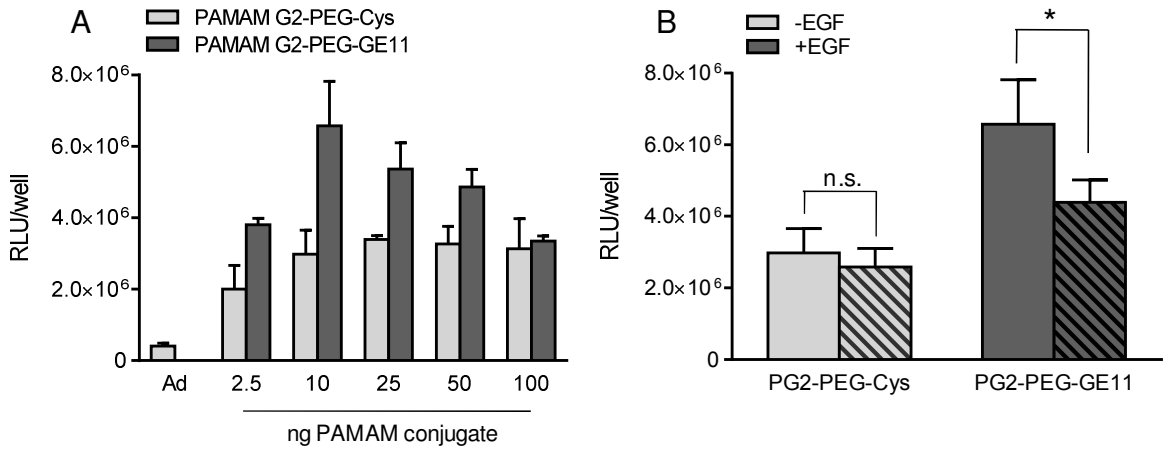

Figure 33. Showing specificity of the PAMAM PEG-GE11 after downregulation of the EGFR (A) $1x10^4$ A549 cells were transduced with Ad-EGFPLuc (MOI 100) coated with PAMAM G2-PEG-GE11 (dark grey) or the control construct PAMAM G2-PEG-Cys (light grey). (B) For the best targeting condition found (10 ng), a pre-incubation with 10 µg/well mEGF is shown. Light and dark grey, respectively, without mEGF pre-incubation, striped bars with mEGF pre-incubation. Mean values (n=3) + std.dev. are shown, unpaired t-test, * $p< 0.05$. Luciferase expression level was evaluated 48 h after transduction, expressed as relative light units per well (RLU/well).

3.10 In vivo experiments on biodistribution

Once the hybrid system of Ad non-covalently coated by PAMAM dendrimers was characterized and optimized in vitro, the protective ability and therefore the inability to target off-target organs like liver and spleen was tested.

For the initial in vivo experiments, the focus was put on biodistribution of the naked versus the PAMAM G5 coated Ad without taking receptor targeting into consideration. Female Balb/c mice with an age of 6-8 weeks where injected intravenously with $3x10^{10}$ VP of Ad-EGFP either uncoated or coated with 250 or 1500 ng PAMAM G5. 72 h later mice were sacrificed by an overdose of isoflurane and organs were harvested. Biodistribution was analyzed by virus copies per cell using qPCR as well as on the transgene expression level by performing laser scanning microscopy on cryosections and fluorometric measurements of liver homogenates.

3.10.1 Fluorometry of liver homogenates

For analysis of transgene expression level, 0.5 g of each mouse liver was homogenized in a conical tissue grinder using 1 ml RIPA buffer (50 mM Tris, 1% NP-40, 0.25% sodium desoxycholate, 150 mM NaCl, 1 mM EDTA, 1 mM PMSF, pH 7.4) and EGFP fluorescence of the supernatant was measured at 488 nm excitation and 512 nm emission

wavelength with a LS50B spectrometer. In the first experiment mice were divided into three groups (n=3), namely Ad only, Ad coated with 250 ng PAMAM G5 and Ad coated with 250 ng of a PAMAM G5 construct carrying a 2 kDa PEG chain and a terminal cysteine (PAMAM G5-PEG-Cys). With 250 ng PAMAM G5 there was already a trend towards increasing fluorescence visible, ranging from Ad over Ad/PAMAM G5-PEG-Cys to Ad/PAMAM G5 (Figure S4, supplementary information). In the second experiment the amount of PAMAM G5 was increased to 1500 ng and two groups were investigated, Ad versus Ad/PAMAM G5 1500 ng (Figure 34). When 1500 ng PAMAM G5 were used for coating a significant 3.2-fold increase in fluorescence intensity for the coated Ad could be seen compared to the uncoated Ad (n=4), therefore exhibiting a targeting rather than a detargeting from the liver.

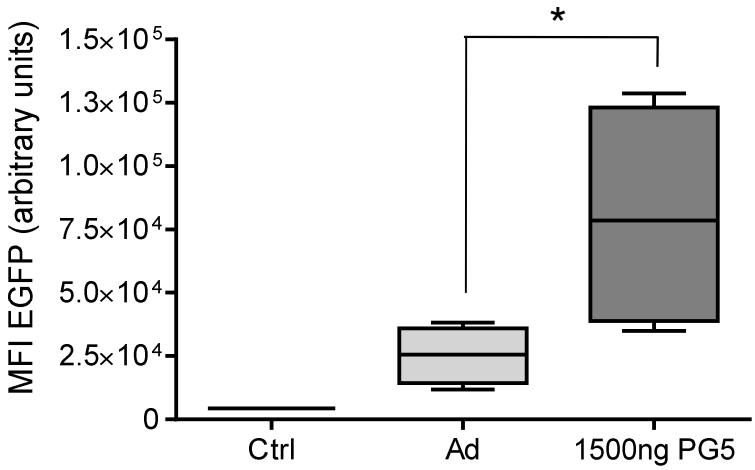

Figure 34. Fluorometric measurement of liver homogenates after Ad versus Ad/PAMAM G5 application

Mice were injected intravenously with either $3x10^{10}$ VP of Ad-EGFP (light grey bar) or Ad-EGFP coated with 1500 ng PAMAM G5 (PG5, dark grey bar) in a PBS/HBG 1:1 mixture. After 72 h mice were sacrificed and prepared liver homogenates were used for EGFP fluorescence measurement at 488 nm excitation and 512 nm emission wavelength. Mean values (n=4) ± std.dev. are shown. Additionally liver fluorescence of an untreated control animal is shown. Unpaired t-test, two-tailed, one sided * $p< 0.05$.

3.10.2 Cryosections

To get an overview of the EGFP expression on a single cell level, 6 µm sections of PFA fixed and Tissue-Tek embedded spleen and liver samples were cut using a Leica CM3050S-cryostat. Samples were analyzed by confocal laser scanning microscopy (Figure 35). Liver sections of Ad coated with 250 ng PAMAM G5 showed again a trend towards higher fluorescence and can be found in the appendix (Figure S4, supplementary information). When

1500 ng of PAMAM G5 was used for Ad coating, liver sections showed a pronounced increase in the number of positive cells and in the intensity of fluorescence, hence matching the results obtained by liver fluorometry. For spleen sections a difference could not be seen by eye for either PAMAM concentration used (Figure 35A).

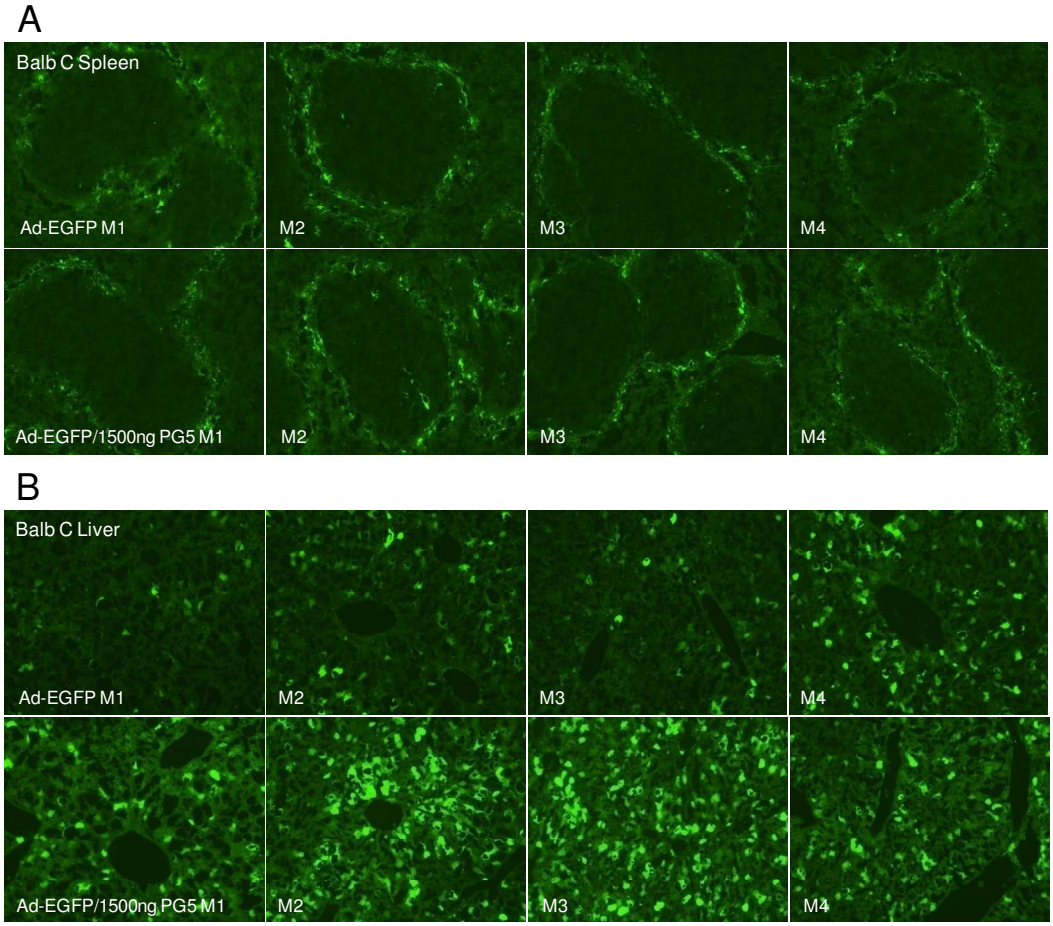

Figure 35. Cryosections of spleen and liver after Ad-EGFP versus Ad-EGFP/PAMAM G5 application

6 µm sections of spleen (A) and liver (B) were cut using a Leica cryostat and analyzed with a confocal laser scanning microscope. Top row in each panel shows Ad only, bottom row shows Ad coated with 1500 ng PAMAM G5 (n=4).

3.10.3 Quantitative real time PCR (qPCR)

Additionally the distribution of virus particles in spleen and liver tissue was analyzed by qPCR (Figure 36). QPCR was carried out by amplification of the Ad E4 gene using 2x Brilliant II SYBR® Green qPCR Master Mix for quantification. C_T values obtained for E4 were normalized to β-actin levels. Copy numbers of Ad/cell were calculated using an E4 standard equation, gained from an E4 standard run in parallel on every plate. The copy numbers of Ad/cell showed a significant increase for the Ad/PAMAM G5 1500 ng liver

samples, while in the spleen samples there was an indication of an increase.

In summary an increase in transgene level, seen by liver fluorometry and cryosections, as well as on the number of virus particles per cell, analyzed by qPCR, was found after PAMAM G5 coating. This effect was more prominent for 1500 ng (equals 1044 molecules/ Ad) than for 250 ng PAMAM G5 (equals 174 molecules/Ad) used for coating.

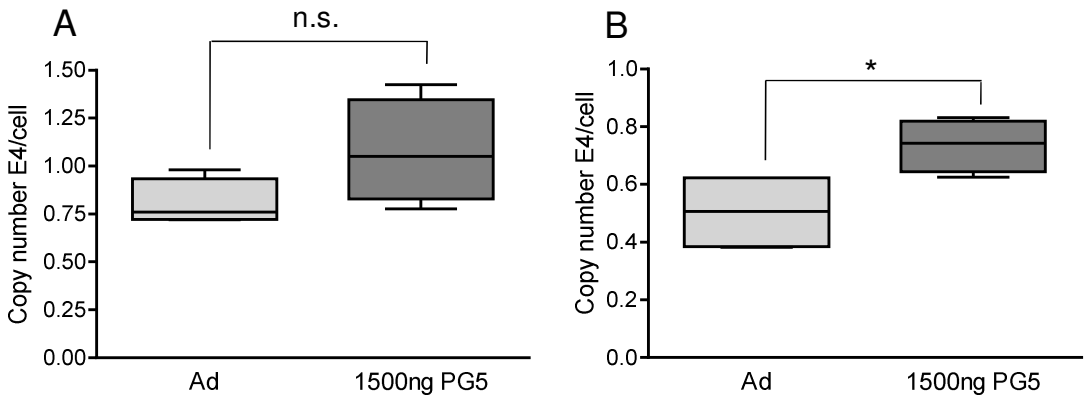

Figure 36. QPCR of Ad E4 gene in spleen and liver tissue after Ad or Ad/PAMAM G5 application A qPCR for the E4 gene of spleen (A) and liver (B) samples after application of Ad (light grey bars) or Ad/PAMAM G5 1500 ng (dark grey bars) application was performed. Samples were run in duplicate and the gained averaged E4 C_T values were normalized against β-actin. Copy numbers of Ad/cell were calculated using an E4 standard run in parallel. Unpaired t-test, two-tailed, * $p< 0.05$.

3.11 Biodistribution study comparing two different mouse strains

The initial animal studies on biodistribution were performed with the immunocompetent BALB/c mice, an albino laboratory-bred strain of the house mouse, which belongs to the most widely used inbred strains. As for tumor implantation an immunodeficient mouse strain was needed, CD 1 nu/nu mice were tested side by side for differences in biodistribution and transgene expression after intravenous Ad (Ad-EGFP) and Ad/PAMAM G5 application. CD 1 nu/nu mice lack a thymus and are therefore unable to produce T-cells, making them ideal models for xenograft research. $2.2x10^{10}$ VP of Ad or Ad coated with 300 ng PAMAM G5 (equals 285 PAMAM molecules/Ad) were injected intravenously in 200 µL of an Opti-MEM/HBG 1:1 mixture. After 72 h mice were sacrificed, and organs harvested for liver fluorometry, laser scanning microscopy of cryosections and qPCR, (Figure 37) as described earlier. After application of Ad/PAMAM G5 compared to Ad only both mouse strains exhibit a clear increase in virus particles per cell (VP/cell) in all organs tested, which was significant for lung of Balb/c and kidney and liver of CD 1 nu/nu. Fluorometry results for Balb/c showed a significant 4.1-fold increase, while results for CD 1 nu/nu showed a trend towards increased fluorometry, but were not

significant due to an outlier in the Ad only group. Cryosections did again confirm the fluorometry results gained. In summary both mice strains indicated an increase of VP/cell as well as in transgene expression levels after PAMAM coating of Ad, with the difference of CD 1 nu/nu displaying an overall higher EGFP expression in the liver, while EGFP expression in the spleen is clearly stronger in the immunocompetent Balb/c. A representative cryosection of lung, kidney (non-target organs) and spleen and liver (natural target organs) is presented in figure 37. An overview of all cryosections can be found in the appendix (Figure S5, supplementary information).

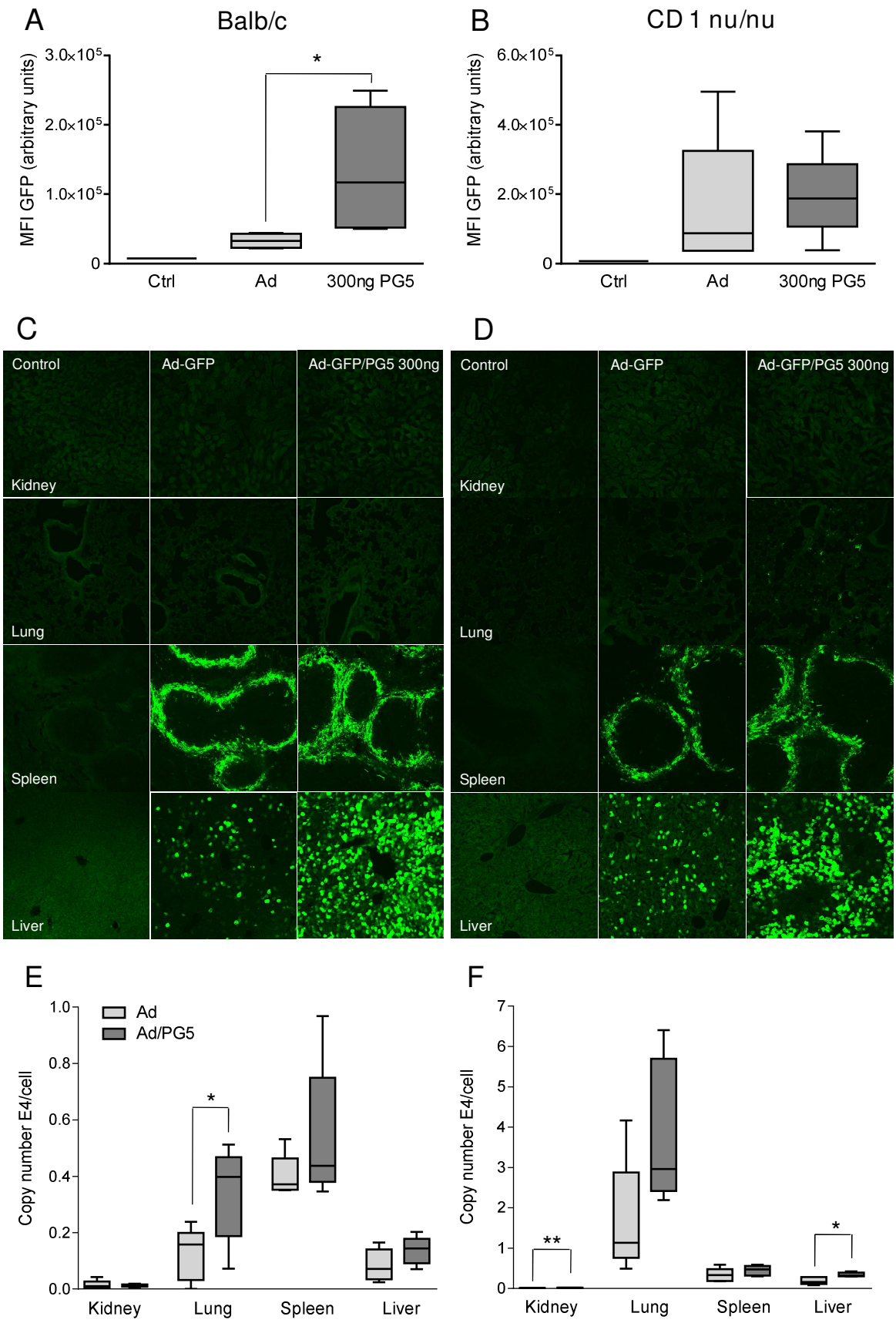

Figure 37. Biodistribution study of i.v. injected Ad versus Ad/PG5 in Balb/c versus CD1 nu/nu Liver fluorometry, cryosections and qPCR results for Balb/c (A, C, E) and CD 1 nu/nu (B, D, F). n= 5, unpaired t-test, two-tailed * $p < 0.05$.

3.12 Establishment of a SKOV-3 intraperitoneal cancer mouse model

In order to reach a well vascularized tumor after intravenous application of Ad, it is important to mediate detargeting from the liver and prevent loss of vector, as well as increasing the circulation half life. As the non-covalent coating approach of Ad-EGFP using PAMAM dendrimers seemed unpromising in mediating this detargeting effect, the idea was to use an alternative application route. Therefore, SKOV-3 LucEGFP ovarian carcinoma cells were implanted intraperitoneally (i.p.) and the Ad should be applied via the same application route, hoping to bypass FX mediated hepatocyte transduction. SKOV-3 cells are known to be hardly transducable by Ad alone,[106] therefore giving the possibility to evidence the PAMAM coating benefit. Additionally up to 60% of ovarian cancers over-express the epidermal growth factor receptor (EGFR),[107] as proved for SKOV-3 cells used in this study, creating the opportunity to target the EGFR using the PAMAM-PEG-GE11 constructs.

3.12.1 In vitro characterization of SKOV-3 LucEGFP cells

3.12.1.1 Quantification of the luciferase and EGFP expression level

The SKOV-3 LucEGFP cells, obtained from the lab of Nori Kasahara, were first tested for their luciferase as well as EGFP expression level (Figure 38). To quantify the luciferase expression 2,000, 5,000 and 10,000 cells were seeded in a 96-well plate and, after 24 h, cells were lysed and a luciferase assay was performed. For 2,000 cells seeded $5.1x10^7$ RLU were found, proving a high luciferase expression level. Additionally the EGFP level was quantified by FACS analysis revealing a mean fluorescence intensity (MFI) of 113 and 94.1% of EGFP positive cells.

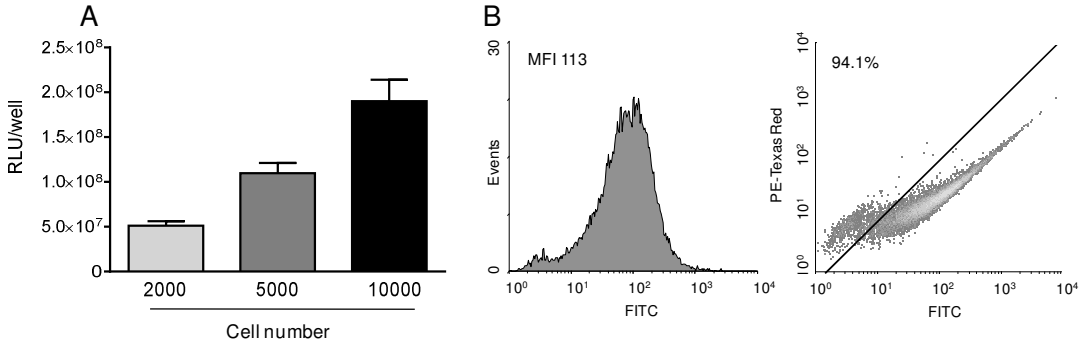

Figure 38. Quantification of the luciferase and EGFP expression level

(A) $2x10^3$, $5x10^3$ and $1x10^4$ SKOV-3 LucEGFP cells were seeded in a 96-well plate. After 24 h, cells were lysed and the luciferase activity was quantified. 2 ng of recombinant luciferase correspond to 10^7 relative light units (RLU). Mean values (n = 6) plus std.dev. are shown.

(B) $2x10^4$ gated cells were analyzed by FACS for EGFP expression using A549 cells as control for laser adjustment (histogram: MFI; density plot: % positive cells).

3.12.1.2 Estimation of the CAR, integrin, TfR and EGFR levels

SKOV-3 LucEGFP cells were analyzed for their coxsackie- and adenovirus receptor (CAR), integrin $\alpha_v\beta_3$ as well as transferrin receptor (TfR) and epidermal growth factor receptor (EGFR) levels using an Alexa 647 labeled secondary antibody (Figure 39). The number of positive cells was obtained by diagonal gating using the APC channel versus the APC Cy7 channel. A low CAR level (MFI 11.7, 28.4% positive) and overexpression of the EGFR (MFI 1346.8, 100% positive) were confirmed.

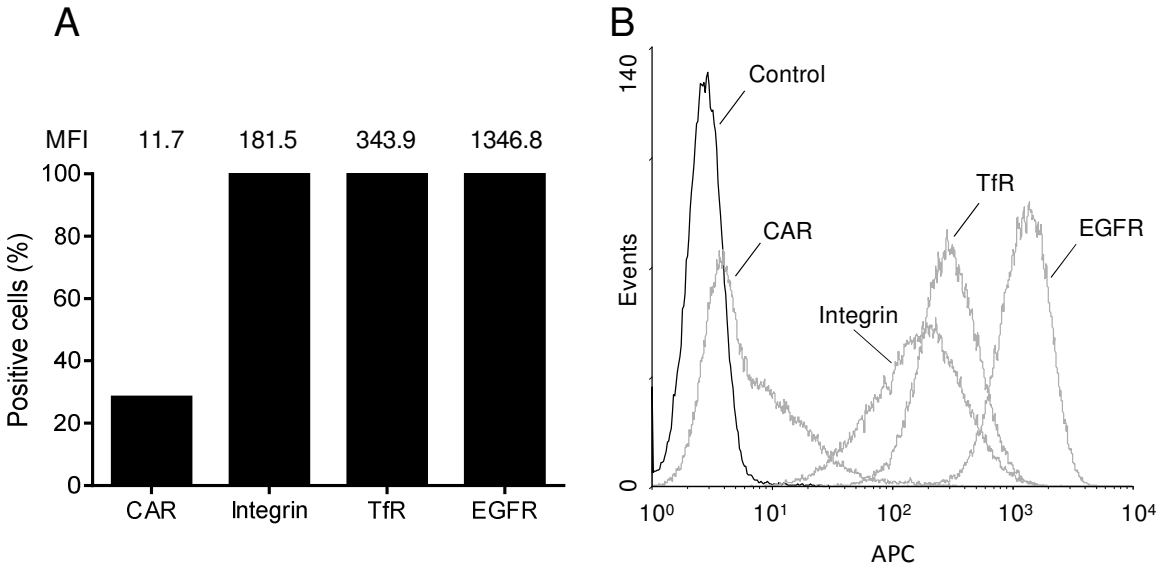

Figure 39. Receptor level estimation of CAR, integrin $\alpha_v\beta_3$, TfR and EGFR
SKOV-3 LucEGFP cells were stained for CAR, integrin $\alpha_v\beta_3$, TfR and EGFR using a 647 labeled secondary antibody and analyzed by flow cytometry. Control staining was performed with a mouse IgG control antibody. The diagram on the left displays the percentage of receptor positive cells for each receptor tested as well as the mean fluorescence intensity (MFI) in the APC channel above each column. The histogram on the right illustrates the shift in the APC channel of receptor positive cells.

To assess the EGFR level of SKOV-3 LucEGFP cells compared with HepG2 (low EGFR expression) and A549 (high EGFR expression) the three cell lines were stained for EGFR using the 647 labeled secondary antibody (Figure 40). For the SKOV-3 LucEGFP a 2.4 fold higher MFI was measured compared to A549, making them the cells with the highest EGF receptor density of the cells analyzed.

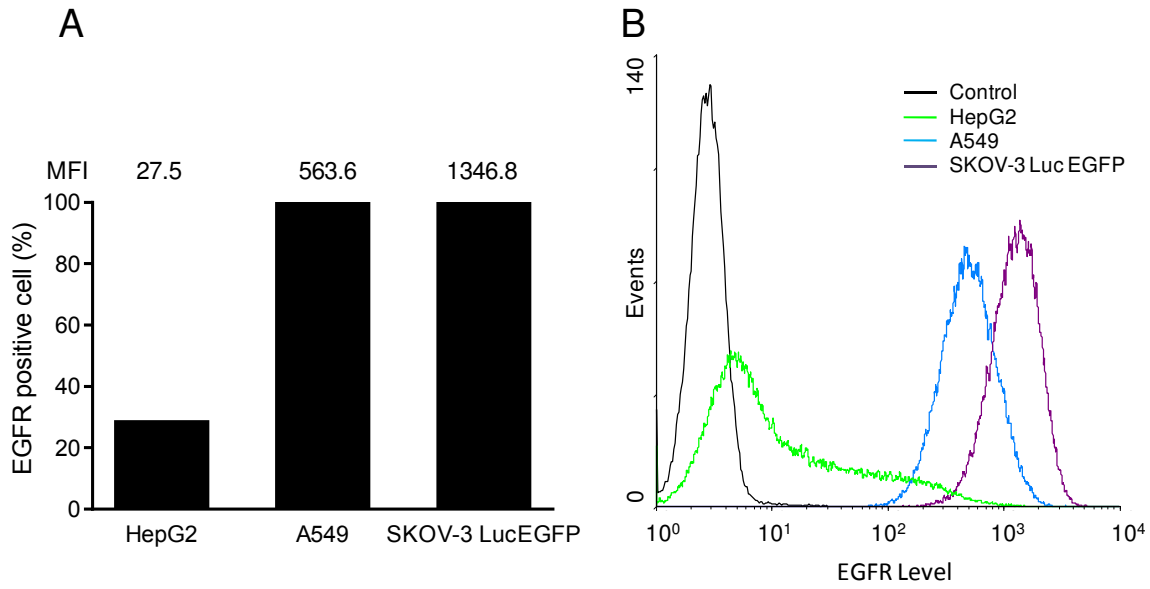

Figure 40. Comparison of the EGFR level of HepG2, A549 and SKOV-3 LucEGFP cells

HepG2, A549 and SKOV-3 LucEGFP were stained for EGFR using a 647 labeled secondary antibody and analyzed by flow cytometry. Control staining was performed with a mouse IgG control antibody. The diagram on the left displays the percentage of receptor positive cells for each cell line as well as the mean fluorescence intensity (MFI) in the APC channel above each column. The histogram on the right illustrates the shift of Alexa 647 positive cells for every cell line.

3.12.2 Establishment of a dual color system

When considering an in vivo application, SKOV-3 LucEGFP provided the opportunity to correlate the luciferase signal with tumor growth, and enabling the best time point for vector application to be found. Additionally due to EGFP expression, tumor tissue can be distinguished from mouse tissue using fluorescence microscopy with an excitation wavelength of 488 nm and a 505/30 band pass filter. To show the possibility that the Ad infected cells are in fact SKOV-3 LucEGFP cells, an Ad expressing a fluorescent transgene with a wavelength distinguishable from that of EGFP was needed. Therefore a mCherry transgene containing construct under an EF1α-promotor was cloned. mCherry has an excitation maximum at 587 nm and an emission maximum of 610 nm. Excitation wavelength and emission filter combinations for both fluorophores were optimized for laser scanning microscopy (LSM) as well as FACS analysis. LSM was performed later using a 488 nm argon laser for extinction and a 505-530 nm band pass filter for detection of EGFP. For mCherry a 543 nm helium-neon laser was used for excitation and a 560 nm long pass filter for detection. For FACS analysis an excitation wavelength of 488 nm was used for EGFP with a 530/40 nm band pass filter for detection. The optimum excitation for mCherry was gained with the 488 nm laser, while for detection a PE-Cy5 filter (680/30 nm)

was used. In the FACS optimization process diagonal gating of the FITC versus the PE, PE-Texas Red, PE-Cy5, PE-Cy7 and APC channel was performed, and are presented in figure S6 in the appendix. A scheme showing the excitation and emission spectra of EGFP and mCherry, as well as the laser excitation wavelengths and emission filters is illustrated below (Figure 41).

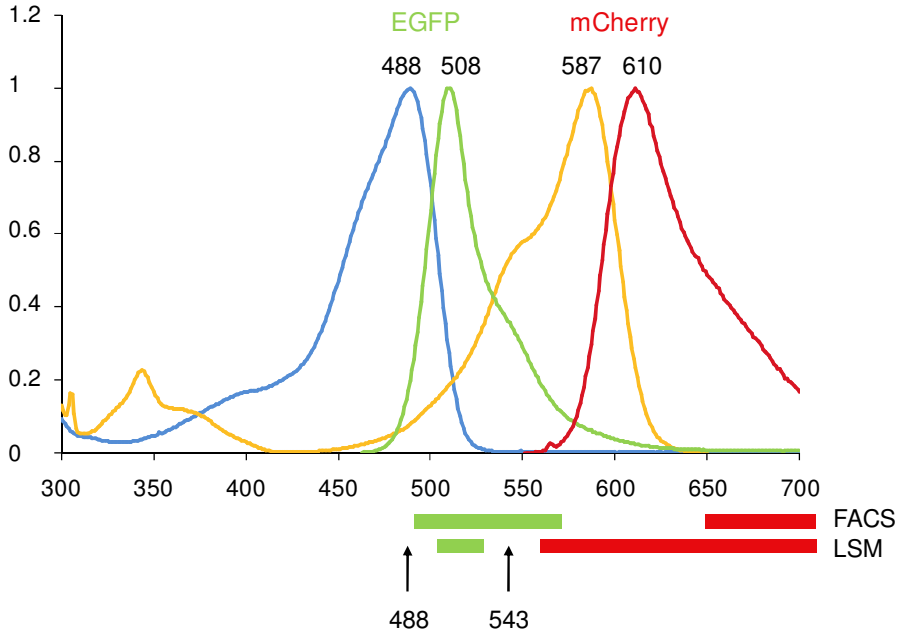

Figure 41. Excitation and emission spectra of EGFP and mCherry

The excitation and emission spectrum for EGFP is illustrated in blue and green respectively. For mCherry the excitation spectrum is shown in orange and the emission spectrum in red. Peak wavelengths are depicted above the spectra and laser excitation wavelengths and emission filters are illustrated with an arrow or colored bar below the spectra. EGFP and mCherry spectra were created using http://www.tsienlab.ucsd.edu/Documents.htm and adapted from (Picard, Experimental Cell Research, 2006).[108]

3.12.2.1 Cloning of the Ad-mCherry construct

As starting vectors the pCpG-hCMV EF1α-TNF and the pCpG-hCMV SCEP-mCherry, cloned by Rudolf Haase, were used. Both were digested with HindIII and SpeI and the EF1α-promotor inserted into the mCherry containing backbone. This resulted in the 3667 bp construct pCpG-hCMV EF1α-mCherry carrying a zeocin resistance. The insertion of the EF1α promotor was verified by digestion with the restriction enzymes SmlI and NheI. In the final step the pCpG-hCMV EF1α-mCherry was digested with PacI and inserted into a pGs66 backbone also cut with PacI (Figure 42). The 38727 bp construct pGs66-hCMV EF1α-mCherry was linearized with SwaI and N52E6 cells were transfected with the help of LPEI for virus production.

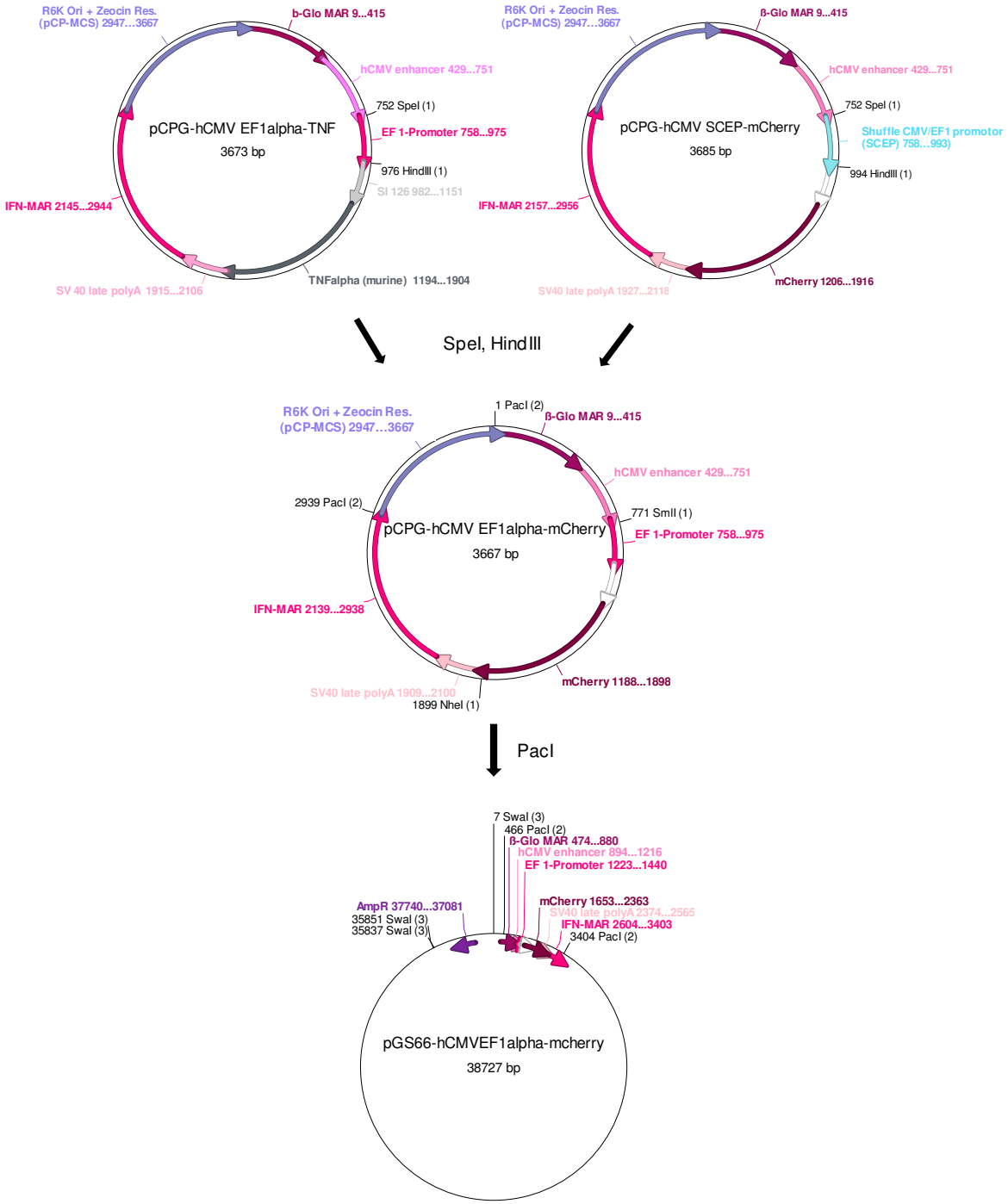

Figure 42. Cloning scheme for Ad-mCherry

Step 1: The EF1α promoter was cut out of the pCpG-hCMV EF1α-TNF construct by HindIII and SpeI and inserted into the pCpG-hCMV-mCherry backbone. Step 2: The hCMV-EF1α-mCherry expression cassette was cut out by PacI and inserted into the PacI site of the pGs66 backbone.

3.12.2.2 Comparison of PAMAM G2, G3 and G5 for coating of Ad-mCherry

SKOV-3 LucEGFP cells were transduced with Ad-mCherry only or coated with PAMAM G2, G3 or G5 at an optimized amount and analyzed by FACS and LSM to prove that both fluorophores could be detected separately (Figure 43 A-C).

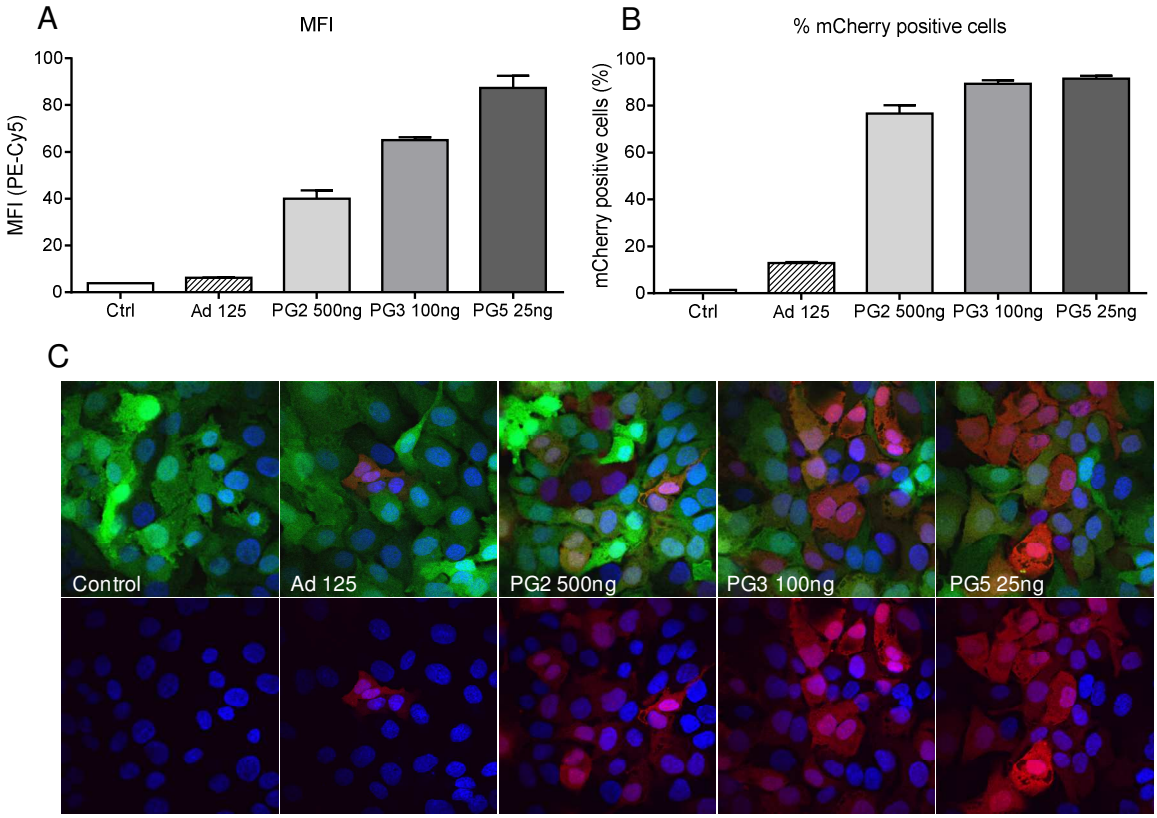

Figure 43. Evaluation of the beneficial effect of PAMAM G2, G3 and G5 coating by FACS and LSM using Ad-mCherry at a MOI of 125

$2.5x10^4$ SKOV-3 LucEGFP cells seeded in 24-well plates (FACS) or 8-well chamber slides (LSM) were transduced at a MOI of 125 with Ad-mCherry alone or coated with the indicated amount of PAMAM G2, G3 and G5. After incubation for 48 h, cells were either subjected to FACS analysis or LSM imaging. (A-B) FACS analysis of SKOV-3 LucEGFP transduced with Ad-mCherry only (stripped bars) or coated with PAMAM G2 (light grey bars), PAMAM G3 (medium grey bars) or PAMAM G5 (dark grey bars). (A) Illustrates the mean fluorescence intensity (MFI) gained in the PE-Cy5 channel, while (B) shows the percentage of transduced cells. Mean values (n=3) plus std.dev. are shown. (C) Laser scanning microscopy (LSM) images of control cells versus Ad-mCherry only and Ad-mCherry coated with PAMAM G2, G3 and G5. Upper panel shows the EGFP signal from SKOV-3 LucEGFP cells as well as the mCherry signal. The lower panel depicts the mCherry signal only.

As seen before, with other low CAR level cell lines using Ad-Luc, the most beneficial effect on transduction was gained by PAMAM G5 coating, followed by G3 and G2. With PAMAM G5 used for coating and Ad-mCherry at a MOI of 125, 91.5% of mCherry positive cells were observed compared to 12.9% with uncoated Ad. The increase in the number of positive cells as well as an increase in the intensity of fluorescence from PAMAM G2 to G5 was confirmed by laser scanning microscopy (LSM) shown in figure 43 C, with a 63x magnification. 10x magnification images of all PAMAMs can be found in figure S7 in the appendix.

When using Ad-mCherry at a MOI of 500 for transduction (Figure 44), the percentage of mCherry expressing cells was above 97% for all the PAMAM generations tested and the increase in MFI reached a maximum of 28-fold higher for PAMAM G5 coating in relation to uncoated Ad-mCherry. Images at 63x magnification and 10x magnification, to give an overview of effectively transduced cells, are exemplified in figure 44C for PAMAM G5 coating.

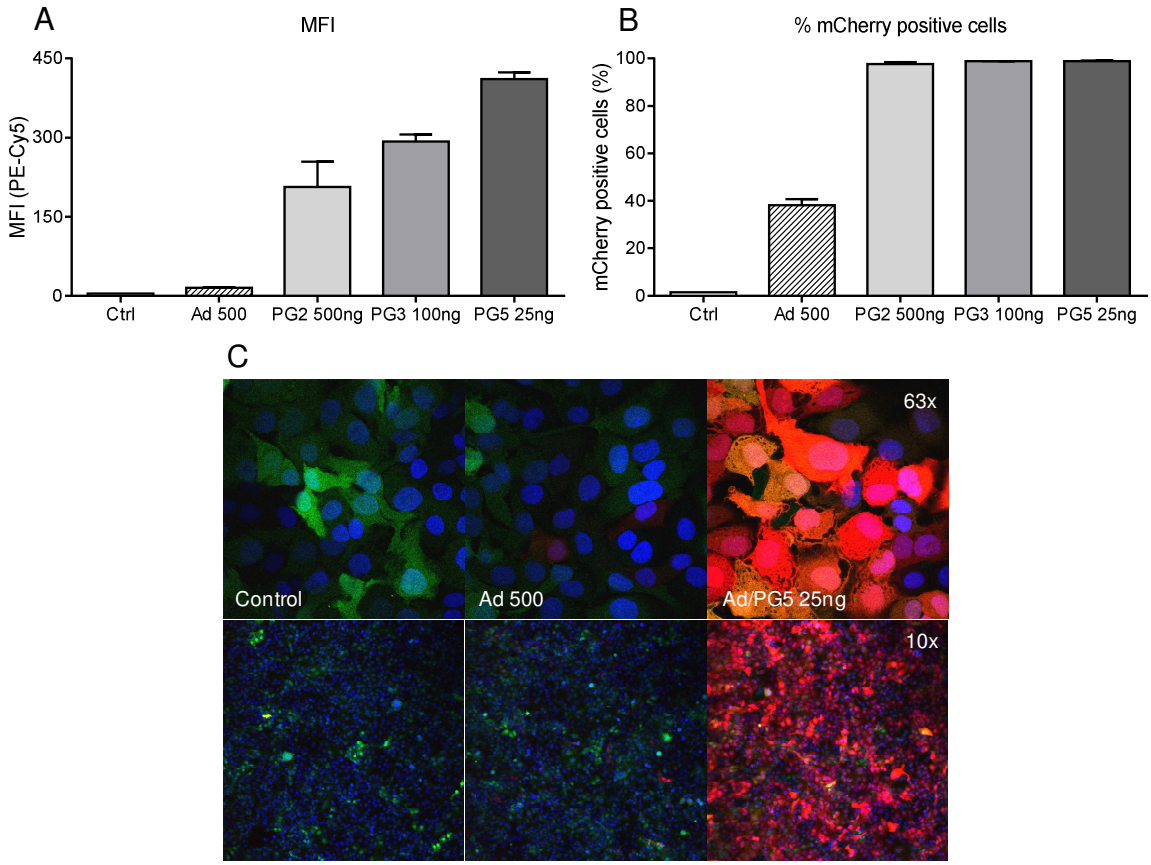

Figure 44. Evaluation of the beneficial effect of PAMAM G2, G3 and G5 coating by FACS and LSM using Ad-mCherry at a MOI of 500

Experimental setup as shown in figure 43. (A-B) FACS analysis illustrating the MFI (A) versus % of positive cells (B). (C) LSM images of control, Ad-mCherry only and PAMAM G5 coated Ad-mCherry in a 63x magnification (top panel) and a 10x magnification (lower panel).

3.12.2.3 Comparing PAMAM-PEG-GE11 generation 2, 3 and 5

Ad coated with PAMAM G2-PEG-GE11, which had been proven to effectively target the EGFR, overexpressed on A549 cells, was directly compared to complexes formed with PAMAM G3-PEG-GE11 and PAMAM G5-PEG GE11. As individual control, a PAMAM-PEG-Cys of the particular generation was used for coating. For PAMAM G2-PEG-GE11 a significant increase in the intensity of fluorescence was measured by FACS analysis compared to the PAMAM G2-PEG-Cys construct. For PAMAM G3-PEG-GE11 a tendency towards higher fluorescence could still be seen, and in the case of PAMAM G5-PEG-GE11 the cysteine construct gained higher fluorescence levels than the targeting construct. As with the lower generation PAMAMs a higher amount of dendrimer was needed for an optimal coating benefit, a higher GE11 density was present in the complexes. In the case of PAMAM G2-PEG-GE11 compared to G3 there was a 6-fold difference in GE11 concentration and an even bigger difference, 56-fold, between generation 2 and 5.

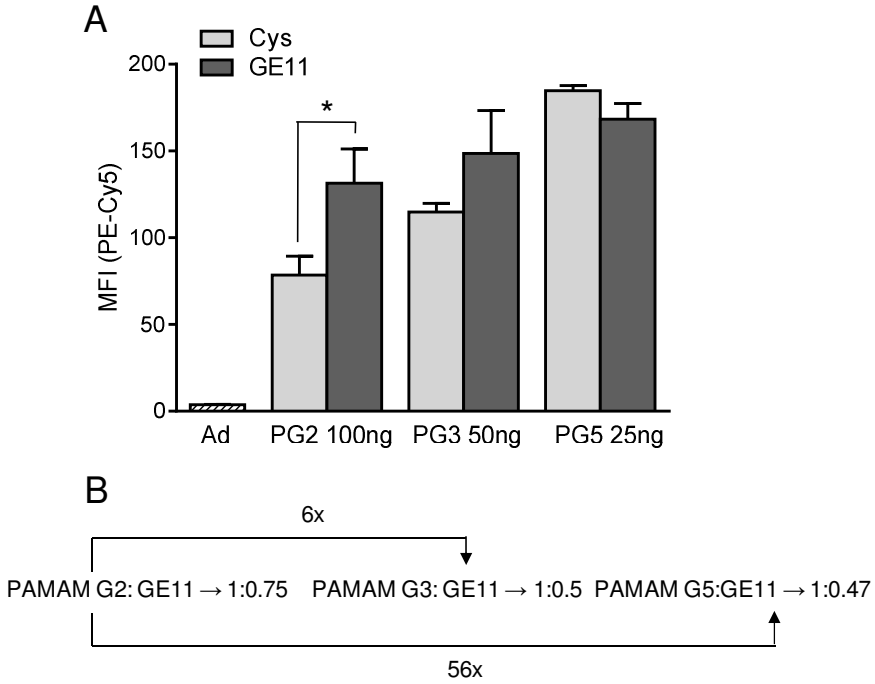

Figure 45. Comparing the different PAMAM-PEG-GE11 constructs for their targeting properties (A) $2.5x10^4$ SKOV-3 LucEGFP cells were seeded in 24-well plates and transduced with Ad (MOI 125) only or coated with PAMAM-PEG-GE11 or the respective control construct PAMAM-PEG-Cys of each generation for 2 h at 37 °C. $2x10^4$ gated cells were analyzed by FACS using the FITC versus the PE-Cy5 channel for diagonal gating. MFI of transduced cells (striped bar: Ad-mCherry, light gray bars: PAMAM-PEG-Cys coated Ad, dark gray bars: PAMAM-PEG-GE11 coated Ad of the indicated PAMAM generations). Mean values (n=3) plus std.dev. are shown.* $p < 0.05$, t test unpaired. (B) Scheme of the coupling ratio of PAMAM to GE11 for every generation, including the fold increase in GE11 present, with respect of the amounts of PAMAM used for coating.

3.12.3 In vivo characterization of SKOV-3 LucEGFP cells

3.12.3.1 Luciferase imaging

After in vitro characterization, including evaluation of the luciferase and EGFP gene expression level, the receptor expression levels as well as the transduction benefit through PAMAM coating of Ad, SKOV-3 LucEGFP cells were tested for their in vivo characteristics. Therefore $5x10^6$ SKOV-3 LucEGFP cells were injected intraperitoneally (i.p.) into Rj:NMRI-nu (nu/nu) mice on day 0 and luciferase imaging was performed twice per week using a CCD camera (IVIS Lumina™) and the Living Image software 3.2 (Caliper Life Sciences, Hopkinton, USA). For imaging mice were anesthetized with 3% isoflurane in oxygen, 100 µL luciferin solution (c=60 mg/mL) was injected i.p. and light efflux recorded after 10 min. Mice showed a lag phase in tumor growth of two to four weeks, where luciferase signals barely remained constantly, after which the signal increased exponentially (Figure 46). At the time point mice were killed tumor nodules were below 5 mm.

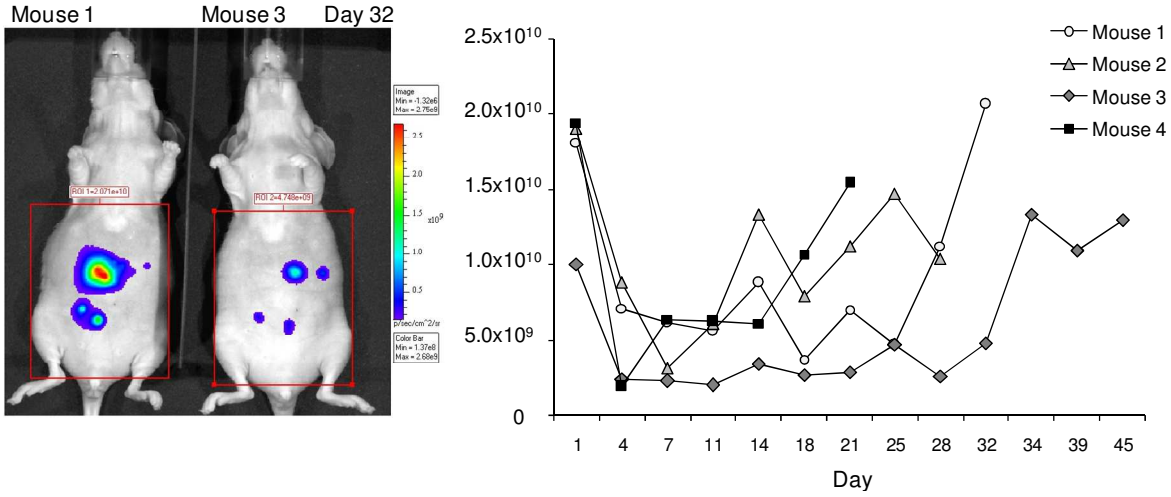

Figure 46. Luciferase imaging of SKOV-3 LucEGFP cells implanted i.p. in NMRI mice
$5x10^6$ SKOV-3 LucEGFP cells were injected intraperitoneally in NMRI nude mice and luciferase imaging performed twice per week. Mice were sacrificed between day 21 and day 45 when the exponential growth phase started. Organs were harvested, fixed with PFA and embedded in paraffin.

After removal of the organs luciferase imaging was performed to highlight the SKOV-3 LucEGFP tumors (Figure 47). Tumor nodules were typically found in the lesser curvature of the stomach, between the liver lobes, in the adherent tissue of the spleen and in the small and large intestines.

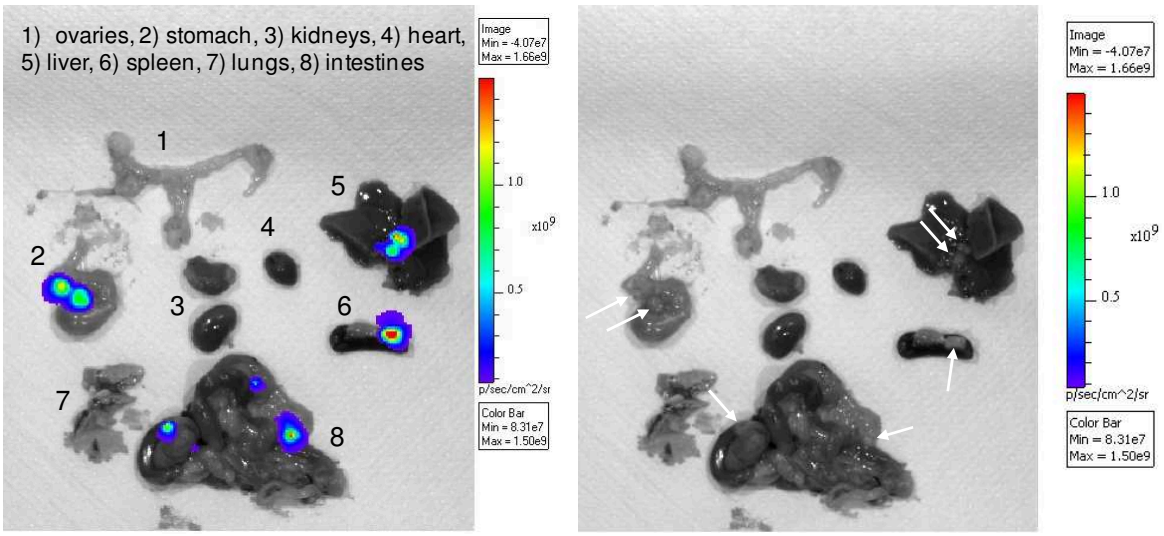

Figure 47. Luciferase imaging of organs carrying tumor nodules

After mouse 3 was sacrificed at day 45, 10 min after luciferin application, organs were removed and a luciferase imaging performed. Numbers refer to the organs listed in the picture on the left. The white arrows on the right depict the tumor nodules.

3.12.3.2 Hematoxylin and eosin (H/E) staining

Organs were fixed in 4% PFA, embedded in paraffin and cut in 5 µm sections before H/E staining was performed. The typical organs with tumor burden, namely liver, spleen, stomach and small intestines were investigated to get an idea of the tumor morphology (Figure 48). Tumor nodules adhering to the stomach and small intestines were rather solid whereas in liver and adherent tissue of the spleen infiltration of tumor cells into healthy tissue could also be seen.

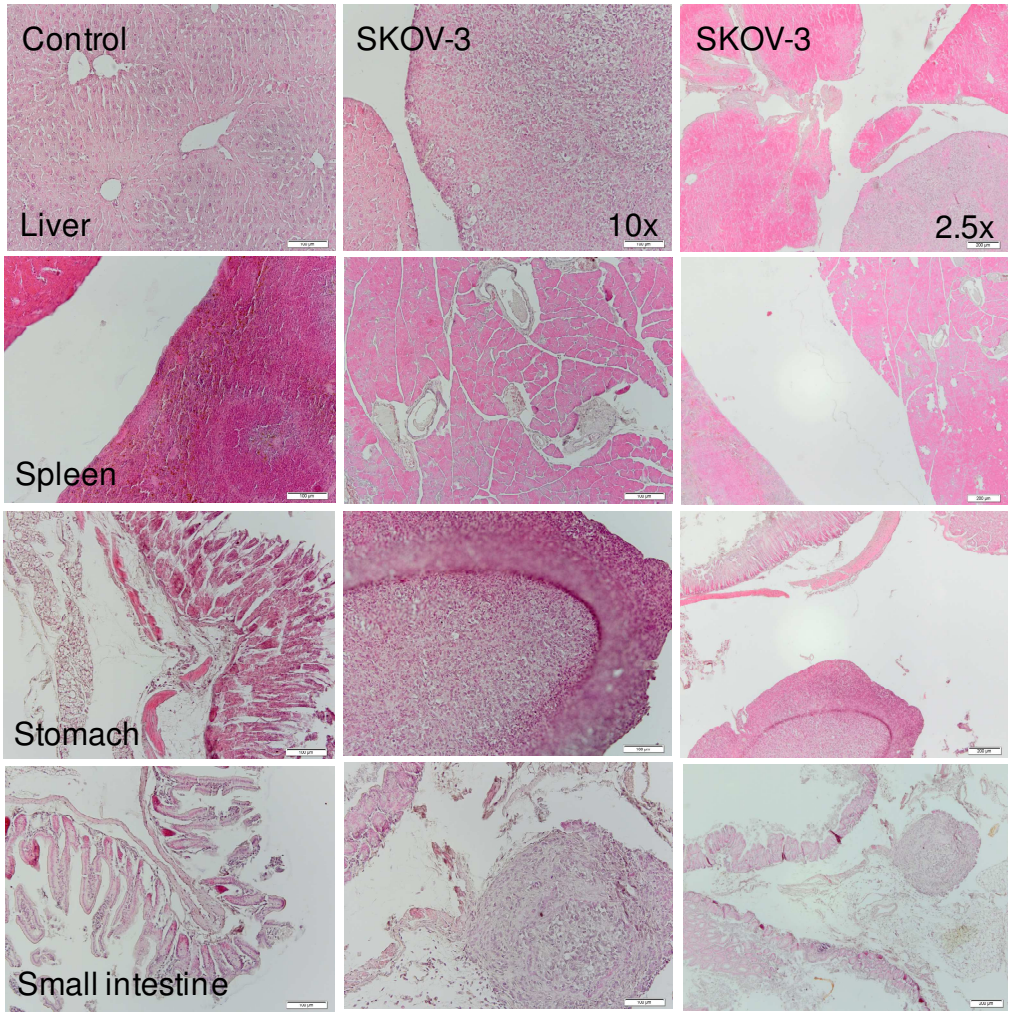

Figure 48. Hematoxylin and eosin staining of SKOV-3LucEGFP i.p. samples and control tissue

PFA fixed and paraffin embedded tissue samples from mouse 3 at day 45, were cut in 5 µm sections and stained with hematoxylin and eosin. Liver, spleen, stomach and small intestine samples are illustrated. First column shows a control animal, second (10x magnification) and third column (2.5x magnification) shows SKOV-3 LucEGFP implemented tumors.

4 DISCUSSION

4.1 In vitro evaluation of non-covalent Ad coating with PAMAM dendrimers or LPEI and BPEI polymers

Chemical modification of adenovirus capsids with polymers or lipids has been described, by several groups, to be beneficial for the reduction of the immune response, enhancement of transduction efficiency and targeting to receptors others than CAR.[46-48] In this study cationic PAMAM dendrimers, linear polyethylenimine (22 kDa) and branched polyethylenimine (25 kDa) were utilized to coat the Ad capsid by virtue of electrostatic interaction to make cell lines with low CAR levels accessible to Ad infection. Targeting to the epidermal growth factor receptor (EGFR) was achieved with the EGFR binding peptide GE11, covalently coupled to the PAMAM dendrimers via a 2 kDa PEG spacer. This represents a significant alternative to genetic targeting approaches, where ligands are usually presented at the distal end of the fiber.[109]

Structural studies of Ad/PAMAM G5 complexes by TEM revealed, that mostly single capsids and some moderate aggregates existed, which were completely coated with PAMAM G5 above a ratio of 200 PAMAM G5 molecules per capsid (Figure 7 and 8). Early studies conducted with cationic liposome-coated Ad showed only large aggregates of several capsids.[72] Nevertheless, for further in vivo studies, e.g., systemic tumor targeting, this would be less beneficial. Furthermore the surface charge of Ad/PAMAM G5 complexes was investigated. When evaluating the surface charge by measuring the zeta potential of Ad, coated with increasing amounts of PAMAM G5, a reversal of charge was observed after coating, leading to positively charged particles (Figure 9). The reverse in surface charge enabled easier binding to the negative cell surface, explaining the enhacement in transduction efficiency seen after coating. To check for the stability of the complexes in solution and during cellular uptake, co-localisation of Ad-Alexa488 and PAMAM G5-Cy5 was analyzed, quantitatively and qualitatively, using the histo and profile tool within the Zeiss 510 META software. With a co-localisation coefficient, calculated according to Manders,[105] of 0.7 to 0.8 a high degree of signal correlation was detected within the cells (Figure 14B) and as PAMAM G5 coated Ad was even found in the perinuclear region of cells (Figure 13 and 14A), it was deduced that Ad/PAMAM G5 complexes were transported together once inside the cell, and that coating did not adversely affect transport toward the nucleus. After evaluating the level of receptors, associated with adenovirus binding and uptake (CAR, $\alpha_v\beta_3$ integrins) (Figure 18 and S1,

supplementary information), in various cancer cell lines, U87MG and HuH7 were chosen as cell lines expressing low and high levels of CAR, respectively, to study differences in uptake of Ad-Alexa488 versus Ad-Alexa488 coated with PAMAM G5-Cy5. When analyzing Ad uptake, semi quantitatively, by flow cytometry, U87MG as a low CAR expressing cell line showed highly elevated levels of cellular uptake after coating (Figure 19A). In contrast, the increase in HuH7 cells was less pronounced, as the uptake rate for uncoated Ad in this cell line was already prominent (Figure 19B), probably due to high basal levels of CAR. This clearly points to a correlation between high CAR level and Ad binding, so that the higher the level the higher the binding, followed by more effective cellular uptake. Ad uptake in cells with low susceptibility to transduction could be improved through non-covalent PAMAM coating. As the binding capacity of negatively charged Ad capsids for cationic molecules is limited, an excess of cationic charge might result in free PAMAM molecules, apart from virus bound ones, which can compete for cellular uptake. This has already been shown for nonviral transfections, where free polycations can be advantageous for the endosomal release of plasmid DNA delivered, but at the same time can also compete for cellular uptake.[100] In addition, it appears that similar effects, in terms of competition, may also occur with Ad. While Ad association could not be further boosted using amounts higher than 10 ng PAMAM G5-Cy5, the fluorescent signal was increased further at a dose of 100 ng, indicating the uptake of free dendrimer (Figure S2, supplementary information). In order to visualize the uptake of PAMAM G5-Cy5 coated Ad-Alexa488 in U87MG and HuH7 cells, laser scanning microscopy (LSM) studies were performed. LSM studies revealed that low amounts of PAMAM G5 enabled internalization of small coated Ad particles, whereas with 100 ng there was a tendency towards the formation of larger particles, which led to strong aggregation at the membrane especially on HuH7 cells (Figure 19H). Additionally, the aggregation behavior of the Ad/PAMAM G5 complexes was compared with Ad/LPEI, as it is known that polyplexes consisting of LPEI and plasmid can rapidly aggregate on the cell surface, when added to the cell culture media.[110] When conducting LSM studies, with 10 ng of each polycation, LPEI/Ad complexes were found to form large aggregates remaining mostly on the cell surface, whereas PAMAM/Ad complexes remained small and were readily internalized (Figure 20).

Initially, cell transductions were carried out in the low and the high CAR expressing cell lines U87MG and HuH7 respectively, to determine optimal amounts of PAMAM G5 needed for Ad coating (Figure 22). In addition, LPEI was utilized for Ad coating, as this polycation is currently one of the most efficient transfection reagents on the market for

nonviral gene delivery.[111] With PAMAM G5, low concentrations boosted transgene expression in U87MG cells, but only marginally increased transduction efficiency in HuH7 cells. In sharp contrast, LPEI only moderately increased the transduction efficiency in U87MG cells, whereas in HuH7 cells LPEI led to a strong decrease. These observations matched the uptake results which indicated an impaired internalization of Ad/LPEI complexes. Interestingly, the beneficial effect was not entirely due to the branched (PAMAM) versus linear (LPEI) structure of the polycation, since the beneficial effect of coating using the highly branched 25 kDa BPEI, which bears a branch point on about one third of nitrogen atoms, was even lower than with LPEI (Figure 23). This is in line with higher transfection efficiency for LPEI over BPEI in non-viral gene therapy, where LPEI supported microtubule associated transport, whereas BPEI did not.[110] One reason for the superiority of PAMAM over LPEI and BPEI seemed to be a difference in cellular toxicity: It has been shown in earlier studies that the PAMAM G5 dendrimer was virtually nontoxic up to a concentration of 20 µg/mL in vitro.[74] When comparing PAMAM G5 and LPEI polyplexes after systemic administration, in vivo, PAMAM G5 was well tolerated up to a dose of almost 7 mg/kg, whereas the LPEI polyplexes [74] and BPEI polyplexes [112] induced liver toxicity at 2 mg/kg. In this study a similar trend was observed, where LPEI and BPEI coated Ad led to pronounced toxicity, in vitro, above 50 ng/well and 100 ng/well respectively, whereas PAMAM G5 was well tolerated up to 1,000 ng/well (Figure 22 C,D and 23 C,D). Besides the toxicity observed, the impaired internalization seen for Ad/LPEI complexes appeared to be the reason for the lower transduction efficiency. It can be concluded from these data, depending on the cell line, that an excess of polycation can induce toxic effects (in the case of LPEI), compete with coated Ad for cell uptake or lead to accumulation on the cell surface (PAMAM and LPEI on HuH7). It was also apparent, that PAMAM coating of Ad could compensate for lack of CAR mediated binding. To confirm that uptake by this route also resulted in successful transduction, the increase in transduction efficiency obtained with PAMAM G5 coating of Ad was correlated to the CAR level in different cell lines with varying CAR expression levels (Figure 25). A clear inverse correlation was seen between the CAR expression level and the increase in transduction efficiency: in SKOV-3 and U87MG cells, which express low levels of CAR, transduction was increased 46- and 38-fold respectively, A549 cells with medium CAR expression levels showed a 10-fold increase, whereas in DU145 and HuH7 cells exhibiting high CAR expression levels, the increase was marginal. For nonviral polyplexes, it has been postulated that cellular binding and internalization occurs via heparan sulfate proteoglycans (HSPGs).[113] It also seems that polycation coated Ad particles can be

retargeted to this pathway, which leads to efficient transduction. Polycation induced toxicity usually increases with molecular weight,[74] hence lower generation PAMAMs (G2 and G3) were screened for their ability to improve Ad transduction (Figure 24). Although on most cell lines the highest increase was found for PAMAM G5, PAMAM G3 and G2 also led to considerable enhancement. With the latter PAMAM generations, however, higher concentrations were necessary to obtain optimal transduction efficiency. Former studies by Haensler et al. demonstrated that only PAMAM G > 4 were able to transfect cells with plasmid.[114] In the case of Ad/PAMAM complexes the increase in cellular binding, followed by enhanced cellular uptake, appeared to be efficient for all dendrimers tested, whereas endosomal escape and nuclear translocation of transferred DNA was achieved by Ad alone. With a polycationic transfection reagent at hand, which enhances both viral and plasmid mediated gene delivery, a side-by-side comparison of both systems was conducted (Figure 26). With an optimized plasmid content of 400 ng and PAMAM G5/plasmid w/w ratio of 2/1, the luciferase activity measured was still 5-fold below the activity achieved with uncoated Ad-EGFPLuc in the low CAR expressing cell line U87MG. When calculating the number of DNA molecules used per well, optimal nonviral transfection still required a 3,700-fold higher number of gene copies when compared to the total Ad particles, and a 57,000-fold higher number in relation to the infectious Ad particles. Although the uptake route of both systems (PAMAM polyplex and PAMAM coated Ad) was similar, this study confirmed the great potential of Ad, once inside the cell, in overcoming intracellular barriers, such as endosomal release and nuclear translocation, but especially mediating efficient transcription. According to mathematical models, the major advantage of Ad lies in post delivery events, as only a small number of intranuclear Ad genomes are necessary to induce high transgene expression levels, i.e., >10,000-fold more efficient than plasmid DNA.[115] In this study a maximum benefit of 3×10^5 to 3.7×10^5, taking the whole Ad particles into account and 4.7×10^6 to 5.8×10^6, when referring to the infectious particles only, was found for HuH7 and U87MG cells respectively, comparing DNA/PAMAM G5 with Ad/PAMAM G5 in matters of transgene expression. The beneficial effect of PAMAM G5 coating on transduction efficiency was also retained in the presence of serum, up to 25%, during the transduction process (Figure 15). Furthermore, in the presence of 100% FCS transduction efficiencies of 36% and 58% were retained after coating with 10 ng and 100 ng, respectively, illustrating the high integrity of the complexes even in the presence of negatively charged albumin.

After intravascular administration, most Ad subtypes interact with several plasma proteins. These interactions determine the fate of the virus: binding of coagulation factor X directs

the Ad to the liver leading to hepatocyte transduction,[43] complement and scavenger receptor binding causes Ad internalization and inactivation by Kupffer cells,[39] while the high prevalence of adenovirus type 5 neutralizing antibodies in the human population leads to inactivation of Ad.[116] As repeated application cycles of gene vectors are usually necessary for efficient treatment of disease, the high immunogenic potential of systemically administered Ad, which will rapidly induce the expression of neutralizing antibodies, represents a serious problem. To test how efficiently the PAMAM coat could prevent antibody binding, a neutralization assay was performed by preincubating uncoated Ad-EGFP and Ad/PAMAM G5 complexes with increasing concentrations of plasma pooled from 60,000, mostly seropositive, donors (Privigen®). Thereafter samples were incubated with A549 cells. While uncoated Ad was rapidly inactivated, PAMAM G5 coated Ad infected 65% of the cells, at the same IgG concentration (Figure 27 and S3, supplementary information). Antibodies able to neutralize Ad vectors bind epitopes either on the hexon or fiber proteins.[117] Here, the PAMAM G5 coating seemed to efficiently protect Ad capsid proteins from this interaction. To make sure that the effect seen was due to masking of the Ad surface by PAMAM and that anti-Ad antibodies were not scavenged by free PAMAM dendrimer, an indirect ELISA was performed. Virus particles absorbed onto a maxisorb flat bottom plate were incubated with Privigen® dilutions, preincubated for 30 min at RT with 100 ng of PAMAM G5 or HBG buffer, as control, before addition to immobilized Ad. For both, PAMAM G5 and HBG preincubations, similar absorption values were observed, indicating that Ad antibodies were able to bind to the Ad surface regardless of PAMAM G5 present in the solvent (Figure 28). Additionally PAMAM G2 and G3 were tested for their protective properties and compared to PAMAM G5 (Figure 29). PAMAM G5 showed the best protection from neutralizing antibodies followed by G3 and G2. This was probably due to the higher charge density of PAMAM G5, resulting from the doubling of primary amines with every PAMAM generation. As the primary amines hold a positive charge at physiological pH, the potential for electrostatic interaction with the Ad capsid rises from generation to generation. Besides inactivation by neutralizing antibodies, there is a high affinity interaction between the coagulation factor X (FX) and the hexon protein, leading to hepatocyte transduction after i.v. administration.[43-45] Therefore, a factor X binding assay was performed to examine the potential of PAMAM G5 to abolish FX-hexon interaction and subsequently hepatocyte transduction (Figure 30). Ad-EGFP and genetically or chemically FX binding-ablated vectors, as controls, were coated with increasing amounts of PAMAM G5 and incubated with SKOV-3 cells with or without the addition of physiological concentrations of factor X (8 µg/mL). 72 h after

transduction, the cells were analyzed for EGFP expression, revealing that only the control vectors showed complete ablation of FX binding. In contrast Ad-EGFP, when coated with amounts of PAMAM G5 as small as 10 ng resulted in even higher EGFP levels in the presence of FX than uncoated Ad, leading to the hypothesis, that both PAMAM and FX contributed to an uptake via heparan sulfate proteoglycans (HSPGs). Only with amounts of PAMAM particles in excess of FX molecules, could a reduction in transgene expression, in the presence of FX, be seen, without a full abolition of FX-hexon interaction.

Besides evaluating adenovirus receptors for cell attachment and uptake, the epidermal growth factor receptor (EGFR) as a possible targeting receptor was investigated (Figure 18 and S1, supplementary information). The EGFR is upregulated in several tumors and is a valid surface marker for targeting of anticancer drugs. Numerous attempts with adenoviral vectors have proven its applicability for targeted gene delivery.[118] In principle, Ad targeting to the EGFR is possible with a non-mitogenic ligand like cetuximab, an anti-EGFR chimeric human/mouse antibody, which led to successful internalization into EGFR positive cells.[85] In this study, the short peptide ligand GE11, which has been identified by phage display technique,[92] was covalently coupled to the PAMAM dendrimers prior to Ad coating. In contrast to the natural ligand EGF, this peptide avoids activation of the EGFR after binding, which could otherwise induce mitogenic activity.[92,97] In the EGFR overexpressing cell line A549, GE11 induced a significant, 2.3-fold higher transgene expression level, when compared to the control conjugate PAMAM G2-PEG-Cys lacking the ligand (Figure 31). In HepG2, which exhibited only low EGFR levels, no significant difference was seen. To prove the specificity of the GE11 mediated targeting effect, A549 cells were preincubated with mEGF, which led to a profound internalization of the EGFR, superior to treatment with Cetuximab, as shown by FACS analysis (Figure 32). Only with PAMAM-PEG-GE11 was transgene expression reduced after mEGF preincubtion, whereas PAMAM-PEG-Cys was unaffected (Figure 33). This clearly demonstrated the selectivity of the system for the EGFR. The affinity of GE11 for the EGFR has been reported to be approximately 10–20-fold lower, when compared to EGF.[92] Hence, a high number of GE11 ligands were necessary to achieve a cooperative binding effect of several GE11 molecules, in close proximity, in order to cluster EGFR.[119] Recently it has been demonstrated that GE11 peptide, per se, as a single molecule had no measurable binding affinity for the EGFR, but when several peptides, covalently attached to LPEI, were incorporated into a particle with nucleic acid, EGFR binding was specific and measurable.[119] Coating of Ad with PAMAM G2-PEG GE11 led to a significant, but less pronounced, targeting effect when compared to other EGFR targeting studies performed

using the natural ligand EGF covalently coupled either via poly[N-2-hydroxypropyl)methacrylamide] (HPMA)[85] or via biotin-streptavidin interaction.[118] Morrison et al. demonstrated that HPMA-coupled mEGF was still able to activate the EGFR leading to its internalization and initiation of downstream signaling.[90] From previous work, performed in our lab, with non-viral gene carriers we learned that this leads to an overall boost in particle uptake due to generally increased surface internalization and macropinocytosis induced by EGFR activation.[97] Still, GE11 can lead to similar effective uptake rates but after prolonged incubation times, with specific binding to the EGFR and subsequent actin-mediated internalization.[120,121] The absence of EGFR activation by PAMAM G2-PEG-GE11, which would otherwise lead to macropinocytosis and mitotic activity, in addition to the fact that non-covalent PAMAM coating does not cause ablation of viral infection as shown for HPMA coated virus, explains the lower increment in transduction efficiency by EGFR targeting. Nevertheless GE11 is a promising and safe candidate for adenovirus targeting studies to cancer cells, and has been proven to specifically enhance transgene expression in EGFR overexpressing tumors after systemic injection of gene carriers.[120]

Taken together, PAMAM coating presents a novel strategy for non-covalent coating of adenoviral capsids. With covalent linkage of polymers to the Ad capsid a restricted endosomal release and interference with intracellular trafficking was often seen;[122] this was not the case using PAMAM dendrimers in this charged base coating strategy, where efficient transduction of cancer cells lacking CAR or with low expression levels was achieved. As low CAR and high EGFR level appear to correlate with the aggressiveness and state of a tumor,[123] this hybrid system, in principle, may be suitable for the treatment of metastatic disease. Furthermore, the dose of Ad applied may be reduced due to enhanced transduction efficiency by targeting, which reduces toxicity and the immune response of the host.

4.2 In vivo evaluation of non-covalent Ad coating with PAMAM G5 dendrimer

After in vitro evaluation of the non-covalent PAMAM coating of Ad, where PAMAM G5 proved best in increasing transduction efficiency as well as showing the highest protection properties against neutralizing antibodies, in vivo studies were performed. Two different PAMAM G5 concentrations, namely 250 ng (equals ~ 200 molecules/Ad) and 1500 ng (equals ~ 1000 molecules/Ad) were assessed as a coating for Ad-EGFP. Instead of a detargeting from the liver, a targeting of the liver could be found with increased Ad

particle numbers revealed by qPCR (Figure 36) as well as increased transgene expression seen by fluorometry of liver homogenates and laser scanning microscopy of cryosections (Figure 34 and 35). Several biodistribution studies with non-viral vectors showed an accumulation of cationic polyplexes mainly in liver, spleen and lungs.[124,125] The accumulation behavior of non-viral gene delivery systems can be explained by the fact, that for therapeutic doses high concentrations of polyplexes are needed, which readily aggregate as their concentration increases.[126] Also with PAMAM coating of adenoviruses a concentration dependent aggregation behavior was observed, in vitro. While coating with 10 ng of PAMAM G5 led to small particles, easily taken up by the cells (Figure 19), coating with 100 ng of PAMAM G5 led to bigger particles and depending on the cell line, aggregation at the membrane was more or less pronounced. Similar results were found by measurement of particle size, performed in the same concentration rage as the in vivo experiments, leading to sizes of the coated Ad-EGFP of 168 nm when coated with 200 molecules PAMAM/Ad and 1128 nm when coated with 1000 molecules PAMAM/Ad. In previous studies it has been shown that even though polyplexes accumulate in the liver, transgene expression is relatively low.[124,125] Burke et al, who evaluated the stability of PEI/DNA complexes showed, that PEI polyplexes remain packaged during circulation in serum, therefore preventing degradation of free DNA by nucleases, but are unpackaged after entering the liver. The unpacking is believed to be a consequence of competitive binding with extracellular matrix components, like collagen and heparan sulfates. A partial uncoating of the adenovirus would, in contrast to naked DNA, reveal a gene vector with high transduction potential.[127] Conform to the factor X binding assay (Figure 30), where complete FX binding ablation was not feasible using this non-covalent PAMAM coating approach, Ad was possibly still able to infect hepatocytes by bridging the Ad to HSPGs on the cell surface, mediated by FX.[43] The observed hepatocyte targeting effect of Ad/PAMAM versus Ad might also be due to a partial escape from ingestion by Kupffer cells, a tendency which was already found, when using 250 ng PAMAM G5 for coating (data not shown). In contrast, PAMAM G5 coating of an adenovirus encoding for NIS (sodium iodide symporter) performed by Geoffrey Grünwald showed a promising 70% detargeting effect from the liver of CD1 nu/nu mice. The sodium iodide symporter can be used for imaging guided analysis of biodistribution and the level of transgene expression, as it is able to transport radio nuclides such as I^{123} after effective implementation of the NIS protein in the cellular membrane.[128] Results were obtained by gamma camera imaging as a reduction in I^{123} uptake in the liver four days after application of Ad-NIS versus Ad-NIS coated with 300 ng PAMAM G5.[129] To rule out differences due to the use of different

mouse strains and operator variability, a side by side evaluation of Ad-EGFP ± coating in Balb/c and CD1 nu/nu mice was performed, where complex formation as well as i.v. application was performed by Geoffrey Grünwald. PAMAM G5 coating of Ad-EGFP led to an increase in transgene expression in the livers of both mouse strains, which could be confirmed by qPCR showing elevated viral particle numbers after coating, not only in the livers, but also in the other organs tested (Figure 37 and S5, supplementary information). Differences either in the virus preparation leading to different aggregation behaviors, in vivo, or specific characteristics of the transmembrane NIS protein may be a reason for the observed differences between Ad-NIS and Ad-EGFP gene transfer. As seen in a study by Klutz et al, where LPEI/NIS polyplexes were administered intravenously, functional NIS expression in the lungs could be abolished due to LPEI-induced membrane damage.[120] Additionally Ad-NIS showed a higher tendency to form aggregates with a broader size distribution after coating with 200 molecules PAMAM G5 per Ad compared to Ad-EGFP (Figure 11). As a qPCR for adenoviral fiber led to similar vector genome quantities for uncoated and 300 ng PAMAM G5 coated Ad-NIS (Geoffrey Grünwald, unpublished observations), complexes might got stuck in the liver sinusoids without efficient hepatocellular uptake.

The in vivo results obtained with Ad-EGFP indicate instability of the Ad/PAMAM G5 complexes after intravenous application combined with insufficient shielding from coagulation factor X. Using PAMAM-PEG-OPSS for covalent attachment of PAMAM to an Ad with a genetically introduced cysteine in the hypervariable region 5 (HVR5) of the hexon protein, might overcome the problem of insufficient shielding, while grafting the PAMAM dendrimer with the peptide ligand GE11 would increase specifity for EGFR overexpressing tumors.

4.3. Establishment of a SKOV-3 i.p. mouse model with dual color imaging facility

Results on biodistribution of intravenously (i.v.) applied Ad-EGFP, coated with PAMAM G5 showed an increase in hepatocyte transduction instead of a detargeting from the liver. As the complex stability and FX shielding ability of non-covalently coated Ad seemed to be insufficient for i.v. administration, an alternative application route, namely intraperitoneally (i.p.) application was considered. I.p. application is especially interesting for the treatment of ovarian cancer. Ovarian cancer is the most lethal form of gynecological malignancy, as the disease is typically detected at a late stage.[130] As a consequence, more than 70% of patients have intraperitoneal metastasis at the time of diagnosis.[131]

The standard treatment of advanced ovarian cancer is represented by a combination of platinum and taxanes directly administered into the peritoneal cavity, following initial surgery.[132] Beside serious side effects such as neurotoxicity, patients often show a relapse within a median time of less than 2 years.[133,134] Here adenovirus gene therapy could act as an alternative or additive therapy approach. As ovarian cancer dissemination is usually confined to the peritoneal cavity even in late stages, Ad can be regionally administered into the peritoneal cavity allowing local exposure of lesions to a high vector concentration.[135] Akiyama et al. showed that only 0.03% of Ad could be detected in the bloodstream, 30 min after i.p. administration of $1x10^{10}$ VP and that no parenchymal liver transgene expression was detectable. The primary target of i.p. administered Ad was found to be the mesothelium present on the exterior of organs,[136] which was infected in a CAR-dependent manner. As SKOV-3 cells are known to be low in CAR and therefore hardly transducable by Ad alone, [106] other methods are needed to improve transduction efficiency and therefore clinical outcome. As proven by in vitro transduction studies, PAMAM dendrimers hold great potential to elevate transduction efficiency in CAR negative and low CAR level cell lines (Figure 24). In the case of SKOV-3 LucEGFP, PAMAM coating of Ad led to infection of 77-92% of the cells for all three PAMAM generations tested, while Ad alone infected only 13% of the cells on average, at a MOI of 125 (Figure 43). On the other hand, in high CAR level cell lines restricted internalization of Ad/PAMAM particles was seen, leading to reduced transgene expression, when increasing the PAMAM concentration. It is therefore interesting to investigate if the transduction of mesothelial cells lining the peritoneal organs, which occurs via CAR, would be negatively influenced by the PAMAM coating. Besides increasing transduction efficiency, in a CAR independent manner, by coating of Ad with PAMAM, the specificity of the system could potentially be increased when using target specific receptors. As 60% of ovarian cancers are stated to over-express the epidermal growth factor receptor (EGFR),[107] proven to be highly expressed in the SKOV-3 LucEGFP cells used in this study (Figure 39 and 40), the specificity of the system can be increased with the use of PAMAM-PEG-GE11 conjugates. Coating of Ad, using PAMAM-PEG-GE11 constructs, showed EGFR specificity in vitro [137] as well as in vivo.[97,138] For detection purposes, a two colored system was established, with SKOV-3 LucEGFP expressing enhanced green fluorescent protein (EGFP), and AdmCherry encoding for the red fluorescent protein mCherry. The detection of both fluorophores was possible, in parallel, using either the same excitation wavelength, but different filters for detection, as used for FACS analysis (extinction at 488 nm, detection at 530/40 nm and 680/30 nm band pass filter for EGFP and mCherry respectively), or by the use of different

excitation wavelengths combined with the appropriate filters (excitation at 488 nm, detection at 505-530 nm band pass filter for EGFP and excitation at 543 nm, detection at 560 nm long pass filter for mCherry), as used for LSM studies. The monomeric fluorophore mCherry, derived from a protein isolated from *Discosoma sp.,* shows high photostability and resistance to photobleaching beside a fast maturation.[139] It is suitable for combination with the well known and extensively studied EGFP, derived from a protein isolated from *Aequorea victoria*. With the establishment of a dual color system, using Ad-mCherry and SKOV-3 LucEGFP cells, it can be easily verified that Ad infected, mCherry expressing, cells are indeed tumor cells. The use of SKOV-3 LucEGFP cells for the establishment of this intraperitoneal ovarian carcinoma mouse model has a further advantage as luciferase imaging can be performed to follow tumor growth and find the best time point for vector administration.

The SKOV-3 LucEGFP model is therefore a potentially useful model for studying the tumor targeting effect of Ad coated with PAMAM dendrimer conjugates and to investigate, how adverse side effects, such as abdominal pain and bowel obstruction [140,141], as well as an unsatisfactory tumor transduction, seen in early clinical trials, could be overcome.[85]

5 SUMMARY

Adenovirus type 5 (Ad) based vectors are the most commonly investigated gene transfer vectors in clinical trials to date due to their high gene transduction efficiency. Transduction efficiency of Ad is dependent on the presence of cellular receptors used to mediate Ad binding and uptake. The coxsackie- and adenovirus receptor (CAR), which is stated to be the key player for efficient cell infection, is often downregulated in tumor cells, correlating with disease progression. Therefore methods have to be established to increase transduction in these Ad-refractory cancer types.

In this thesis cationic PAMAM dendrimers generation 2, 3, and 5 were used for non-covalent coating of the negatively charged adenovirus capsid by the virtue of electrostatic interaction. Complexes were studied with respect to their biophysical and biological properties. Co-localisation studies using Ad-Alexa488 as well as PAMAM G5-Cy5 confirmed the high stability of the complexes also during cellular binding and uptake. Intracellular trafficking which is often restricted when using covalent coating strategies, was thereby not impaired. Additionally, PAMAM dendrimers showed great potential in increasing transduction efficiency of CAR negative to medium CAR level cancer cell lines, while showing no toxicity up to a concentration of 1 mg/well. Therefore PAMAM dendrimers proved superior to commonly used Ad coating polymers based on polyethylenimine in relation to enhanced transduction as well as reduced toxicity. As the majority of the human population carries anti-Ad antibodies it was important, in regards to future clinical applications, to check the protective abilities of the different PAMAM generations. Protection from neutralizing antibodies prevents loss of functional vector after application and, if needed, might allow second and third rounds of vector administration. PAMAM G5, with 128 primary amines and therefore the highest potential for electrostatic interaction with the negatively charged Ad capsid, gave the highest protection from neutralizing antibodies, followed by G3 and G2.

To increase the specificity for cancer cells, PAMAM conjugates were synthesized, carrying the epidermal growth factor receptor-targeting ligand GE11 covalently coupled to the PAMAM dendrimers via a 2 kDa PEG spacer. The PEG spacer had the function of presenting the GE11 on the particle surface to make it available for receptor interaction. In contrast to the natural ligand EGF, GE11 shows a much lower mitotic activity, making it favorable for clinical applications. Coating of the Ad with PAMAM-PEG-GE11 conjugates led to specific uptake in EGFR overexpressing A549 cells. This could be proven by EGFR downregulation prior to transduction, along with the help of a control

construct, carrying a terminal cysteine instead of the GE11 peptide. Furthermore HepG2 cells were used as control cell line expressing low EGFR levels.

When considering therapy of tumor metastases, intravenous injection of the adenovirus vector would be favorable. Liver toxicity however is profound after i.v. application as the Ad has a natural tropism for the liver due to clearance by KCs as well as transduction of hepatocytes mediated by coagulation factor X-hexon interaction. Ablating this inherited tropism was the goal of several studies on genetic and chemical modifications of the virus capsid. A vector designed to prevent liver targeting and with increased circulation kinetics would have the possibility of accumulating in tumors by the enhanced permeability and retention (EPR) effect. Based on the in vitro data gained in this study, Geoffrey Grünwald was able to show a detargeting from the liver of 70%, when using 300 ng PAMAM G5 for coating of an intravenously administered Ad encoding for the sodium iodide symporter (NIS). This could not be repeated in this study using an Ad encoding for enhanced green fluorescent protein (EGFP). The influence of the virus preparation, as well as the specific characteristics of the NIS transgene, has to be further elucidated to understand the requirement for non-covalent coating approaches to mediate efficient liver detargeting.

Intraperitoneally (i.p.) Ad application is, beside intravenous administration, an interesting application route, when thinking about the treatment of ovarian tumors. In order to study transduction enhancement of PAMAM dendrimers in vivo, a SKOV-3 ovarian carcinoma mouse model was established. Ovarian carcinomas are known to be restricted mostly to the peritoneal cavity even in a late stage of disease. Using i.p. implanted SKOV-3 tumors offers the possibility of applying Ad locally, circumventing the sequestration of Ad in the liver, seen after intravenous administration. SKOV-3 cells are known to be hardly transducable by Ad alone due to a low and inhomogeneous CAR expression and show a high EGFR level. In this thesis enhancement of transduction as well as specificity for the EGFR could be shown, in vitro, using a two color system. The feasibility of a side by side evaluation of EGFP expressing SKOV-3 LucEGFP cells and mCherry expressing Ad transduced cells, makes an estimation of target versus non-target Ad-infected cells convenient.

Non-covalent coating of the Ad using PAMAM dendrimers holds great potential for increasing transduction efficiency in otherwise refractory cancer cells in vitro. Further studies are required to see if i.p. administered Ad can overcome difficulties associated with Ad therapy in clinical trials of ovarian carcinoma, to date, such as bowel obstruction and low transduction efficiency.

6 REFERENCES

1 Fujiwara, T. *et al.* Induction of chemosensitivity in human lung cancer cells in vivo by adenovirus-mediated transfer of the wild-type p53 gene. *Cancer Res* 54, 2287-2291 (1994).

2 Tanaka, T. *et al.* Adenovirus-mediated prodrug gene therapy for carcinoembryonic antigen-producing human gastric carcinoma cells in vitro. *Cancer Res* 56, 1341-1345 (1996).

3 Choi, K. J., Zhang, S. N., Choi, I. K., Kim, J. S. & Yun, C. O. Strengthening of antitumor immune memory and prevention of thymic atrophy mediated by adenovirus expressing IL-12 and GM-CSF. *Gene therapy* 19, 711-723, doi:10.1038/gt.2011.125 (2012).

4 Rowe, W. P., Huebner, R. J., Gilmore, L. K., Parrott, R. H. & Ward, T. G. Isolation of a cytopathogenic agent from human adenoids undergoing spontaneous degeneration in tissue culture. *Proc Soc Exp Biol Med* 84, 570-573 (1953).

5 Walsh, M. P. *et al.* Computational analysis of two species C human adenoviruses provides evidence of a novel virus. *J Clin Microbiol* 49, 3482-3490, doi:10.1128/JCM.00156-11 (2011).

6 Russell, W. C. Adenoviruses: update on structure and function. *J Gen Virol* 90, 1-20, doi:10.1099/vir.0.003087-0 (2009).

7 Abou El Hassan, M. A., van der Meulen-Muileman, I., Abbas, S. & Kruyt, F. A. Conditionally replicating adenoviruses kill tumor cells via a basic apoptotic machinery-independent mechanism that resembles necrosis-like programmed cell death. *Journal of virology* 78, 12243-12251, doi:10.1128/JVI.78.22.12243-12251.2004 (2004).

8 Cattaneo, R., Miest, T., Shashkova, E. V. & Barry, M. A. Reprogrammed viruses as cancer therapeutics: targeted, armed and shielded. *Nature reviews. Microbiology* 6, 529-540, doi:10.1038/nrmicro1927 (2008).

9 Vorburger, S. A. & Hunt, K. K. Adenoviral gene therapy. *The oncologist* 7, 46-59 (2002).

10 Stevens, C. W., Zeng, M. & Cerniglia, G. J. Ionizing radiation greatly improves gene transfer efficiency in mammalian cells. *Human gene therapy* 7, 1727-1734, doi:10.1089/hum.1996.7.14-1727 (1996).

11 Peng, Z. Current status of gendicine in China: recombinant human Ad-p53 agent for treatment of cancers. *Human gene therapy* 16, 1016-1027, doi:10.1089/hum.2005.16.1016 (2005).

12 Raty, J. K., Pikkarainen, J. T., Wirth, T. & Yla-Herttuala, S. Gene therapy: the first approved gene-based medicines, molecular mechanisms and clinical indications. *Curr Mol Pharmacol* 1, 13-23 (2008).

13 Barker, D. D. & Berk, A. J. Adenovirus proteins from both E1B reading frames are required for transformation of rodent cells by viral infection and DNA transfection. *Virology* 156, 107-121 (1987).

14 McConnell, M. J. & Imperiale, M. J. Biology of adenovirus and its use as a vector for gene therapy. *Human gene therapy* 15, 1022-1033, doi:10.1089/hum.2004.15.1022 (2004).

15 Majhen, D. & Ambriovic-Ristov, A. Adenoviral vectors--how to use them in cancer gene therapy? *Virus research* 119, 121-133, doi:10.1016/j.virusres.2006.02.001 (2006).

16 Coughlan, L. *et al.* Tropism-modification strategies for targeted gene delivery using adenoviral vectors. *Viruses* 2, 2290-2355, doi:10.3390/v2102290 (2010).

17 Rekosh, D. M., Russell, W. C., Bellet, A. J. & Robinson, A. J. Identification of a protein linked to the ends of adenovirus DNA. *Cell* 11, 283-295 (1977).

18 Christensen, J. B. *et al.* Presence of the adenovirus IVa2 protein at a single vertex of the mature virion. *Journal of virology* 82, 9086-9093, doi:10.1128/JVI.01024-08 (2008).

19 Everitt, E., Lutter, L. & Philipson, L. Structural proteins of adenoviruses. XII. Location and neighbor relationship among proteins of adenovirion type 2 as revealed by enzymatic iodination, immunoprecipitation and chemical cross-linking. *Virology* 67, 197-208 (1975).

20 van Oostrum, J. & Burnett, R. M. Molecular composition of the adenovirus type 2 virion. *Journal of virology* 56, 439-448 (1985).

21 Bergelson, J. M. *et al.* Isolation of a common receptor for Coxsackie B viruses and adenoviruses 2 and 5. *Science* 275, 1320-1323 (1997).

22 Dechecchi, M. C., Tamanini, A., Bonizzato, A. & Cabrini, G. Heparan sulfate glycosaminoglycans are involved in adenovirus type 5 and 2-host cell interactions. *Virology* 268, 382-390, doi:10.1006/viro.1999.0171 (2000).

23 Wickham, T. J., Mathias, P., Cheresh, D. A. & Nemerow, G. R. Integrins alpha v beta 3 and alpha v beta 5 promote adenovirus internalization but not virus attachment. *Cell* 73, 309-319 (1993).

24 Huang, S., Kamata, T., Takada, Y., Ruggeri, Z. M. & Nemerow, G. R. Adenovirus interaction with distinct integrins mediates separate events in cell entry and gene delivery to hematopoietic cells. *Journal of virology* 70, 4502-4508 (1996).

25 Davison, E. *et al.* Adenovirus type 5 uptake by lung adenocarcinoma cells in culture correlates with Ad5 fibre binding is mediated by alpha(v)beta1 integrin and can be modulated by changes in beta1 integrin function. *J Gene Med* 3, 550-559, doi:10.1002/jgm.223 (2001).

26 Li, E. *et al.* Integrin alpha(v)beta1 is an adenovirus coreceptor. *Journal of virology* 75, 5405-5409, doi:10.1128/JVI.75.11.5405-5409.2001 (2001).

27 Salone, B. *et al.* Integrin alpha3beta1 is an alternative cellular receptor for adenovirus serotype 5. *Journal of virology* 77, 13448-13454 (2003).

28 Meier, O. *et al.* Adenovirus triggers macropinocytosis and endosomal leakage together with its clathrin-mediated uptake. *J Cell Biol* 158, 1119-1131, doi:10.1083/jcb.200112067 (2002).

29 Wiethoff, C. M., Wodrich, H., Gerace, L. & Nemerow, G. R. Adenovirus protein VI mediates membrane disruption following capsid disassembly. *Journal of virology* 79, 1992-2000, doi:10.1128/JVI.79.4.1992-2000.2005 (2005).

30 Kelkar, S. A., Pfister, K. K., Crystal, R. G. & Leopold, P. L. Cytoplasmic dynein mediates adenovirus binding to microtubules. *Journal of virology* 78, 10122-10132, doi:10.1128/JVI.78.18.10122-10132.2004 (2004).

31 Trotman, L. C., Mosberger, N., Fornerod, M., Stidwill, R. P. & Greber, U. F. Import of adenovirus DNA involves the nuclear pore complex receptor CAN/Nup214 and histone H1. *Nature cell biology* 3, 1092-1100, doi:10.1038/ncb1201-1092 (2001).

32 Greber, U. F. *et al.* The role of the nuclear pore complex in adenovirus DNA entry. *The EMBO journal* 16, 5998-6007, doi:10.1093/emboj/16.19.5998 (1997).

33 Rein, D. T., Breidenbach, M. & Curiel, D. T. Current developments in adenovirus-based cancer gene therapy. *Future Oncol* 2, 137-143, doi:10.2217/14796694.2.1.137 (2006).

34 Balague, C. *et al.* Sustained high-level expression of full-length human factor VIII and

restoration of clotting activity in hemophilic mice using a minimal adenovirus vector. *Blood* 95, 820-828 (2000).

35 Duffy, M. R., Parker, A. L., Bradshaw, A. C. & Baker, A. H. Manipulation of adenovirus interactions with host factors for gene therapy applications. *Nanomedicine (Lond)* 7, 271-288, doi:10.2217/nnm.11.186 (2012).

36 Shayakhmetov, D. M., Gaggar, A., Ni, S., Li, Z. Y. & Lieber, A. Adenovirus binding to blood factors results in liver cell infection and hepatotoxicity. *Journal of virology* 79, 7478-7491, doi:10.1128/JVI.79.12.7478-7491.2005 (2005).

37 Stone, D. *et al.* Adenovirus-platelet interaction in blood causes virus sequestration to the reticuloendothelial system of the liver. *Journal of virology* 81, 4866-4871, doi:10.1128/JVI.02819-06 (2007).

38 Othman, M., Labelle, A., Mazzetti, I., Elbatarny, H. S. & Lillicrap, D. Adenovirus-induced thrombocytopenia: the role of von Willebrand factor and P-selectin in mediating accelerated platelet clearance. *Blood* 109, 2832-2839, doi:10.1182/blood-2006-06-032524 (2007).

39 Xu, Z., Tian, J., Smith, J. S. & Byrnes, A. P. Clearance of adenovirus by Kupffer cells is mediated by scavenger receptors, natural antibodies, and complement. *Journal of virology* 82, 11705-11713, doi:10.1128/JVI.01320-08 (2008).

40 Smith, J. S., Xu, Z., Tian, J., Stevenson, S. C. & Byrnes, A. P. Interaction of systemically delivered adenovirus vectors with Kupffer cells in mouse liver. *Human gene therapy* 19, 547-554, doi:10.1089/hum.2008.004 (2008).

41 Haisma, H. J. *et al.* Scavenger receptor A: a new route for adenovirus 5. *Mol Pharm* 6, 366-374, doi:10.1021/mp8000974 (2009).

42 Vrancken Peeters, M. J., Perkins, A. L. & Kay, M. A. Method for multiple portal vein infusions in mice: quantitation of adenovirus-mediated hepatic gene transfer. *Biotechniques* 20, 278-285 (1996).

43 Waddington, S. N. *et al.* Adenovirus serotype 5 hexon mediates liver gene transfer. *Cell* 132, 397-409, doi:10.1016/j.cell.2008.01.016 (2008).

44 Vigant, F. *et al.* Substitution of hexon hypervariable region 5 of adenovirus serotype 5 abrogates blood factor binding and limits gene transfer to liver. *Molecular therapy : the journal of the American Society of Gene Therapy* 16, 1474-1480, doi:10.1038/mt.2008.132 (2008).

45 Kalyuzhniy, O. *et al.* Adenovirus serotype 5 hexon is critical for virus infection of hepatocytes in vivo. *Proc Natl Acad Sci U S A* 105, 5483-5488, doi:10.1073/pnas.0711757105 (2008).

46 Fasbender, A. *et al.* Complexes of adenovirus with polycationic polymers and cationic lipids increase the efficiency of gene transfer in vitro and in vivo. *J Biol Chem* 272, 6479-6489 (1997).

47 Kreppel, F. & Kochanek, S. Modification of adenovirus gene transfer vectors with synthetic polymers: a scientific review and technical guide. *Molecular therapy : the journal of the American Society of Gene Therapy* 16, 16-29, doi:10.1038/sj.mt.6300321 (2008).

48 Fisher, K. D. & Seymour, L. W. HPMA copolymers for masking and retargeting of therapeutic viruses. *Advanced drug delivery reviews* 62, 240-245, doi:10.1016/j.addr.2009.12.003 (2010).

49 Freimuth, P. A human cell line selected for resistance to adenovirus infection has reduced levels of the virus receptor. *Journal of virology* 70, 4081-4085 (1996).

50 Carlisle, R. C. *et al.* Human erythrocytes bind and inactivate type 5 adenovirus by presenting

Coxsackie virus-adenovirus receptor and complement receptor 1. *Blood* 113, 1909-1918, doi:10.1182/blood-2008-09-178459 (2009).

51 Wilson, J. M. Adenovirus-mediated gene transfer to liver. *Advanced drug delivery reviews* 46, 205-209 (2001).

52 Kaneda, Y. Update on non-viral delivery methods for cancer therapy: possibilities of a drug delivery system with anticancer activities beyond delivery as a new therapeutic tool. *Expert Opin Drug Deliv* 7, 1079-1093, doi:10.1517/17425247.2010.510511 (2010).

53 Sonawane, N. D., Szoka, F. C., Jr. & Verkman, A. S. Chloride accumulation and swelling in endosomes enhances DNA transfer by polyamine-DNA polyplexes. *J Biol Chem* 278, 44826-44831, doi:10.1074/jbc.M308643200 (2003).

54 Kreiss, P. *et al.* Plasmid DNA size does not affect the physicochemical properties of lipoplexes but modulates gene transfer efficiency. *Nucleic Acids Res* 27, 3792-3798 (1999).

55 Corsi, K., Chellat, F., Yahia, L. & Fernandes, J. C. Mesenchymal stem cells, MG63 and HEK293 transfection using chitosan-DNA nanoparticles. *Biomaterials* 24, 1255-1264 (2003).

56 Fishburn, C. S. The pharmacology of PEGylation: balancing PD with PK to generate novel therapeutics. *Journal of pharmaceutical sciences* 97, 4167-4183, doi:10.1002/jps.21278 (2008).

57 Ogris, M. & Wagner, E. To be targeted: is the magic bullet concept a viable option for synthetic nucleic acid therapeutics? *Human gene therapy* 22, 799-807, doi:10.1089/hum.2011.065 (2011).

58 Kamiya, H., Tsuchiya, H., Yamazaki, J. & Harashima, H. Intracellular trafficking and transgene expression of viral and non-viral gene vectors. *Advanced drug delivery reviews* 52, 153-164 (2001).

59 Kurachi, S. *et al.* Characterization of capsid-modified adenovirus vectors containing heterologous peptides in the fiber knob, protein IX, or hexon. *Gene therapy* 14, 266-274, doi:10.1038/sj.gt.3302859 (2007).

60 Belousova, N., Krendelchtchikova, V., Curiel, D. T. & Krasnykh, V. Modulation of adenovirus vector tropism via incorporation of polypeptide ligands into the fiber protein. *Journal of virology* 76, 8621-8631 (2002).

61 Einfeld, D. A., Brough, D. E., Roelvink, P. W., Kovesdi, I. & Wickham, T. J. Construction of a pseudoreceptor that mediates transduction by adenoviruses expressing a ligand in fiber or penton base. *Journal of virology* 73, 9130-9136 (1999).

62 Wu, H. *et al.* Identification of sites in adenovirus hexon for foreign peptide incorporation. *Journal of virology* 79, 3382-3390, doi:10.1128/JVI.79.6.3382-3390.2005 (2005).

63 Grill, J. *et al.* Combined targeting of adenoviruses to integrins and epidermal growth factor receptors increases gene transfer into primary glioma cells and spheroids. *Clinical cancer research : an official journal of the American Association for Cancer Research* 7, 641-650 (2001).

64 Gaggar, A., Shayakhmetov, D. M. & Lieber, A. CD46 is a cellular receptor for group B adenoviruses. *Nature medicine* 9, 1408-1412, doi:10.1038/nm952 (2003).

65 Short, J. J., Vasu, C., Holterman, M. J., Curiel, D. T. & Pereboev, A. Members of adenovirus species B utilize CD80 and CD86 as cellular attachment receptors. *Virus research* 122, 144-153, doi:10.1016/j.virusres.2006.07.009 (2006).

66 Miyazawa, N., Crystal, R. G. & Leopold, P. L. Adenovirus serotype 7 retention in a late endosomal compartment prior to cytosol escape is modulated by fiber protein. *Journal of virology* 75,

1387-1400, doi:10.1128/JVI.75.3.1387-1400.2001 (2001).

67 Arcasoy, S. M., Latoche, J. D., Gondor, M., Pitt, B. R. & Pilewski, J. M. Polycations increase the efficiency of adenovirus-mediated gene transfer to epithelial and endothelial cells in vitro. *Gene therapy* 4, 32-38, doi:10.1038/sj.gt.3300349 (1997).

68 Han, J. *et al.* Combination of adenovirus and cross-linked low molecular weight PEI improves efficiency of gene transduction. *Nanotechnology* 21, 105106, doi:10.1088/0957-4484/21/10/105106 (2010).

69 Kasman, L. M., Barua, S., Lu, P., Rege, K. & Voelkel-Johnson, C. Polymer-enhanced adenoviral transduction of CAR-negative bladder cancer cells. *Mol Pharm* 6, 1612-1619, doi:10.1021/mp9000958 (2009).

70 Meunier-Durmort, C., Grimal, H., Sachs, L. M., Demeneix, B. A. & Forest, C. Adenovirus enhancement of polyethylenimine-mediated transfer of regulated genes in differentiated cells. *Gene therapy* 4, 808-814, doi:10.1038/sj.gt.3300450 (1997).

71 Park, K. H. *et al.* Enhanced delivery of adenovirus, using proteoliposomes containing wildtype or V156K apolipoprotein A-I and dimyristoylphosphatidylcholine. *Human gene therapy* 21, 579-587, doi:10.1089/hum.2008.207 (2010).

72 Qiu, C., De Young, M. B., Finn, A. & Dichek, D. A. Cationic liposomes enhance adenovirus entry via a pathway independent of the fiber receptor and alpha(v)-integrins. *Human gene therapy* 9, 507-520, doi:10.1089/hum.1998.9.4-507 (1998).

73 Chollet, P., Favrot, M. C., Hurbin, A. & Coll, J. L. Side-effects of a systemic injection of linear polyethylenimine-DNA complexes. *J Gene Med* 4, 84-91 (2002).

74 Navarro, G. *et al.* Low generation PAMAM dendrimer and CpG free plasmids allow targeted and extended transgene expression in tumors after systemic delivery. *J Control Release* 146, 99-105, doi:10.1016/j.jconrel.2010.04.030 (2010).

75 Tomalia DA, B. H., Dewald J, Hall M,Kallos G, Martin S, et al. A new class of polymers: starburst dentritic macromolecules. *Polymer Journal*, 117-132 (1985).

76 Tomalia, D. A. Birth of a new macromolecular architecture: dendrimers as quantized building blocks for nanoscale synthetic polymer chemistry. *Progress in Polymer Science* 30, 294-324, doi:http://dx.doi.org/10.1016/j.progpolymsci.2005.01.007 (2005).

77 Awasthi, V. D., Garcia, D., Goins, B. A. & Phillips, W. T. Circulation and biodistribution profiles of long-circulating PEG-liposomes of various sizes in rabbits. *Int J Pharm* 253, 121-132 (2003).

78 O'Riordan, C. R. *et al.* PEGylation of adenovirus with retention of infectivity and protection from neutralizing antibody in vitro and in vivo. *Human gene therapy* 10, 1349-1358, doi:10.1089/10430349950018021 (1999).

79 Doronin, K., Shashkova, E. V., May, S. M., Hofherr, S. E. & Barry, M. A. Chemical modification with high molecular weight polyethylene glycol reduces transduction of hepatocytes and increases efficacy of intravenously delivered oncolytic adenovirus. *Human gene therapy* 20, 975-988, doi:10.1089/hum.2009.028 (2009).

80 Prill, J. M. *et al.* Modifications of adenovirus hexon allow for either hepatocyte detargeting or targeting with potential evasion from Kupffer cells. *Molecular therapy : the journal of the American Society of Gene Therapy* 19, 83-92, doi:10.1038/mt.2010.229 (2011).

81 Croyle, M. A., Yu, Q. C. & Wilson, J. M. Development of a rapid method for the PEGylation

of adenoviruses with enhanced transduction and improved stability under harsh storage conditions. *Human gene therapy* 11, 1713-1722, doi:10.1089/10430340050111368 (2000).

82 Fisher, K. D. *et al.* Polymer-coated adenovirus permits efficient retargeting and evades neutralising antibodies. *Gene therapy* 8, 341-348, doi:10.1038/sj.gt.3301389 (2001).

83 Subr, V. *et al.* Coating of adenovirus type 5 with polymers containing quaternary amines prevents binding to blood components. *J Control Release* 135, 152-158, doi:10.1016/j.jconrel.2008.12.009 (2009).

84 Green, N. K. *et al.* Extended plasma circulation time and decreased toxicity of polymer-coated adenovirus. *Gene therapy* 11, 1256-1263, doi:10.1038/sj.gt.3302295 (2004).

85 Morrison, J. *et al.* Cetuximab retargeting of adenovirus via the epidermal growth factor receptor for treatment of intraperitoneal ovarian cancer. *Human gene therapy* 20, 239-251, doi:10.1089/hum.2008.167 (2009).

86 Kobrin, M. S., Yamanaka, Y., Friess, H., Lopez, M. E. & Korc, M. Aberrant expression of type I fibroblast growth factor receptor in human pancreatic adenocarcinomas. *Cancer Res* 53, 4741-4744 (1993).

87 Casscells, W. *et al.* Elimination of smooth muscle cells in experimental restenosis: targeting of fibroblast growth factor receptors. *Proc Natl Acad Sci U S A* 89, 7159-7163 (1992).

88 Werner, S. *et al.* Large induction of keratinocyte growth factor expression in the dermis during wound healing. *Proc Natl Acad Sci U S A* 89, 6896-6900 (1992).

89 Nicholson, R. I., Gee, J. M. & Harper, M. E. EGFR and cancer prognosis. *Eur J Cancer* 37 Suppl 4, S9-15 (2001).

90 Morrison, J. *et al.* Virotherapy of ovarian cancer with polymer-cloaked adenovirus retargeted to the epidermal growth factor receptor. *Molecular therapy : the journal of the American Society of Gene Therapy* 16, 244-251, doi:10.1038/sj.mt.6300363 (2008).

91 Kawaguchi, Y. *et al.* Cetuximab induce antibody-dependent cellular cytotoxicity against EGFR-expressing esophageal squamous cell carcinoma. *Int J Cancer* 120, 781-787, doi:10.1002/ijc.22370 (2007).

92 Li, Z. *et al.* Identification and characterization of a novel peptide ligand of epidermal growth factor receptor for targeted delivery of therapeutics. *FASEB J* 19, 1978-1985, doi:10.1096/fj.05-4058com (2005).

93 Stevenson, M. *et al.* Incorporation of a laminin-derived peptide (SIKVAV) on polymer-modified adenovirus permits tumor-specific targeting via alpha6-integrins. *Cancer Gene Ther* 14, 335-345, doi:10.1038/sj.cgt.7701022 (2007).

94 Nejjari, M. *et al.* alpha6beta1 integrin expression in hepatocarcinoma cells: regulation and role in cell adhesion and migration. *Int J Cancer* 83, 518-525 (1999).

95 Dingli, D., Russell, S. J. & Morris, J. C., 3rd. In vivo imaging and tumor therapy with the sodium iodide symporter. *J Cell Biochem* 90, 1079-1086, doi:10.1002/jcb.10714 (2003).

96 Schaffert, D. *et al.* Poly(I:C)-mediated tumor growth suppression in EGF-receptor overexpressing tumors using EGF-polyethylene glycol-linear polyethylenimine as carrier. *Pharm Res* 28, 731-741, doi:10.1007/s11095-010-0225-4 (2011).

97 Schäfer, A. *et al.* Disconnecting the yin and yang relation of epidermal growth factor receptor (EGFR)-mediated delivery: a fully synthetic, EGFR-targeted gene transfer system avoiding receptor activation. *Human gene therapy* 22, 1463-1473, doi:10.1089/hum.2010.231 (2011).

98 Snyder, S. L. & Sobocinski, P. Z. An improved 2,4,6-trinitrobenzenesulfonic acid method for the determination of amines. *Anal Biochem* 64, 284-288, doi:10.1016/0003-2697(75)90431-5 (1975).

99 Carlsson, J., Drevin, H. & Axen, R. Protein thiolation and reversible protein-protein conjugation. N-Succinimidyl 3-(2-pyridyldithio)propionate, a new heterobifunctional reagent. *Biochem J* 173, 723-737 (1978).

100 Boeckle, S. *et al.* Purification of polyethylenimine polyplexes highlights the role of free polycations in gene transfer. *J Gene Med* 6, 1102-1111, doi:10.1002/jgm.598 (2004).

101 Schiedner, G., Hertel, S. & Kochanek, S. Efficient transformation of primary human amniocytes by E1 functions of Ad5: generation of new cell lines for adenoviral vector production. *Human gene therapy* 11, 2105-2116, doi:10.1089/104303400750001417 (2000).

102 Kreppel, F., Biermann, V., Kochanek, S. & Schiedner, G. A DNA-based method to assay total and infectious particle contents and helper virus contamination in high-capacity adenoviral vector preparations. *Human gene therapy* 13, 1151-1156, doi:10.1089/104303402320138934 (2002).

103 Spitzweg, C. *et al.* In vivo sodium iodide symporter gene therapy of prostate cancer. *Gene therapy* 8, 1524-1531, doi:10.1038/sj.gt.3301558 (2001).

104 Chen, H. Comparative observation of the recombinant adeno-associated virus 2 using transmission electron microscopy and atomic force microscopy. *Microsc Microanal* 13, 384-389, doi:10.1017/S1431927607070808 (2007).

105 Manders, E. M. M., Verbeek, F. J. & Aten, J. A. Measurement of co-localization of objects in dual-colour confocal images. *Journal of microscopy* 169, 375-382, doi:10.1111/j.1365-2818.1993.tb03313.x (1993).

106 Kanerva, A. *et al.* Gene transfer to ovarian cancer versus normal tissues with fiber-modified adenoviruses. *Molecular therapy : the journal of the American Society of Gene Therapy* 5, 695-704, doi:10.1006/mthe.2002.0599 (2002).

107 Siwak, D. R. *et al.* Targeting the epidermal growth factor receptor in epithelial ovarian cancer: current knowledge and future challenges. *J Oncol* 2010, 568938, doi:10.1155/2010/568938 (2010).

108 Picard, D., Suslova, E. & Briand, P. A. 2-color photobleaching experiments reveal distinct intracellular dynamics of two components of the Hsp90 complex. *Exp Cell Res* 312, 3949-3958, doi:10.1016/j.yexcr.2006.08.026 (2006).

109 Alemany, R. Designing adenoviral vectors for tumor-specific targeting. *Methods Mol Biol* 542, 57-74 (2009).

110 Wightman, L. *et al.* Different behavior of branched and linear polyethylenimine for gene delivery in vitro and in vivo. *J Gene Med* 3, 362-372, doi:10.1002/jgm.187 (2001).

111 Vicennati, P., Giuliano, A., Ortaggi, G. & Masotti, A. Polyethylenimine in medicinal chemistry. *Curr Med Chem* 15, 2826-2839 (2008).

112 Russ, V. *et al.* Novel degradable oligoethylenimine acrylate ester-based pseudodendrimers for in vitro and in vivo gene transfer. *Gene therapy* 15, 18-29, doi:10.1038/sj.gt.3303046 (2008).

113 Kopatz, I., Remy, J. S. & Behr, J. P. A model for non-viral gene delivery: through syndecan adhesion molecules and powered by actin. *J Gene Med* 6, 769-776, doi:10.1002/jgm.558 (2004).

114 Haensler, J. & Szoka, F. C., Jr. Polyamidoamine cascade polymers mediate efficient transfection of cells in culture. *Bioconjug Chem* 4, 372-379 (1993).

115 Varga, C. M. *et al.* Quantitative comparison of polyethylenimine formulations and adenoviral

vectors in terms of intracellular gene delivery processes. *Gene therapy* 12, 1023-1032, doi:10.1038/sj.gt.3302495 (2005).

116 Chirmule, N. *et al.* Immune responses to adenovirus and adeno-associated virus in humans. *Gene therapy* 6, 1574-1583, doi:10.1038/sj.gt.3300994 (1999).

117 Bradley, R. R., Lynch, D. M., Iampietro, M. J., Borducchi, E. N. & Barouch, D. H. Adenovirus serotype 5 neutralizing antibodies target both hexon and fiber following vaccination and natural infection. *Journal of virology* 86, 625-629, doi:10.1128/JVI.06254-11 (2012).

118 Pereboeva, L., Komarova, S., Roth, J., Ponnazhagan, S. & Curiel, D. T. Targeting EGFR with metabolically biotinylated fiber-mosaic adenovirus. *Gene therapy* 14, 627-637, doi:10.1038/sj.gt.3302916 (2007).

119 Abourbeh, G. *et al.* PolyIC GE11 polyplex inhibits EGFR-overexpressing tumors. *IUBMB life* 64, 324-330, doi:10.1002/iub.1002 (2012).

120 Klutz, K. *et al.* Epidermal growth factor receptor-targeted (131)I-therapy of liver cancer following systemic delivery of the sodium iodide symporter gene. *Molecular therapy : the journal of the American Society of Gene Therapy* 19, 676-685, doi:10.1038/mt.2010.296 (2011).

121 Mickler, F. M. *et al.* Tuning nanoparticle uptake: live-cell imaging reveals two distinct endocytosis mechanisms mediated by natural and artificial EGFR targeting ligand. *Nano letters* 12, 3417-3423, doi:10.1021/nl300395q (2012).

122 Espenlaub, S. *et al.* Capsomer-specific fluorescent labeling of adenoviral vector particles allows for detailed analysis of intracellular particle trafficking and the performance of bioresponsive bonds for vector capsid modifications. *Human gene therapy* 21, 1155-1167, doi:10.1089/hum.2009.171 (2010).

123 Matsumoto, K., Shariat, S. F., Ayala, G. E., Rauen, K. A. & Lerner, S. P. Loss of coxsackie and adenovirus receptor expression is associated with features of aggressive bladder cancer. *Urology* 66, 441-446, doi:10.1016/j.urology.2005.02.033 (2005).

124 Fischer, D., Osburg, B., Petersen, H., Kissel, T. & Bickel, U. Effect of poly(ethylene imine) molecular weight and pegylation on organ distribution and pharmacokinetics of polyplexes with oligodeoxynucleotides in mice. *Drug Metab Dispos* 32, 983-992 (2004).

125 Merdan, T. *et al.* PEGylation of poly(ethylene imine) affects stability of complexes with plasmid DNA under in vivo conditions in a dose-dependent manner after intravenous injection into mice. *Bioconjug Chem* 16, 785-792, doi:10.1021/bc049743q (2005).

126 Morille, M., Passirani, C., Vonarbourg, A., Clavreul, A. & Benoit, J. P. Progress in developing cationic vectors for non-viral systemic gene therapy against cancer. *Biomaterials* 29, 3477-3496, doi:10.1016/j.biomaterials.2008.04.036 (2008).

127 Burke, R. S. & Pun, S. H. Extracellular barriers to in Vivo PEI and PEGylated PEI polyplex-mediated gene delivery to the liver. *Bioconjug Chem* 19, 693-704, doi:10.1021/bc700388u (2008).

128 Willhauck, M. J. *et al.* The potential of 211Astatine for NIS-mediated radionuclide therapy in prostate cancer. *Eur J Nucl Med Mol Imaging* 35, 1272-1281, doi:10.1007/s00259-008-0775-4 (2008).

129 Geoffrey K Grünwald, A. V., Kathrin Klutz, Michael J Willhauck, Nathalie Schwenk, Reingard Senekowitsch-Schmidtke, Markus Schwaiger, Christian Zach, Ernst Wagner, Burkhard Göke, Per S Holm, Manfred Ogris, Christine Spitzweg. Non-Covalent Dendrimer Coating of Adenoviral Vectors for Systemic Sodium Iodide Symporter (NIS)-

Mediated Radiovirotherapy. *JNM* (2013).

130 Ferlay, J. *et al.* Estimates of the cancer incidence and mortality in Europe in 2006. *Ann Oncol* 18, 581-592, doi:10.1093/annonc/mdl498 (2007).

131 Cannistra, S. A. Cancer of the ovary. *N Engl J Med* 351, 2519-2529, doi:10.1056/NEJMra041842 (2004).

132 Safra, T. *et al.* Combined weekly carboplatin and paclitaxel as primary treatment of advanced epithelial ovarian carcinoma. *Gynecol Oncol* 114, 215-218, doi:10.1016/j.ygyno.2009.04.008 (2009).

133 Muggia, F. M. *et al.* Phase III randomized study of cisplatin versus paclitaxel versus cisplatin and paclitaxel in patients with suboptimal stage III or IV ovarian cancer: a gynecologic oncology group study. *J Clin Oncol* 18, 106-115 (2000).

134 Ozols, R. F. *et al.* Phase III trial of carboplatin and paclitaxel compared with cisplatin and paclitaxel in patients with optimally resected stage III ovarian cancer: a Gynecologic Oncology Group study. *J Clin Oncol* 21, 3194-3200, doi:10.1200/JCO.2003.02.153 (2003).

135 Wolf, J. K. & Jenkins, A. D. Gene therapy for ovarian cancer (review). *Int J Oncol* 21, 461-468 (2002).

136 Akiyama, M. *et al.* Ablating CAR and integrin binding in adenovirus vectors reduces nontarget organ transduction and permits sustained bloodstream persistence following intraperitoneal administration. *Molecular therapy : the journal of the American Society of Gene Therapy* 9, 218-230, doi:10.1016/j.ymthe.2003.10.010 (2004).

137 Vetter, A. *et al.* Adenoviral vectors coated with PAMAM dendrimer conjugates allow CAR independent virus uptake and targeting to the EGF receptor. *Mol Pharm* 10, 606-618, doi:10.1021/mp300366f (2013).

138 Geoffrey K Grünwald, A. V., Kathrin Klutz, Michael J Willhauck, Nathalie Schwenk, Reingard Senekowitsch-Schmidtke, Markus Schwaiger, Christian Zach, Ernst Wagner, Burkhard Göke, Per S Holm, Manfred Ogris and Christine Spitzweg. EGFR-Targeted Adenovirus for Improved Systemic Delivery of the Theranostic NIS Gene and Image-Guided Radiovirotherapy. *Molecular Therapy, submitted* (2013).

139 Shaner, N. C. *et al.* Improved monomeric red, orange and yellow fluorescent proteins derived from Discosoma sp. red fluorescent protein. *Nature biotechnology* 22, 1567-1572, doi:10.1038/nbt1037 (2004).

140 Ganly, I. *et al.* A phase I study of Onyx-015, an E1B attenuated adenovirus, administered intratumorally to patients with recurrent head and neck cancer. *Clinical cancer research : an official journal of the American Association for Cancer Research* 6, 798-806 (2000).

141 Zeimet, A. G. & Marth, C. Why did p53 gene therapy fail in ovarian cancer? *Lancet Oncol* 4, 415-422 (2003).

7 APPENDIX

7.1 Abbreviations

Ad	Adenovirus type 5
BPEI	Branched polyethylenimine (25 kDa)
CAR	Coxsackie- and adenovirus receptor
C4BP	C4b-binding protein
CD4	Cluster of differentiation 4
CpG	Cytosine phosphate guanine
Cy5	Cyanine 5
Cys	Cysteine
CR-3	Complement receptor 3
CsCl	Cesium chloride
D	Aspartic acid
DAB	Diaminobutane
DAPI	4',6-Diamidino-2-phenylindole
DLS	Dynamic light scattering
DMEM	Dulbecco's Modified Eagle's Medium
DMSO	Dimethyl sulfoxide
DNA	Deoxyribonucleic acid
DTT	Dithiothreitol
EDTA	Ethylenediaminetetraacetic acid
EGFP	Enhanced green fluorescent protein
EGF	Epidermal growth factor
EGFR	Epidermal growth factor receptor
EPR effect	Enhanced permeability and retention effect
EtBr	Ethidium bromide
EtOH	Ethanol
FACS	Fluorescence-activated cell sorting
FCS	Fetal calf serum
FGF	Fibroblast growth factor
FGFR	Fibroblast growth factor receptor
FS	Forward scatter
FIX	Coagulation factor IX
FX	Coagulation factor X

G	Glycine
GM-CSF	Granulocyte macrophage colony stimulating factor
HBG	HEPES-buffered glucose
HBS	HEPES-buffered saline
HEK 293	Human embryonic kidney cells
HEPES	N-(2-hydroxyethyl) piperazine-N'-(2-ethansulfonic acid)
H-L-Cysteine	L-Cysteine hydrochloride monohydrate
HPLC	High pressure liquid chromatography
HPMA	N(2-hydroxypropyl)methacrylamide
Hsc70	Heat shock cognate 70 kDa protein
HSV-TK	Herpes simplex virus thymidine kinase
HVR	Hypervariable region
IgG	Immunoglobulin G
INF	Interferon
i.p.	Intraperitoneal
i.v.	Intravenous
K	Lysine
kb	Kilobase
kDa	Kilo Dalton
KCs	Kupffer cells
LPEI	Linear polyethylenimine (22 kDa)
LSM	Laser scanning microscopy
Luc	Luciferase
mEGF	murine epidermal growth factor
MFI	Mean fluorescence intensity
miRNA	Micro RNA
MOI	Multiplicity of infection
MTT	3-(4,5-Dimethylthiazol-2-yl)-2,5-diphenyltetrazolium bromide
MW	molecular weight
NEAA	Non essential amino acids
NIS	Sodium iodide symporter
NPC	Nuclear pore complex
OPSS	=PDP, Ortho-pyridyldisulfide
o.n.	over night
p53	Protein 53

PAMAM	Polyamidoamine dendrimer
PBS	Phosphate-buffered saline
PCR	Polymerase chain reaction
pDNA	Plasmid DNA
PDI	Polydispersity index
PDP	Pyridyldithio propionyl group
PEI	Polyethylenimine
PEG	Polyethylene glycol
PFA	Paraformaldehyde
PFU	Plaque forming units
PG 2/3/5	PAMAM generation 2/3/5
PMSF	Phenylmethylsulfonyl fluoride
PTA	Phosphotungstic acid
qPCR	Quantitative real time PCR
R	Arginine
RLU	Relative light units
RNA	Ribonucleic acid
ROI	Region of interest
RPMI	Roswell Park Memorial Institute
RT	Room temperature
SS	Sideward scatter
SR-A	Scavanging receptor-A
TEM	Transmission electron microscopy
T	Threonine
Tf	Transferrin
TfR	Transferrin receptor
TFA	Trifluoroacetic acid
TFP	Tetrafluorophenyl esters
TGF beta	Transforming growth factor beta
TNBS	Trinitrobenzenesulfonic acid
TP	Terminal protein
TRAIL	Tumor Necrosis Factor Related Apoptosis Inducing Ligand
Tris	Tris(hydroxymethyl)aminomethane
VP	Viral particles
w/w ratio	Weight to weight ratio (conjugate to nucleic acid)

7.2 Buffer List

Buffer/ Solution	Ingredient	Amount
DMEM (low glucose, 1g/L)	Biochrom DMEM medium powder $NaHCO_3$ FCS Penicillin Streptomycin Stable glutamine (NEAA if required) Adjusted to pH 7.4	10.15 g/L 3.7 g/L 10% 1% 1% 1% 1%
DMEM/Ham's F12 1:1	Biochrom DMEM/Ham F12 medium powder $NaHCO_3$ FCS Penicillin Streptomycin Stable glutamine Adjusted to pH 7.4	12.12 g/L 2.44 g/L 10% 1% 1% 1%
RPMI	Biochrom RPMI 1640 medium powder $NaHCO_3$ FCS Penicillin Streptomycin Stable glutamine Adjusted to pH 7.4	10.48 g/L 2 g/L 10% 1% 1% 1%
PBS	KCl KH_2PO_4 NaCl Anhydrous Na_2PO_4 Adjusted to pH 7.4 MilliQ water	0.2 g 0.2 g 8.0 g 1.15 g ad 1000 mL
HBG	HEPES (20 mM) Glucose monohydrate pH adjusted to 7.4 MilliQ water	4.76 g/L 55 g/L ad 1000 mL
LAR	1 M glycylglycine solution (pH 8.0) 100 mM $MgCl_2$ solution 0.5 M EDTA solution (pH 8.0) DTT ATP Coenzyme A (stock: 42.6 mg/mL) pH adjusted to 8.0-8.5 MilliQ water Luciferine-Solution (stock: 10 mM)	2 mL (20 mM) 1 mL (1 mM) 20 µL (0.1 mM) 50.8 mg (3.2 mM) 27.8 mg (0.55 mM) 0.5 mL (0.27 mM) ad 100 mL ad 0.5 mM
Luciferine stock (10 mM)	Luciferine-Na 1 M glycylglycine solution (pH 8.0) pH adjusted to 8.0 MilliQ water	240 mg 2.35 mL ad 80 mL

7.2 Buffer list continued

Buffer/ Solution	Ingredient	Amount
LB	Bacto trypton Yeast extract NaCl MilliQ water For agar plates: Agar Relevant antibiotics in working conc.: Ampicillin (100 µg/mL) Kanamycin (50 µg/mL) Zeocin (25 µg/mL)	10 g 5 g 5 g ad 1 L 15 g/L
50xTAE	Tris EDTA-Na_2x2H_2O Eisessig	242.3 mg 18.6 g/L 60.05 g/L
NaOAc (3M)	NaOAc pH adjusted to 5.2 with HOAc MilliQ water	12.3g ad 50 mL
Tris/EDTA (10mmol/1mmol)	Tris EDTA (stock: 0.5M, pH 8 with NaOH) pH adjusted to 8.5 MilliQ water	121.14 mg 200 µL ad 100 mL
ELISA Coating Buffer	 0.2 M $NaHCO_3$ 0.2 M Na_2CO_3 pH 9.5	 100 mL 50 mL
Blocking Buffer	BSA PBS	7.5 g ad 250 mL
Wash Buffer 0.05 % Tween	Tween 20 PBS	0.5 g ad 1000 g
Substrate solution	0.2 M Na_2HPO_4 1M Citric acid pH adjusted to 5 MilliQ water o-Phenylendiamine dihydrochoride (Sigma) 30% H_2O_2	2.57 mL 2.43 mL ad 10 mL 2 tablets 4 µL
RIPA Buffer	Tris NP-40 Na-deoxycholate NaCl EDTA (stock 0.5M) pH adjusted to 7.4 MilliQ water PMSF (protease inhibitor, stock 200mM)	6.072 g 10 mL 2.5 g 8.75 2 mL ad 1000 mL 5mL

7.3 Supporting information chapter 3.4

Receptor level study

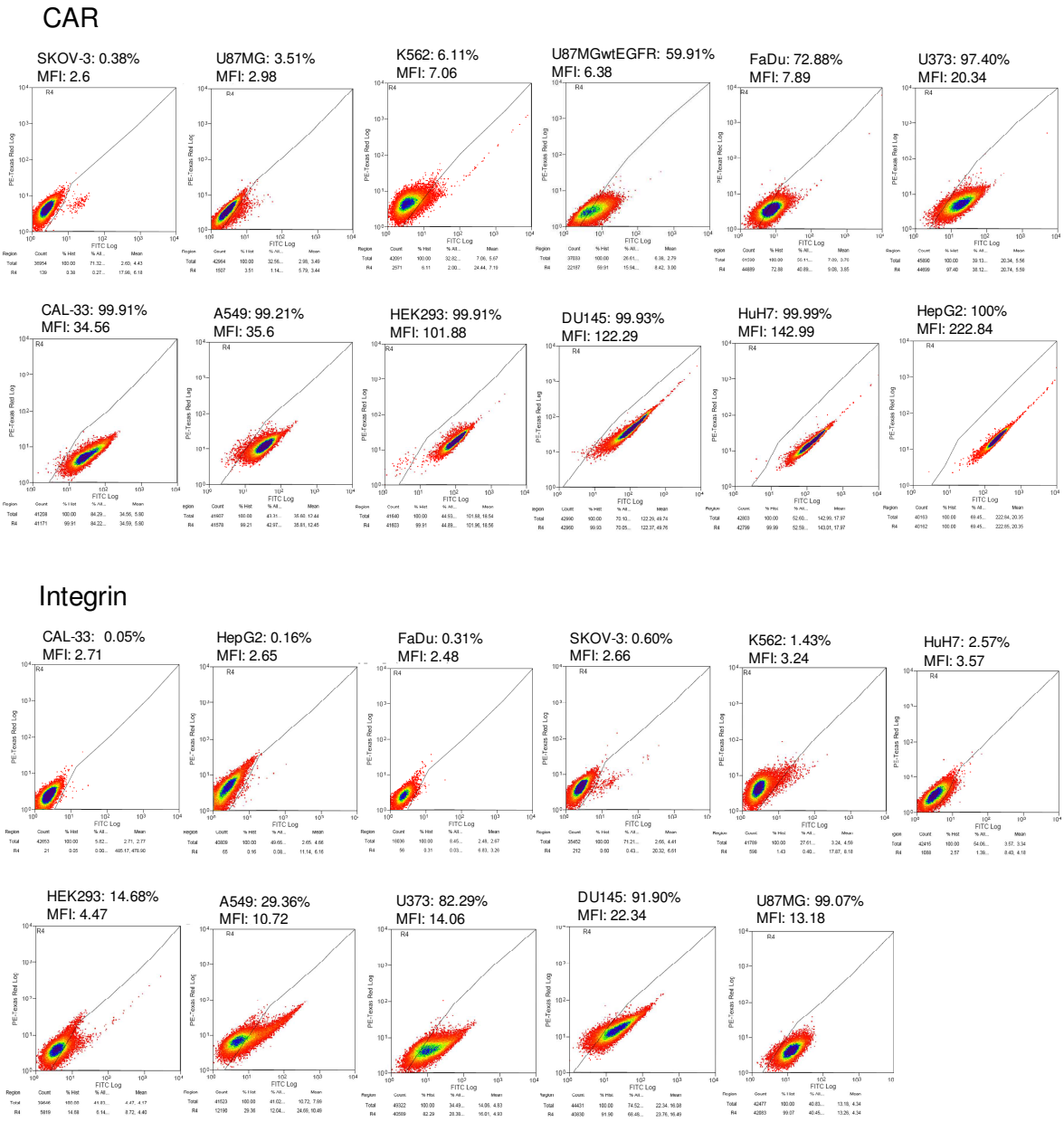

Receptor level study continued

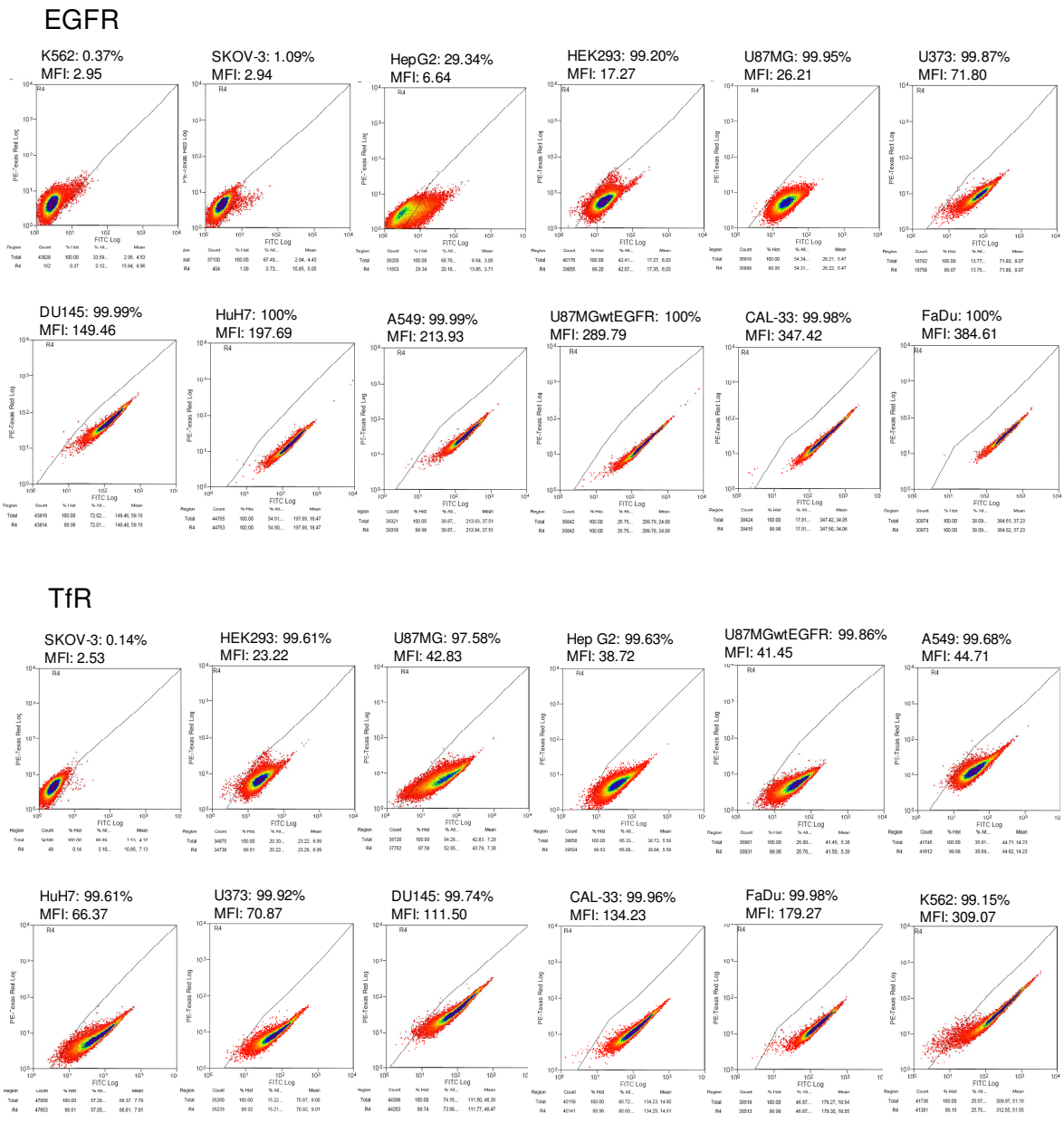

Figure S1. Receptor level estimation of CAR, integrin $\alpha_v\beta_3$, EGFR and TfR

Indicated cell lines were stained for CAR, integrin $\alpha_v\beta_3$, EGFR and TfR and analyzed by flow cytometry. Control staining was performed with mouse IgG control antibody.

For every cell line, the mean fluorescence intensity (MFI) in the FITC channel, as well as the percentage of receptor positive cells is shown, going from the receptor low cell lines in the upper left corner to the receptor high cell lines in the lower right corner, for every receptor tested.

7.4 Supporting information chapter 3.5

Co-localisation study by FACS analysis

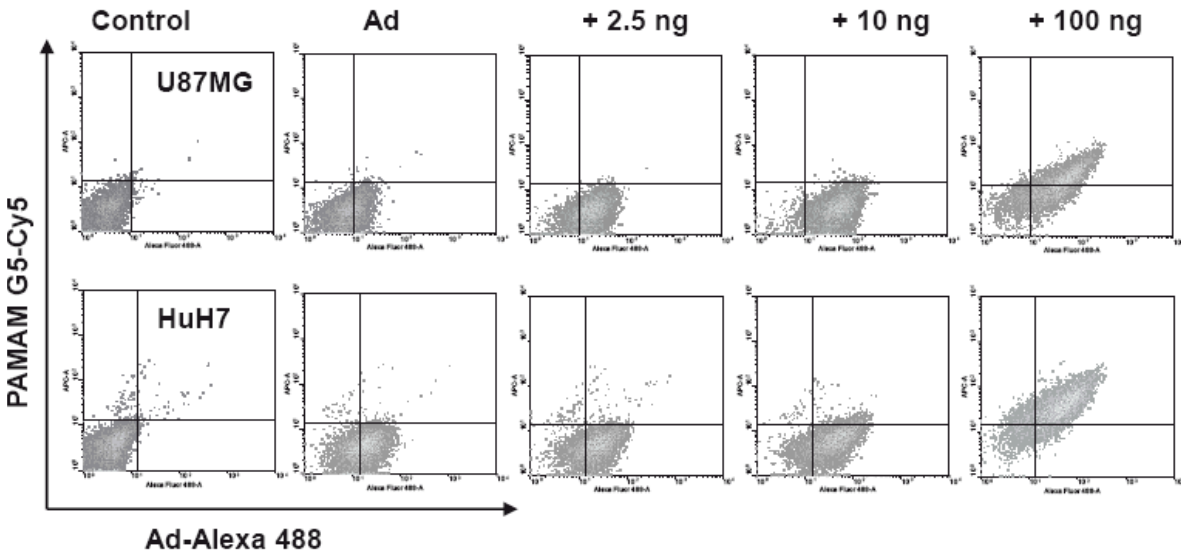

Figure S2. Cellular association of Alexa488-labeled Ad and Cy5-labeled PAMAM G5 dendrimer $5x10^4$ U87MG and HuH7 cells seeded in 24-well plates were transduced with Ad-Alexa488 alone or coated with indicated amounts of PAMAM G5-Cy5 (MOI 500, 10,000 virus particles/cell). After a 2 h incubation period, at 37 °C, cells were analyzed by flow cytometry. Dot plots of 10,000 gated events (x-axis: Ad-Alexa488 signal, y-axis: PAMAM G5-Cy5 signal) of U87MG (top row) or HuH7 cells (bottom row) are shown.

7.5 Supporting information chapter 3.7

Neutralization assay on cellular level

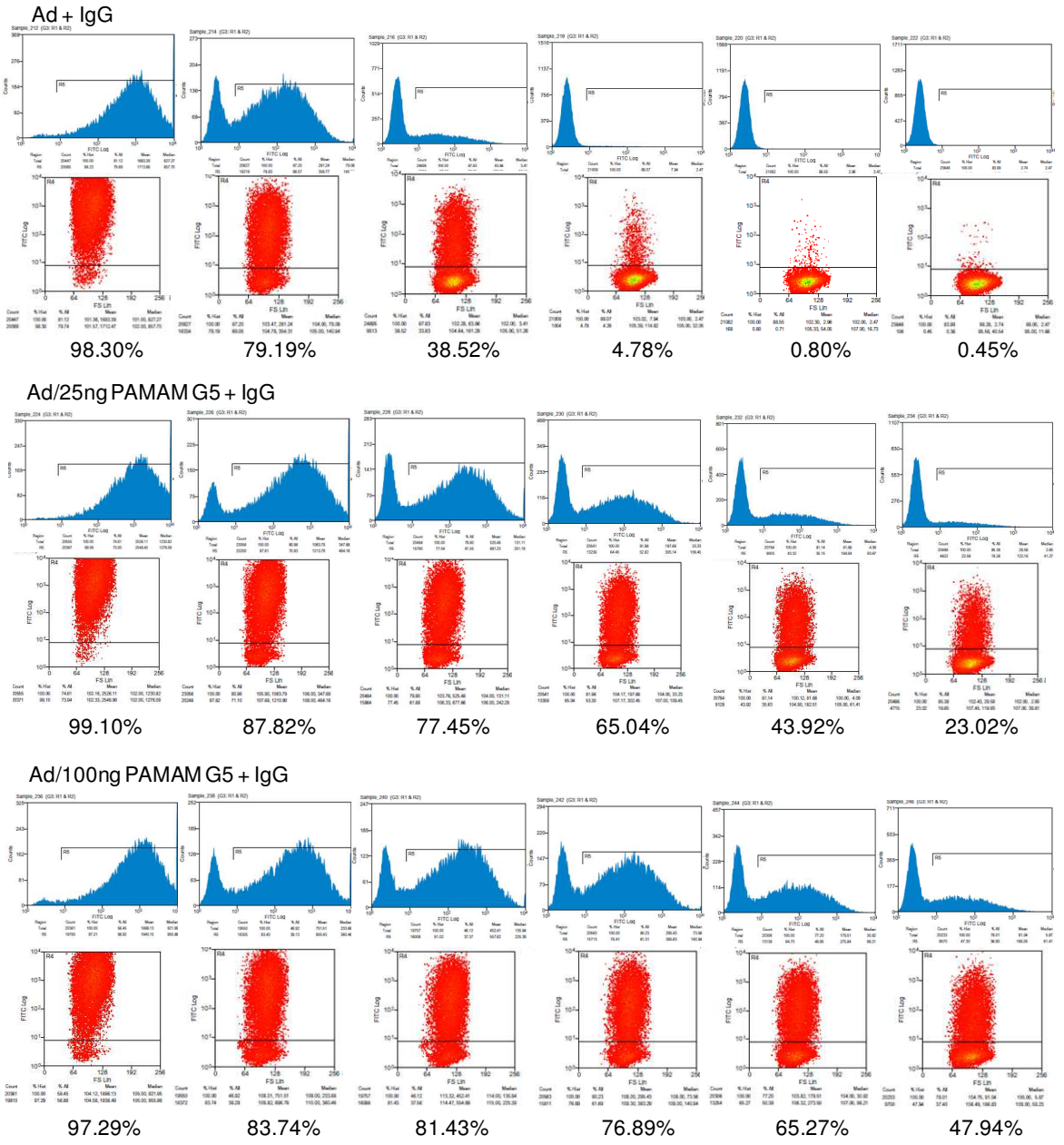

Figure S3. The protective effect of PAMAM G5 coating on transduction in the presence of anti-adenovirus neutralizing antibodies

$5x10^4$ A549 cells, seeded in 24-well plates, were transduced with Ad-EGFP alone (triangles) or coated with 25 ng or 100 ng of PAMAM G5 at a MOI of 100. A range of IgG concentrations (Privigen®) were incubated with uncoated Ad or Ad/PAMAM G5 complexes for 30 min before application to A549 cells. After 48 h, EGFP expression was analyzed by flow cytometry. The first row in each panel shows histograms, illustrating the shift of EGFP positive cells. The second row in each panel shows density plots depicting the amount of EGFP positive cells. Representative data out of three independent experiments are shown.

7.6 Supporting information chapter 3.10

Biodistribution study with Ad/PAMAM G5 250ng

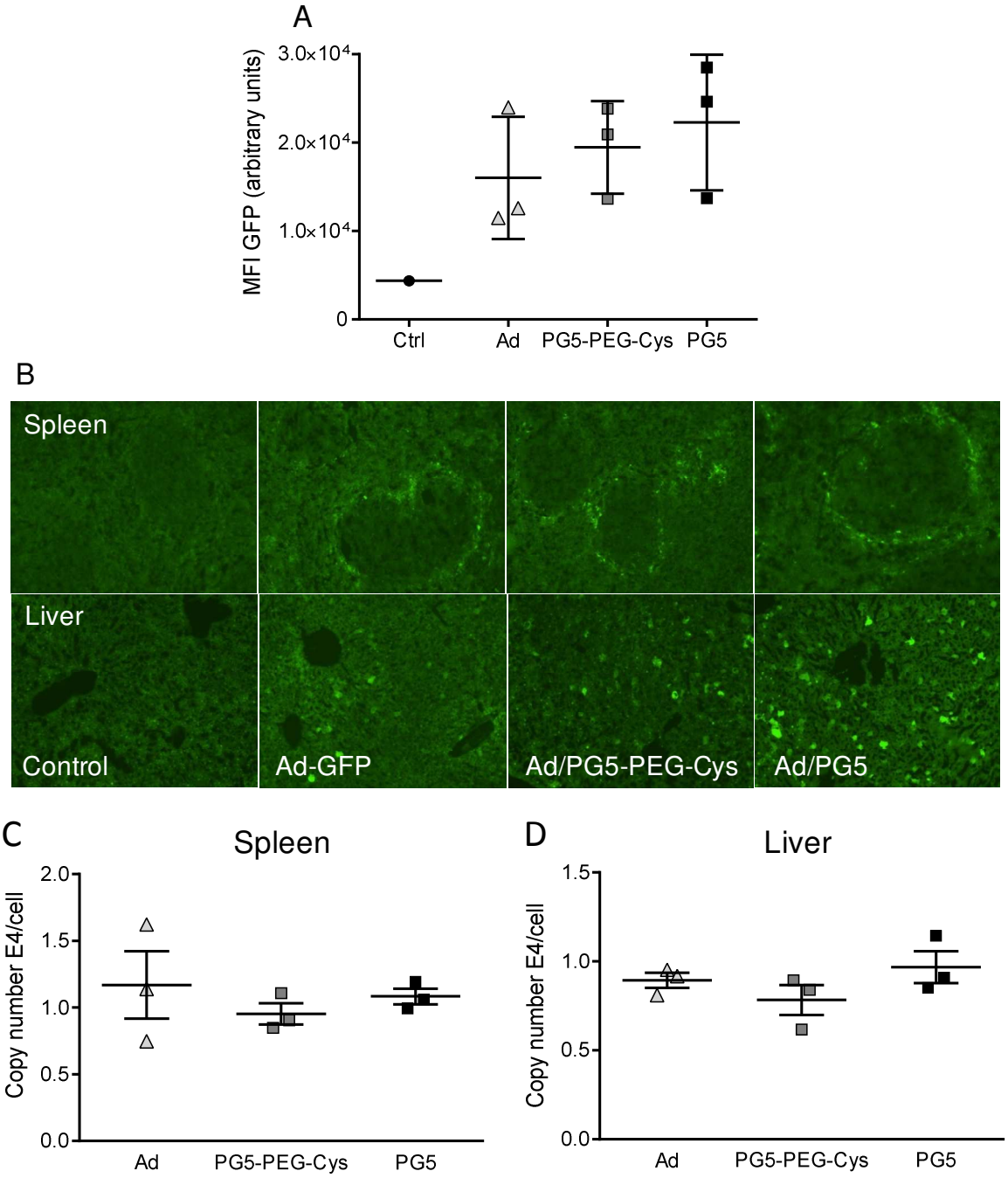

Figure S4. Biodistribution study after application of Ad-EGFP or Ad/PAMAM G5 250 ng

(A) Fluorometric measurement of liver homogenates of Balb/c after intravenous injection of $3x10^{10}$VP of Ad-EGFP (light grey triangles), Ad/PAMAM G5-PEG-Cys 250 ng (dark grey squares) or Ad/PAMAM G5 250 ng (black squares). (B) Cryosections of spleen (top row) and liver samples (bottom row) showing a representative of each treatment group plus an untreated control animal. (C, D) QPCR of spleen (C) and liver (D) samples of Ad-EGFP (light grey triangles), Ad/PAMAM G5-PEG-Cys 250 ng (dark grey squares) or Ad/PAMAM G5 250 ng (black squares). n=3 per group, plus untreated control animal.

7.7 Supporting information chapter 3.11

Cryosections – Biodistribution study with two mouse strains

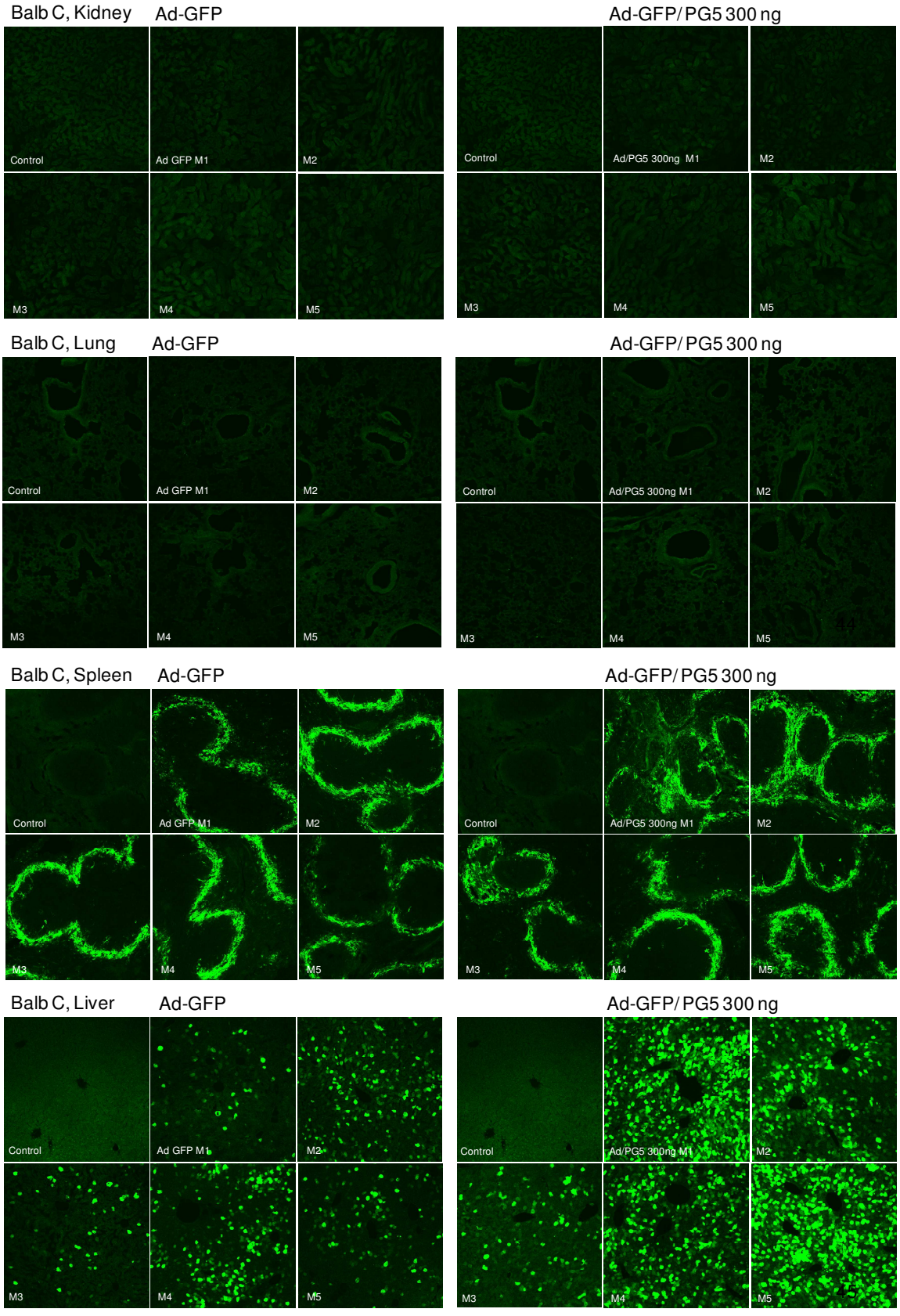

Cryosections – Biodistribution study with two mouse strains continued

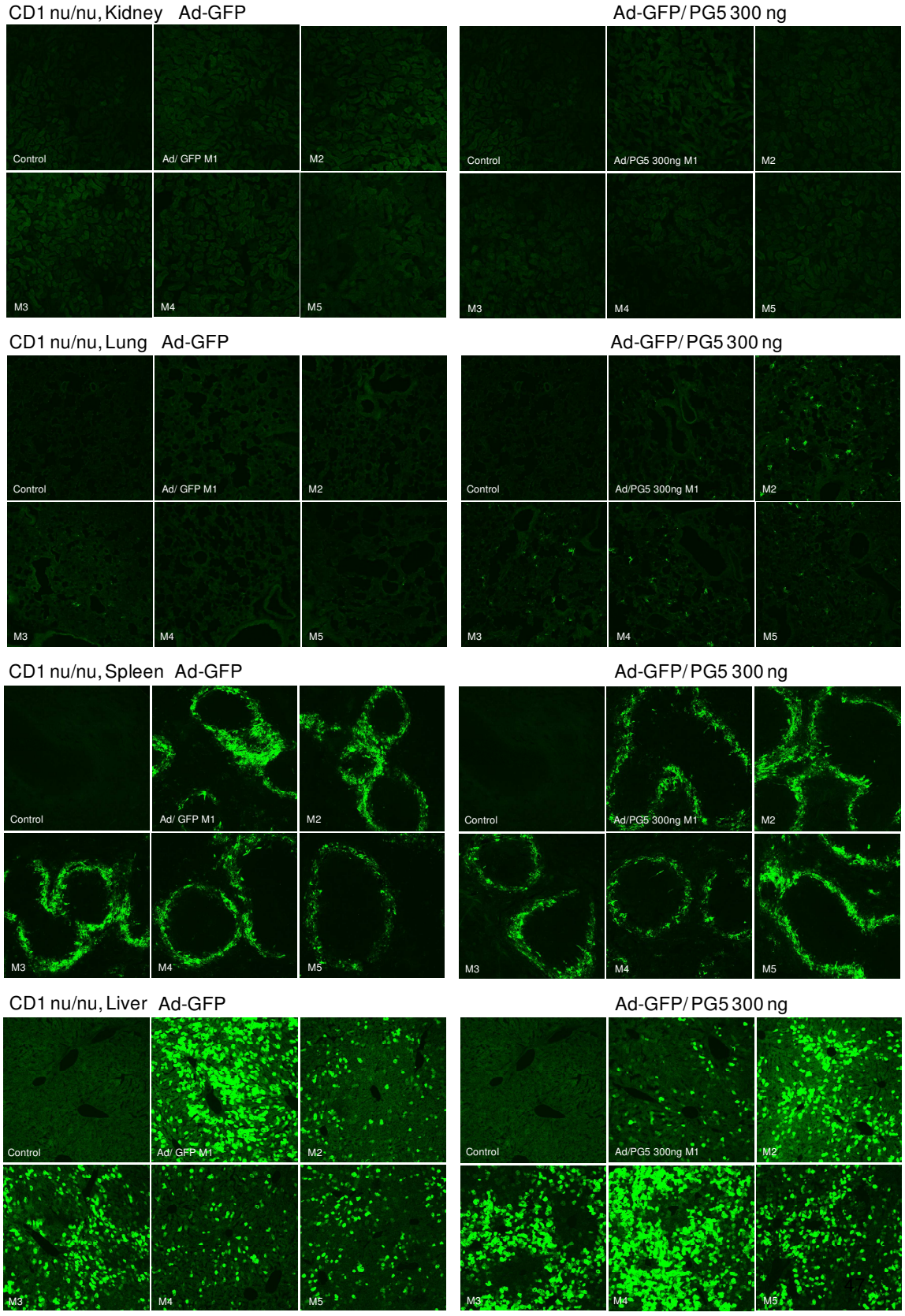

Figure S5. Cryosections after i.v. application of Ad versus Ad/PG5 in Balb/c versus CD1 nu/nu LSM images of cryosections of kidney, lung, spleen und liver of two different mouse strains, Balb/c and CD1 nu/nu, after application of $2.2x10^{10}$ VP Ad-EGFP or Ad-EGFP coated with 300 ng PAMAM G5 (PG5).

7.8 Supporting information chapter 3.12

Diagonal gating to find the best channel combination for mCherry evaluation

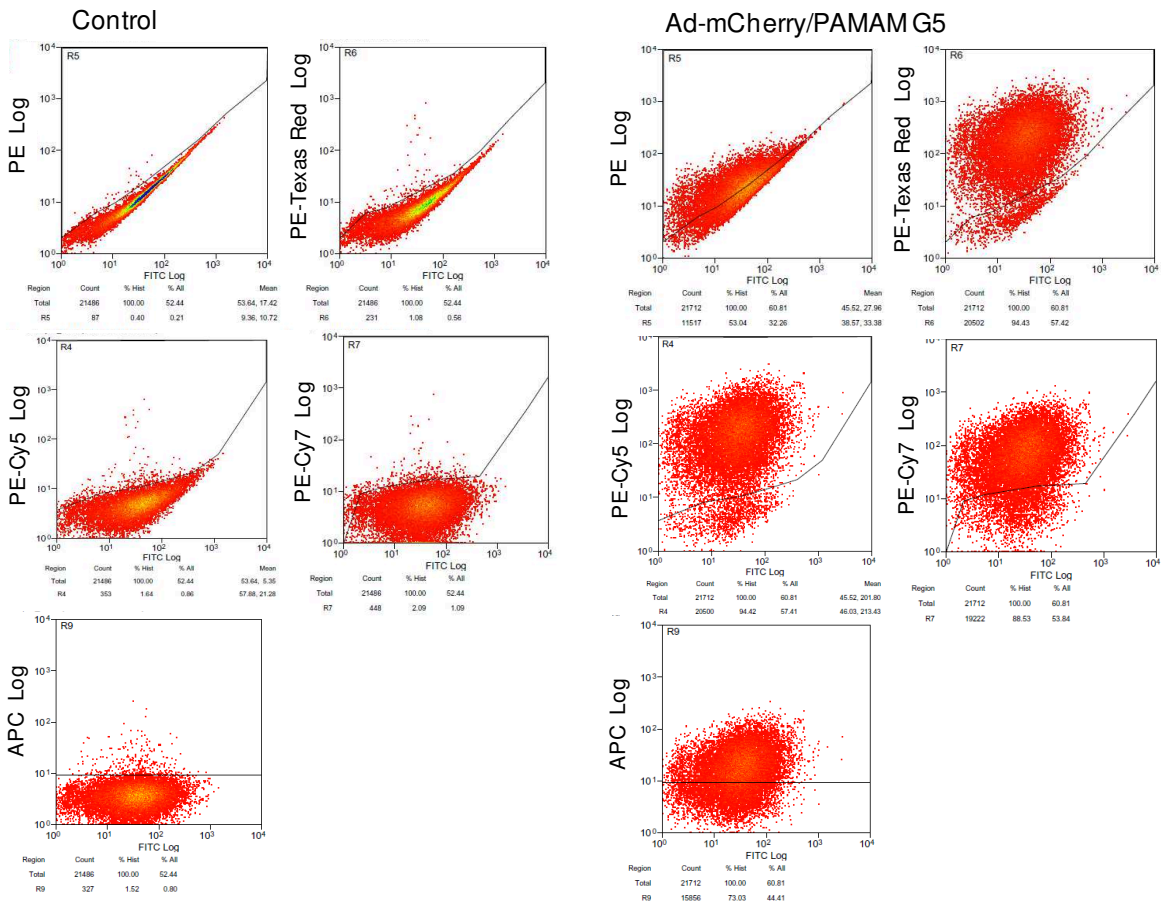

Figure S6. Optimization of diagonal gating with different channel combinations

To find the best channel combination for diagonal gating, cells excitated with a 488 nm or 635 nm laser respectively were plotted against the FITC channel (530/40) using either the PE (575/25), PE-Texas Red (613/20), PE-Cy5 (680/30), PE-Cy7 (750 LP) or APC (665/20) channel for diagonal gating. Excitation with the 488 nm laser and diagonal gating of PE-Cy5 against the FITC channel resulted in the best separation between mCherry positive and negative cells. Almost equivalent results were found with PE-Texas Red against the FITC channel.

Transduction of SKOV-3 LucEGFP with Ad-mCherry - overview 10x

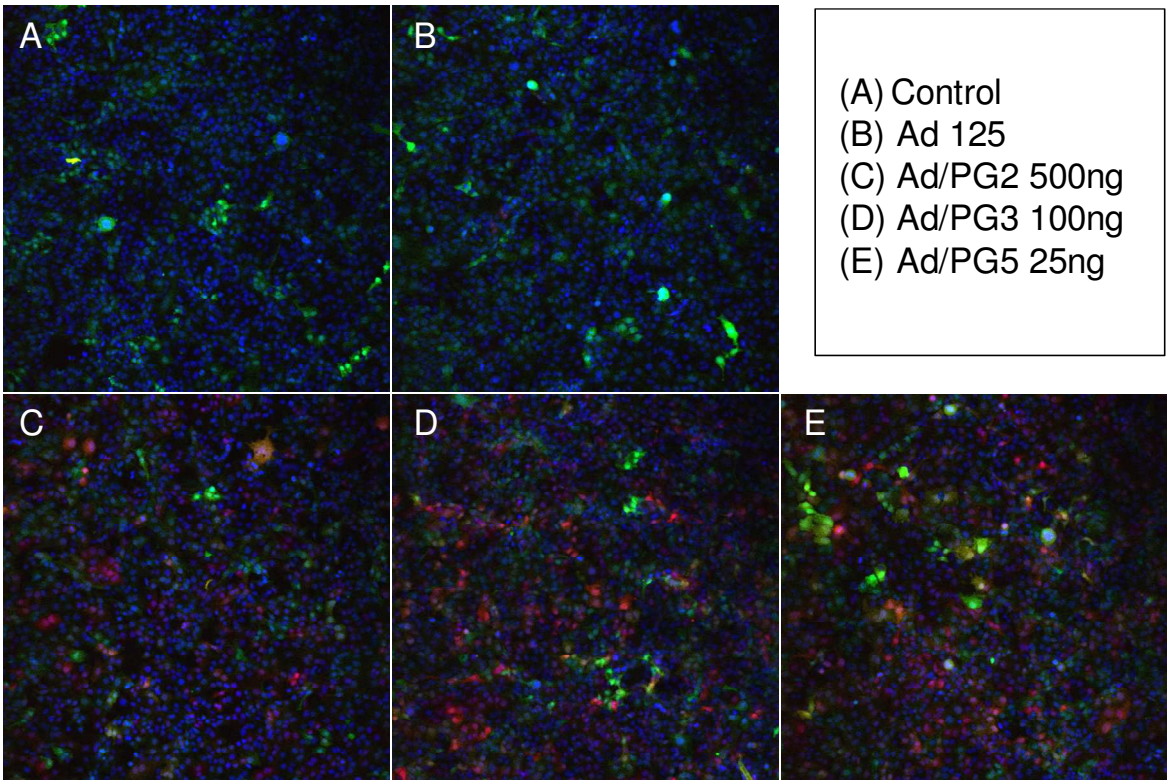

Figure S7. Evaluation of the coating benefit of PAMAM G2, G3 and G5 by LSM using Ad-mCherry at a MOI of 125

$2.5x10^4$ SKOV-3 LucEGFP cells seeded in 8-well chamber slides were transduced at a MOI of 125 with Ad-mCherry alone or coated with the indicated amounts of PAMAM G2, G3 and G5. After an incubation time of 48 h, cells were subjected to LSM imaging. (A-E) Laser scanning microscopy (LSM) images of control cells (A) versus Ad-mCherry only (B) and Ad-mCherry coated with PAMAM G2 (C), G3 (D) and G5 (E). Pictures show the EGFP signal from SKOV-3 LucEGFP as well as the mCherry signal in a 10x magnification.

7.9 Publications

7.9.1 Original papers

Schäfer A, Pahnke A, Schaffert D, van Weerden WM, de Ridder CM, Rödl W, Vetter A, Spitzweg C, Kraaij R, Wagner E, Ogris M; *Disconnecting the yin and yang relation of epidermal growth factor receptor (EGFR)-mediated delivery: a fully synthetic, EGFR-targeted gene transfer system avoiding receptor activation*, Hum Gene Ther. 2011 Dec;22(12):1463-73. doi: 10.1089/hum.2010.231. Epub 2011 Aug 10.

Vetter A, Virdi KS, Espenlaub S, Rödl W, Wagner E, Holm PS, Scheu C, Kreppel F, Spitzweg C, Ogris M.; *Adenoviral vectors coated with PAMAM dendrimer conjugates allow CAR independent virus uptake and targeting to the EGF receptor*, Molecular Pharmaceutics, 2013 Feb 4;10(2):606-18. doi: 10.1021/mp300366f. Epub 2013 Jan 18.

Grünwald GK, Vetter A, Klutz K, Willhauck MJ, Schwenk N, Senekowitsch-Schmidtke R, Schwaiger M, Zach C, Wagner E, Göke B, Holm PS, Ogris M, Spitzweg C.
Systemic Image-Guided Liver Cancer Radiovirotherapy Using Dendrimer-Coated Adenovirus Encoding the Sodium Iodide Symporter (NIS) as Theranostic Gene, J. Nucl. Med., 2013, in press

Manuscripts in preparation

Grünwald GK, Vetter A, Klutz K, Willhauck MJ, Schwenk N, Senekowitsch-Schmidtke R, Schwaiger M, Zach C, Wagner E, Göke B, Holm PS, Ogris M, Spitzweg C.
EGFR-Targeted Adenovirus Dendrimer Coating for Improved Systemic Delivery of the Theranostic NIS Gene, Mol. Ther. Nucleic Acids, 2013, in revision

7.9.2 Poster presentations

A. Vetter, K.S. Virdi, S. Espenlaub, W. Rödl, E. Wagner, P.S. Holm, F. Kreppel, C. Scheu, C. Spitzweg and M. Ogris; *Chemical modification of the adenovirus capsid for enhanced viral uptake into target cells*, 17th annual meeting of the German Society for Gene Therapy, Munich, 2010

A. Vetter, K.S. Virdi, S. Espenlaub, W. Rödl, E. Wagner, P.S. Holm, F. Kreppel, C. Scheu, C. Spitzweg and M. Ogris; *Non-covalent polymer coating of the adenovirus capsid allows for increased uptake into target cells*, 21st annual meeting of the Society of Virology, Freiburg, 2011

A. Vetter, S. Espenlaub, W. Rödl, E. Wagner, P.S. Holm, F. Kreppel, C. Spitzweg and M. Ogris; *Comparison of PAMAM G5 dendrimer and linear polyethylenimine for coating of adenovirus vectors*, 18th annual meeting of the German Society for Gene Therapy, Frankfurt, 2012

A. Vetter, Kulpreet S. Virdi, S. Espenlaub, W. Rödl, E. Wagner, F. Kreppel, C. Spitzweg and M. Ogris; *Non-covalent coating of adenoviral vectors with PAMAM dendrimer conjugates allows for CAR independent virus uptake and targeting to the EGF receptor*
16th Annual Meeting of the American Society of Gene & Cell Therapy, Salt Lake City, 2013

8 ACKNOWLEDGEMENTS

The last pages I want to dedicate to all the people who supported me throughout my doctoral thesis and there were many.

First of all I want to thank Prof. Dr. Ernst Wagner for giving me the opportunity to join his research group and have the freedom to work on a viral related topic in an otherwise non-viral environment. Thanks for providing me space for my S2 work and all the equipment needed. Special thanks go to PD Dr. Manfred Ogris as my direct supervisor for his mixture of guidance and freedom for individual development. Thanks for your patience during our 'ja aber' discussions, the countless jokes and the opportunity not only to join a scientific meeting each year, but also courses on presentations techniques and scientific writing provided by the SFB 824. I also want to thank Prof. Dr. Christine Spitzweg as my second supervisor for her guidance, the regular meetings during the set up of the project as well as for the productive research outcome. Additionally, I want to thank PD Dr. Florian Kreppel for his professional research guidance on adenovirus related topics. It was a pleasure to work with you and feel your passion about research. Thanks for your time spent on discussions, ideas and creative input.

Besides the people who supervised me, special thanks go to all the people in the lab, who made it easy for me to love going to the lab every single day. I want to thank our core facility, Ursula, Anna and Markus and for keeping it all going. Thanks to our technician Miriam for introducing me to cell culture work when I started and also for helping with my first FACS experiments and immunohistochemistry staining. Also to Wolfgang, for holding it all together, solving computer related topics, repairing several machines- I don't know if there is a single machine you hadn't had your hands on- as well as introducing me into chemical synthesis. Thanks to Rudi, the fastest Bavarian tongue I ever met and passionate cloning master. It was a pleasure to work with and learn from you. At this point thanks to Ursula for preparing as Rudi always stated 'the best competent cells ever'. Furthermore I want to thank Kulpreet for doing several TEM sessions with me. 'You're the boss, I am the driver' and I know it can be difficult to satisfy my wishes. It was always fun with you.

Thanks to all the people in the Kreppel/Kochanek lab, without you this thesis would hardly have been feasible. Thanks for virus supply, protocols and introducing me into virus propagation. Thanks for welcoming me with open arms and our going out event to the beer garden. Special thanks to Siggi for the Alexa 488, as well as the first covalent coupling

studies of the Ad-PEG-PAMAMs. Thanks to Lea for following up on aggregation studies and freezing thawing studies with the Ad-PEG-PAMAMs. Also special thanks to Jan for fluorescence measurement of liver homogenates, helping with qPCR and silver staining and being the man to answer my questions during my stay in Ulm. Additionally, thanks a lot to Matthias for his hands on the in vivo experiments on biodistribution as well as the help with the setting up of the ELISA. Thanks to Erika for introducing me into cloning of big vectors, creating the Ad-HP, Ad-HP-mir143bs, Ad-AFP and Ad-AFP-mir143bs and to Sandra for her work on cloning the Ad-mCherry.

I also want to thank my cooperation partner Geoffrey who followed up on my in vitro results with adenoviral NIS gene transfer, in vivo. Thanks for your help with the biodistribution study comparing two different mouse strains. Thanks also go to Alke Schopp of the group of Elisabeth Deindl, who did the H/E staining of the SKOV-3 i.p. tumors. Last but not least thanks to Daniel, Flo, Andi, Kevin, Tommy, Uli, Christian, Irene, Petra, Rebekka and the rest of the crew for the best working atmosphere ever, for fun times on the skiing trips, Pharma parties etc. Couldn't have any better colleagues than you guys! Thanks to the 'Laufgruppe Wagner', even though mostly consisting of two people and to Martina for the well organized botanical excursions and diversity of practical courses I could supervise. Special thanks also go to my former lab colleague in Cardiff, Lindy Goddard, for her great job on proof reading this thesis.

Big thanks to my family especially my Mum for providing me backing and supporting me throughout every big decision in my life and to Gordon for his tolerance and respect on my decision to go to Munich and simply for being there, whenever most of the time mentally.

…To make an end is to make a beginning…

T.S. Eliot